Master of Science Thesis

Application of fracture mechanics in a blended numerical framework for progressive damage analysis of CFRPs in FEM

A.P. van Oostrum

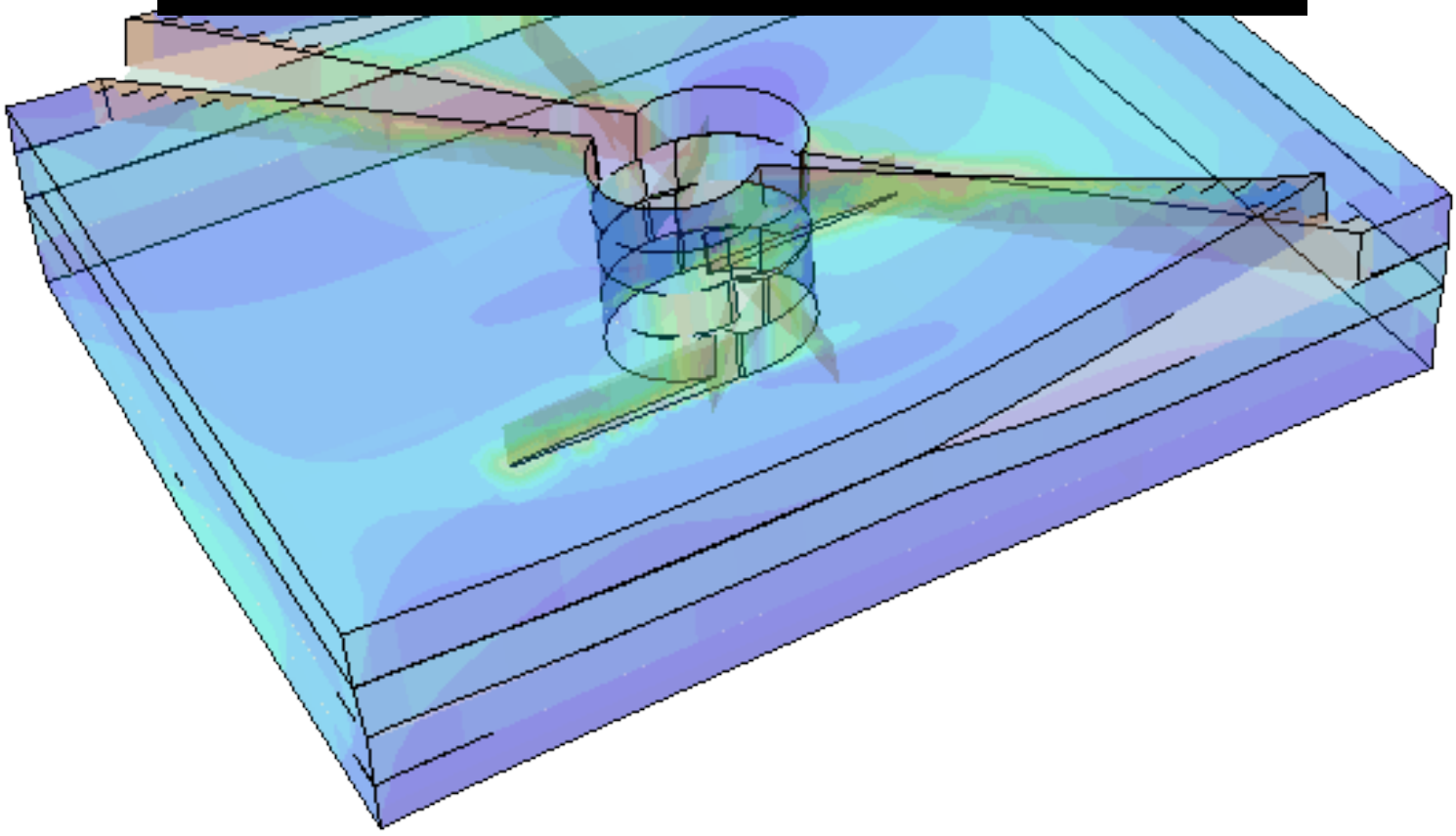

Faculty of Aerospace Engineering · Delft University of Technology

TU Delft Delft University of Technology

Application of fracture mechanics in a blended numerical framework for progressive damage analysis of CFRPs in FEM

Master of Science Thesis

For obtaining the degree of Master of Science in Aerospace Engineering
at Delft University of Technology

A.P. van Oostrum

6 October 2017

Faculty of Aerospace Engineering · Delft University of Technology

Delft University of Technology
Faculty of Aerospace Engineering
Department of Aerospace Structures and Materials

GRADUATION COMMITTEE

Dated: 6 October 2017

Chair holder:

Prof.dr.ir. R. Benedictus

Committee members:

Dr. D.S. Zarouchas

Dr. C.D. Rans

Dr.ir. J.M.J.F. van Campen

Abstract

The unique strength and directional properties of composite materials make them increasingly interesting to be applied in structural applications. This applies specifically if low weight is important such as in the aerospace industry where composites are increasingly used. However, at the same time composites are not well understood on multiple different fronts. One of such aspects is the progression of damage. This thesis worked towards increasing the fidelity of current progressive damage analysis methods by blending stress-strain and fracture mechanics based methods and more particularly it focussed on the fracture mechanics. This high fidelity model should be accurate, computationally efficient and allow for application in generic specimens.

Within these fracture mechanics based methods two meso mechanical types of failure are modelled. Delaminations, using cohesive zone modelling, and matrix cracks using a combination of cohesive zone modelling and XFEM to provide mesh in-dependency. A stress-strain based continuum damage model (CDM) is provided as part of partly parallel research to model fibre failure. These models are combined in a framework using Abaqus. The model was tested on four ply-scaled CFRP laminates in a open hole tensile test, as well as validated on an in-house experimental campaign. Preliminary models, previously presented in the parallel study, featured severe convergence issues due to Abaqus's implementation of XFEM. This is partly resolved in this thesis and a consistent set of results is presented.

The model performs very well in terms of final failure loads with errors within a few percent points. Also damage progression looks promising, with progression rates and failure patterns for both delaminations and matrix cracks mostly in line with experimental CT scan results. Only the matrix crack patterns can not be matched in all layers. This is related the aforementioned convergence issues which also prevents multiple parallel cracks to be modelled at the same time. Attempts to overcome this have proven to be unsuccessful in the current framework. This presents a clear issue as damage can be underestimated without any quantification on the consequence.

Two main recommendations are presented. The model performed significantly better than more traditional CDM implementations, presenting also more physically sensible failure patterns. Continuation is therefore recommended, further investigating the current model. Although all the obtained results are very promising they are by far not enough to validate the model. Only a small subset of possible laminates and loading conditions is considered and it is unknown how the model will respond under failure that is more driven by interactions of failure modes or different failure mechanisms such as compressive fibre failure which was left outside the scope of this thesis.

Secondly, the framework with Abaqus's implementation of XFEM is too constrained and this can not be overcome. The presented framework in this thesis may be sufficient for some cases, but can not be extended to any generic laminate. The possibility that damage is underestimated is dangerous and the move to a less limited framework with more control is advised, hereby moving away from commercial software.

Preface

Dear reader,

The work presented here is the accumulation of 8 months of errors, debugging and small victories. I started with only one expectation; nothing will work. Failure in composites features just to much interactions, small complexities and unknowns to make everything work. Even in the very limited scope of this thesis. I just needed to confirm myself, and was not disappointed. For every small victory new hurdles, and solutions, present themselves. Working with composites will never bore you this way and sometimes it was hard to stop. I hope the reader can appreciate the results presented in this thesis as much as I do.

I would like to thank my supervisor Dr. D. Zarouchas for his feedback and support during the writing of this thesis. Moreover I'd like to thank B.R van Dongen for his cooperation, feedback and criticism during the past months. Finally I'd like to thank my friends and family who had to put up with me, and did so.

Delft, University of Technology
6 October 2017

A.P. van Oostrum

"Life is really simple, but we insist on making it complicated."

— *Confucius*

Table of Contents

Acronyms

CDM Continuum Damage Model.

CFRP Carbon Fibre Reinforced Plastics.

CLF Crack Limiting Function.

CT Computerized Tomography.

CTE Crack Tip Elements.

CZM Cohesive Zone Modelling.

DCB Double Cantilever Beam.

DIC Digital Image Correlation.

DoF Degrees of Freedom.

ECT Edge Crack Torsion.

ELS End Loaded Split.

ENF End Notched Flexure.

FEM Finite Element Method.

LEFM Linear Elastic Fracture Mechanics.

MMB Mixed Mode Bending.

ODB Output DataBase.

OHT Open Hole Tensile.

PDA Progressive Damage Analysis.

RVE Representative Volume Element.

SERR Strain Energy Release Rate.

UDMGINI User Damage Imitation.

UEXTERNALDB User External Database.

UMAT User Defined Material.

URDFIL User Read File.

VCCT Virtual Crack Closure Technique.

VCE Virtual Crack Extension.

WWFE World Wide Failure Exercise.

XFEM Extended Finite Element Method.

List of Symbols

Symbol	Unit	Description
CTE	$[m/deg]$	Coefficient of thermal expansion
E	$[Pa]$	Elastic modulus
FI	$[-]$	Failure Index
G	$[Pa]$	Shear modulus
G_c	$[J/m^2]$	Fracture toughness
G_I	$[J/m^2]$	Strain energy release rate mode I
G_{II}	$[J/m^2]$	Strain energy release rate mode II
G_{III}	$[J/m^2]$	Strain energy release rate mode III
k	$[Pa]$	Stiffness
$\boldsymbol{K}$	$[-]$	Stiffness matrix
l	$[m]$	Element length
N	$[-]$	Number of elements
p	$[-]$	Inclination parameter
r	$[m]$	Radial distance from crack tip
R	$[-]$	Random number
R	$[m]$	Radius
S	$[Pa]$	Shear strength
t	$[m]$	Thickness
W	$[-]$	Weight
X	$[Pa]$	Fibre strength
Y	$[Pa]$	Transverse strength
Z	$[Pa]$	Transverse strength
α	$[-]$	Stiffness coefficient
α_1	$[-]$	Power law coefficient
α_2	$[-]$	Power law coefficient
α_3	$[-]$	Power law coefficient
β	$[1/Pa^3]$	Shear non-linearity coefficient
δ_c	$[m]$	Separation displacement
η	$[-]$	B-K interaction criteria coefficient

Symbol	Unit	Description
ν	$[-]$	Poisson ratio
σ	$[Pa]$	Stress
σ_u	$[Pa]$	Ultimate strength
τ	$[Pa]$	Stress
θ	$[rad]$	Fracture angle

List of Figures

List of Tables

1 Introduction

Composite structures are increasingly applied in lightweight structures. Their directional properties allow them to be tailored to specific needs, allowing for more efficient and stronger structures. Especially in weight critical applications, such as is common in e.g. the aerospace industry, the advantages are therefore ever increasingly applied. However, the anisotropy that provides composites structures their strength makes them also not well understood [11, 12] and difficult to work with. One of the aspects that is not well understood is initiation and progression of damage. The presence of both fibres and a matrix presents a wide range of different types of failure. Moreover interactions between the fibres and matrix, but also between the different failure modes adds to the complexity of the problem. This specifically applies as damage progresses. This complexity of interactions and different failure modes provides the basis for this research. This research works towards blending stress-strain and fracture mechanics based methods with the objective to improve the fidelity of current Progressive Damage Analysis (PDA) methods under quasi-static loading. Fidelity in this aspect refers to applicability on generic laminates, taking into account the complete framework from accuracy to computational effort. The work presented in this thesis focussed primarily on fracture mechanics based methods and a combination of matrix and delamination failure. The stress-strain based methods are only used as input for the blended framework and are provided from a parallel research. Blending these two methods is currently done only in a very limited extent [13–15]. With increasing understanding and modelling capabilities a framework can be built which will allow these models to be employed in more complex loading situations, such as where failure is less predictable or stimulated by e.g. fatigue loading. Working towards accurately predicting failure is key to move forward in understanding and effectively utilizing composite structures by allowing for smaller safety margins or longer operational use. The objective of this thesis sets small steps towards that goal.

This chapter introduces the research objective and provides the broader picture in which the research objective is placed. First however, damage in composites is shortly discussed to provide an introduction to what damage in composites in this thesis encompasses. Hereafter a partly parallel work activity is shortly discussed. This work provided part of the input for the final model and a joined preliminary model was previously presented. Based on these two preliminaries the research objective and scope is discussed. Finally an outline for the rest of this thesis is presented which highlights the focus of the work presented in this thesis.

1.1 Failure in composites

A first important distinction that needs to be made when describing failure is the scale at which this is described. Typically this considers the macro, meso, micro and nano scales. What types of failure modes can be distinguished differs per scale level, and will also to some degree affect accuracy. At the meso mechanical level, which this thesis will mostly be modelled in, the most common distinction is made between fibre failure, matrix failure and delaminations, with the former two in either tensile or compressive loading. The definition of how this failure is defined follows from the lower scale levels, specifically the micro scale.

1.1.1 Fibre Failure

Tensile fibre failure is in its simplest form just a breakage of fibres. Compressive fibre failure is more complex and not one clear failure mode can be distinguished. Under compressive loading fibres may show a form of local micro buckling, or fibre kinking.

The definition of this failure is also strongly dependent on the constituent behaviour of the surrounding matrix material. Such aspects are described at the lower scale levels via e.g. a Representative Volume Element (RVE)

1.1.2 Matrix Failure

Matrix failure is a form of intra-laminar fracture in which cracks form in the matrix material in between the fibres. This fracture can follow not only from a regular tensile normal separation, but also under compressive loading with the fracture planes (at angle) slipping over each other.

Interactions with the fibres are again strongly present, not only with the fibres dictating the direction the cracks can follow, but also acting as crack stoppers at a micro mechanical level. Moreover interaction with delaminations can be strong with compressive loading creating a wedging effect driving delaminations. In other cases a normal opened crack may initiate in the matrix but continue as a delamination.

1.1.3 Delaminations

Finally delaminations consider a separation of the individual plies. Although this does not distinguish between tensile and compressive loading, as the latter simply closes the fracture plane, it can still be distinguished at lower scale levels with the typical distinction considering how a crack is opened. This refers to the crack modes, with mode I tensile cracks or mode II (longitudinal) and mode III (transverse) shear cracks.

The list and description of failure modes described previously is far from complete or unambiguous. Depending on the exact scale level failure modes can be clustered, or considered individually, making further divisions in the short descriptions above. This thesis will

implement failure at a meso mechanical level and with a limitation of just tensile loading, will mostly consider the high level terms fibre failure, matrix failure and delamination failure. This thesis will not consider any new failure theories but builds on pre-existing work. The ultimate definition of failure, in this thesis, therefore follows from the implemented failure theories. These failure theories may, and preferably are, based on lower scale levels as this more likely to capture the physics of the problem.

1.2 Parallel research

A partly parallel and precursor study by Van Dongen[2] focused on stress-strain based methods in order to model the initiation and progression of damage in composites. These methods base damage on the local stress-strain state in a laminate. Damage progression is modelled using a selective stiffness reduction in the form of a Continuum Damage Model (CDM) in an attempt to emulate the development of damage. These models are relatively easy to implement, but can completely undermine the physical meaning of the damage.

This thesis considers damage from a fracture mechanics based perspective. Rather than smearing the damage as CDMs do, cracks are modelled discretely with identifiable fracture surfaces. Moreover, fracture is now not driven by the stress-strain state, but to a large extent also by the energy that is released when these fracture surfaces are separated, thereby increasing the physical meaning when such methods are employed.

The fracture mechanics based methods discussed in this thesis and the partly parallel work by Van Dongen[2] are also combined in this thesis. An overview of how these works integrate is also provided in Figure 1.1 and is further discussed under the outline of this thesis in Section 1.4. The work by Van Dongen is shown in Figure 1.1 as a dotted line. The focus in the results reported in this thesis are based on a continuation of this parallel work from the preliminary model onwards as also discussed in the next section.

1.3 Research Objectives, questions and scope

This section discusses the research objectives and research questions for this thesis. As this work was also part of the previously mentioned parallel work, a very clear focus is put on some of these research questions following from the conclusions by Van Dongen [2]. This is further explained in the scope of this section.

1.3.1 Research objectives and questions

The high level research objective for this thesis is defined as:

> "To provide a high fidelity numerical framework for modelling of progressive damage for CFRP by using a combined fractures mechanics and stress-strain based approach implemented in FEM."

High fidelity herein refers to the algorithm not being constrained by specific laminate layup requirements or failure modes describable by either fracture mechanics or stress-strain based approaches only. Moreover it considers an internal trade-off between accuracy and speed or computational effort. The objective considers the complete framework in which this PDA is performed considering expandability to more complex load cases and corresponding models. Two main sub-objectives could therefore consider providing a general framework with a high accuracy and a framework with a low computational cost. A final sub-objective is identifying how these aspects relate to each other.

In order to meet this objective the leading research questions are among similar lines. To reach the objective the following three research questions are therefore most important to consider: What are the driving aspects for the accuracy of the implemented models? What are the driving aspects of the computational cost of the implemented model?; And finally, in order to conclude on the generality of the framework, it is important to provide an answer to the question; what are the limitations of the implemented model?

1.3.2 Scope and limitations

Both the research objectives and questions have been aligned as part of the parallel research towards the same uniform objective. Within the work presented in this thesis focus is laid on the blended implementation of a stress-strain and fracture mechanics based method within a general framework. A restriction is made considering only Open Hole Tensile (OHT) experiments for Carbon Fibre Reinforced Plastics (CFRP) laminates. In assessing the framework and its suitability this restriction is lowered and also more complex loading conditions and laminates are considered.

As the work focusses around both the framework as well as the implementation, it is also a limited review of what can be achieved with current state of the art methods in commercial software. This thesis therefore does not propose new damage models. As the framework is set as part of the parallel work, a limitation was made to the commercial Finite Element Method (FEM) software Abaqus. This imposes a set of restrictions on what can be achieved and investigated.

A final important limitation that needs to be considered are the laminates. Even under constant loading conditions in OHT tests different laminates will yields different failure modes and failure patterns, depending on the materials and stacking sequences. Only a very select number of laminates can be considered. Therefore focus in the work is on the progression and sequencing of failure patterns, rather than failure loads, as this can provide more confidence in the scalability to different laminates and loading conditions.

1.4 Outline

After this introduction, Chapter 2 will provide an overview of fracture mechanics based methods to model damage in composites. It will provide a high level discussion and motivate the choice and selection of these fracture mechanics based methods. An important aspect

herein is their suitability within a blended framework. In parallel a similar review was performed by Van Dongen [2] for the stress-strain based CDMs.

Hereafter Chapter 3 will discuss the implementation of the selected models in a blended framework. This will consider two parts: the model integration within the commercial software of Abaqus and the implementation of the failure models, considering also in short the stress-strain based models which are not discussed in Chapter 2. Focus of this chapter is to provide an overview of how this model can be recreated within Abaqus, highlighting all the important elements and how these interact with each other and where these are defined. This description is relatively detailed as a lot of subsequent discussion and problems relate to this framework, its integration within Abaqus and the limitations this creates. As not all of these follow logically, a discussion on resulting issues can only be attempted if a complete description is provided.

Hereafter follows arguably the most important Chapter 4. Chapter 4 is the focal chapter of this thesis and discusses the verification model in several aspects, together with its underlying problems. This chapter discusses two main variants of the same model. The single crack model, and the multiple crack model. The single crack model is limited in the amount of damage it can describe and has no scalability to more generic laminates or loading conditions. It is however relatively stable to run. This model is used to investigate the models performance in terms of accuracy and computational effort. The multiple crack model is less stable, but provides a framework for scalability of the model and an attempt to remove the limitations of the single crack model. To appreciate the multiple crack model a strong understanding of the issues present in the single crack model is therefore first required.

Chapter 5 provides a validation of the resulting model from Chapter 4 on a in-house experimental campaign. It does not present real new issues with the models, but provides an new set of results in an attempt to provide additional validations of the models performance. However, as only single layup is tested the best overview of the performance of the model is still provided in Chapter 4.

Finally Chapter 6 discusses the main conclusions of the presented models and recommendations on how to move forward. All chapters will end with an individual conclusion which highlights the most important aspects of the chapter and provides a limited discussion on applicability and shortcomings. This final chapter follows from these individual conclusions.

An overview of how these chapters integrate with the model's development, the focus of the chapters and the partly parallel work by Van Dongen [2] is provided in Figure 1.1.

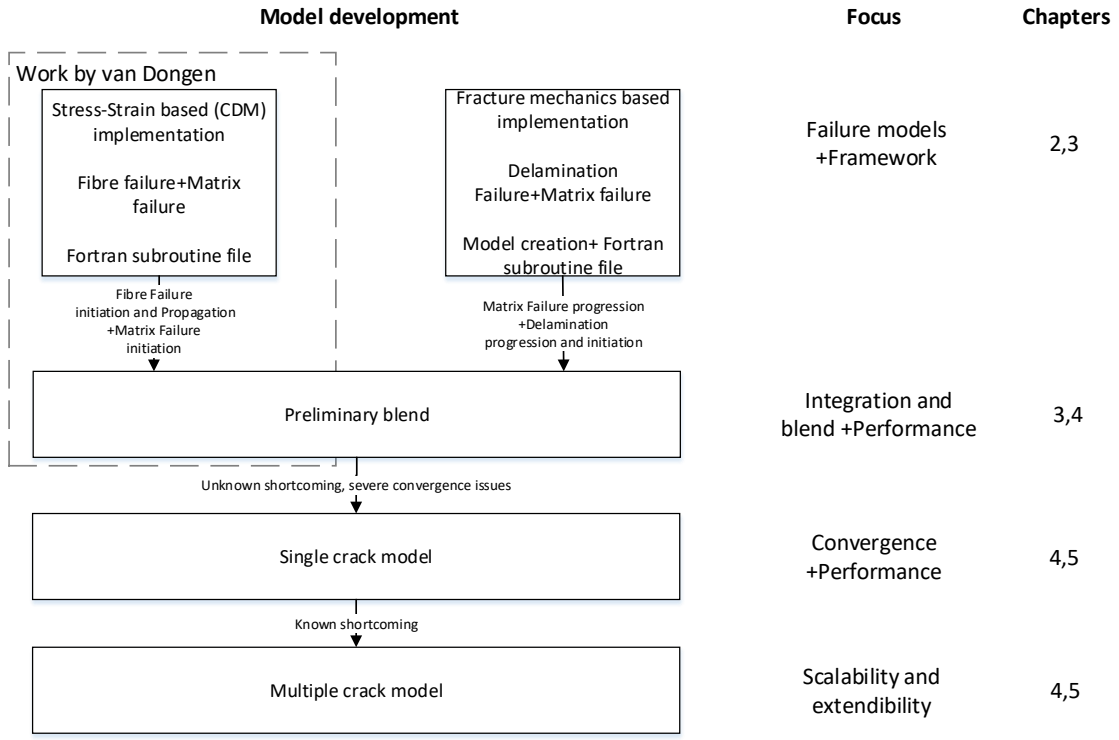

Figure 1.1: Outline of model elements and integration within thesis

2 Fracture mechanics damage progression models

This chapter discusses fracture mechanics based damage models, their underlying theories and their applicability for a high fidelity PDA framework for CFRPs. This chapter highlights the most important aspects, considerations and the selection of a model. Only matrix cracks and delaminations can effectively be captured by these methods as these failures provide a relatively clear fracture plane. Fibre damage is therefore not considered within this chapter. Details on how the selected method is translated in the PDA framework and more insight in the actual implementation is provided in the next chapter. This next chapter also blends with stress-strain based models which will incorporate the fibre damage that is not considered in this chapter.

These stress-strain based methods, which are not further considered in this chapter, consider a form of property degradation to simulate the development of damage and are also known as a Continuum Damage Model (CDM). This chapter will consider models in which fracture considers a true separation, in which a clear fracture plane can be identified. Two main methods can be identified in this context: The Virtual Crack Closure Technique (VCCT) in the framework of Linear Elastic Fracture Mechanics (LEFM) and Cohesive Zone Modelling (CZM). The VCCT describes the progression of cracks by the release of nodes in between elements to model the evolution of cracks. CZM on the other hand uses interface elements with degrading stiffness to model the progression of cracks. Besides these techniques, which describe a model for both the crack progression and crack path, the applicability of the relatively novel Extended Finite Element Method (XFEM) is also considered. The Extended Finite Element Method (XFEM) provides methods which allows for arbitrary crack paths, unlike the basic implementations of VCCT and CZM, by using local enrichment of elements.

This chapter provides the necessary pre-required knowledge to motivate why these models are selected together with the basic knowledge required for the implementations of the damage models which is discussed in the next chapter. Practical application, in terms of numerical formulation, is not so much considered as part of the practical application will be provided by Abaqus and is not controllable. Numerical aspects that are relevant for the actually chosen model, at the end of this chapter, are discussed in the subsequent chapter.

First fracture criteria are discussed in Section 2.1. Section 2.2 discusses fracture within the LEFM framework, predominantly applicable for the VCCT. Hereafter, in Section 2.3, the cohesive zone model is shortly explained. Section 2.4 discusses the advantages and

applicability of XFEM. Finally the choice for a combination of CZM and XFEM is discussed in Section 2.5 and is concluded upon in Section 2.6. The basis for some of these sections follow partly or entirely from a pre-cursor unpublished literature review and are repeated to familiarize the reader with the subject and to present the basis for the selection of methods in Section 2.5, which is the focal point of this chapter.

2.1 Fracture criteria

Fracture criteria find their origin in isotropic materials such as metals and the stress fields around the crack tip. The stress state around the crack tip determines whether a crack will progress or not. Analytical formulations for the stress field around the crack tip follow from LEFM and a stress intensity factor (K) is defined based on this stress field [1, 16]. Materials subsequently have a critical value (K_c) for this stress intensity factor which dictates fracture. The value of K_c depends on the mode in which a crack is opened and is therefore in principle different for all three crack modes.

The physical relevance of these stress based fracture criteria is arguable [11]. However, for isotropic materials is has been shown that these fracture criteria are equivalent to an energy based counterpart [17, 18]. Specifically for composite, anisotropic, materials these energy based fracture criteria make physically more sense. Rather than a stress intensity factor these energy based fracture criteria are based on the energy that is released per unit of formed crack area. This is quantified via the Strain Energy Release Rate (SERR) as also shown in equation 2.1.

$$G_I \geq G_{c_I} \qquad G_{II} \geq G_{c_{II}} \qquad G_{II} \geq G_{c_{III}} \tag{2.1}$$

These values differ for each crack mode and require some sort of interaction criteria if multiple modes are active at the same time. The use of interaction criteria is an important one with for example the most typical failure mode of delamination occurring commonly under mixed mode I + II conditions [19]. It is clear that fracture, under mixed mode conditions is most likely to occur before any of the individual criteria for the fracture modes is satisfied.

The value for fracture toughness values for delaminations can be obtained by tests for which a limited amount of standards exist. Typical tests are for example a Double Cantilever Beam (DCB) test for mode I cracks, and End Notched Flexure (ENF) and End Loaded Split (ELS) tests for mode II delaminations [19, 20]. For mode III cracks for a long time no methods existed. Moreover mode III cracks are typically less significant [21] and focus has historically been pointed less towards this [22]. For the mode III Edge Crack Torsion (ECT) tests have been developed, the development hereof however being only a recent one with limited data available. Currently, for mode I and II cracks of unidirectional composites ASTM standards exist [23, 24]. Moreover methods considering multiple modes at once exist [19] such as Mixed Mode Bending (MMB) tests. Further determination of these fracture toughness parameters is for now not considered, though it is noted that accurate knowledge of these parameters is a key requirement for the proper modelling of failure.

An extensive overview of interaction criteria, for both 2D and 3D models is provided by

Reeder [22]. An important point to note is that none of the criteria is physically based and all require a curve fit [22]. This requires the addition of combined mode tests like MMB. The lack of a physical basis for the interaction criteria makes the choice of one in some sense rather arbitrary. The BK and power law criterion are commonly applied[22, 25] but this can primarily be driven by their small amount of experimental parameters. These criteria are given in Equation (2.2) and (2.3) respectively.

- Modified B-K criterion:

$$\frac{G_I + G_{II} + G_{III}}{G_{Ic} + (G_{IIc} - G_{Ic})(\frac{G_{II}+G_{II}}{G_I+G_{II}+G_{III}})^\eta + (G_{IIIc} - G_{Ic})(\frac{G_{II}+G_{III}}{G_I+G_{II}+G_{III}})^\eta} \geq 1 \tag{2.2}$$

- Power law criterion:

$$(\frac{G_I}{G_I})^{\alpha_1} + (\frac{G_{II}}{G_{IIc}})^{\alpha_2} + (\frac{G_{III}}{G_{IIIc}})^{\alpha_3} \geq 1 \tag{2.3}$$

2.2 Models in the framework of LEFM

This chapter deals with models that consider the crack tip as a sharp discontinuity, as defined by the analytical formulation of LEFM. Fracture in these models is directly linked to the fracture criteria discussed previously. An alternative method, discussed in the next section, does not consider the crack tip as sharp. Rather, cohesive zone models consider a gradual degradation of stiffness at the fracture plane. In cohesive zone models the interface is explicitly modelled. In the models of this chapter on the other hand, primarily the crack tip is modelled.

From the framework of LEFM in proximity to the crack tip a singularity of the type $1/r$ exists, with r referring to the distance from the crack tip. Models based on the framework of LEFM need to include this behaviour to accurately determine fracture. Using regular FEM elements an extremely fine mesh is required. Moreover, convergence is troublesome due to the presence of a singular expression. To overcome this, in the framework of LEFM, typically second order quarter point elements are used. These special Crack Tip Elements (CTE) have additional nodes placed at a quarter position of the element edges which introduces a singular expression. This allows for the reproduction of the characteristic $1/\sqrt{r}$ behaviour. In numerical implementations these special elements are typically placed as a “waiver" around the crack tip [1].

Only for delaminations there is clearly defined fracture plane due to presence of a resin rich layer which would allow for proper placement of such elements. For matrix cracks it has been shown that the singularity of the order $1/\sqrt{r}$ is not correct, but a lower order is applicable [26]. Moreover matrix cracks may not have a clearly defined initial fracture plane hindering possible implementation by depending strongly on adaptive meshing techniques. For this reason only delaminations are considered in the framework of LEFM and the remainder of this section. It is clear that describing only a specific type damage poses a severe limitation.

The use of these special Crack Tip Elements (CTE) introduces a very strong mesh dependency, as they should move along with the crack tip. This requires the mesh to be continuously updated. The optional addition of XFEM removes this strong mesh dependency by allowing for mesh independent fracture planes and singularities by using special enrichment functions. The use of XFEM is further discussed in Section 2.4.

2.2.1 Failure determination

The determination of crack progression, for example by equation (2.1), or under mixed mode conditions requires the determination of the SERR. If multiple fracture modes are present than this quantity needs to be subdivided into the SERR components corresponding to each mode. This section discusses two methods to determine the SERR. The Virtual Crack Closure Technique (VCCT) technique is thereof most commonly applied due to its easy separation into the different fracture modes. Alternatively the Virtual Crack Extension (VCE) method can be used. This method is however rarely applied.

2.2.1.1 Virtual crack closure technique

The Virtual Crack Closure Technique (VCCT) is most commonly applied in order to compute the strain energy release rate. If different crack modes are present then the global strain energy release rate is of little use. The combined loading criteria of Section 2.1 require a distinction between the energy available for each of these modes separately. The VCCT is able to relatively easily provide this distinction of modes making it a commonly applied method [27]. The total SERR is provided by the summation of the individual crack modes. The principles of this method are based on the analytical formulation of the J-integral to compute the SERR, employed in the numerical FEM domain assuming there is small process zone ahead of the crack tip. In the VCCT the SERR is determined by a virtual extension of the crack from a to $a + \Delta a$. Energies, for each crack mode, are computed by a multiplication of internal nodal forces and displacements around the crack tip. The SERR is determined by subtraction of the energy prior to the extension of the crack and by a division over the area of the newly fracture surface. There exist two formulation of the VCCT, a one step and a two step method. Both methods are similar, with the one step method being slightly simpler by assuming nodal forces to not have changed significantly by the virtual extension of the crack, which allows them to be reused. The distinction in different crack modes is automatically provided as released energies are computed for each mode separately. A complete overview of the VCCT technique, and it implementations is provided by [27] for the 2D case, the 3D solid case and for special plate or shell elements. Moreover non-linear cases are considered as well. Implementation of the VCCT for delamination in composites is provided by for example [21, 28] among others, but no implementations are found in the form of a full PDA as discussed in this thesis.

2.2.1.2 Virtual crack extension technique

The VCE method is based on the principle of virtual extension of the crack, but does unlike the VCCT does not dictate a method to do so. It is however therefore typically not capable

of providing mode separation as the SERR is determined on global level, unlike the VCCT which locally used the J-integral. The global SERR release rate follows from deviating the potential energy with respect to the change in crack area [1]. In FEM formulation the energy release can be obtained by differentiation of the stiffness matrix $\boldsymbol{K}$ [1]. By using the total potential energy the approximation of the crack tip is of lesser importance and the use of CTE may not be required. Moreover the method is relatively quick. However, as the energy release is determined at a global level a distinction in different fractures modes can not be provided by default. This severely limits the applicability. This inability to not provide mode separation made the VCE technique to be primarily used by mode I cracks with no interactions. However, as early as 1975, formulations for mixed modes have been provided for the VCE [29–33]. In the context of composites the method has been applied more recently for the modelling of delamination [34]. It provided a novelty by including the mode separation, but no results including mode separation for composites have been reported after this for the VCE method. Moreover the work by Davis [34] provided little to no comments on the accuracy of this method and functioned primarily as proof of concept. This lack of practical application for models with multiple modes present makes limits the applicability of this technique in the context of this thesis.

2.2.2 Crack progression

Section 2.2.1 provided a means to determine the SERR which, if coupled to a fracture criterion, determines whether a crack should progress. The VCCT already dictated the method by which this crack should progress. The VCE method left this unspecified. This section outlines the most important methods of crack progression.

As the VCCT is most commonly applied to determine the SERR, the node release method, which must be used in conjunction for the VCCT is also the most commonly applied method for the progression of cracks. The node release method simulates the progression of cracks by the release of FEM nodes. Alternatively, to prevent the addition of nodes during the progression of cracks additional nodes may pre-exist at the fracture plane which are coupled by rigid elements and are uncoupled as cracks progresses [21, 28]. In the node release method the direction as well as the growth of cracks is directly coupled to the mesh orientation and size. Prime disadvantages of this method would be [1, p.328]: The requirement of a pre-crack and possible strong mesh dependency by following the crack path. Moreover Lord [35] mentions as additional problems the requirement to recompute the stiffness matrix and possible ‘discontinuities in the originally smooth delamination front’ [35, p.1] as a crack progresses.

To overcome the strong mesh dependency found in the node release method, alternatives which consider more freely defined fracture paths are considered. As also the SERR needs to be determined these methods are less commonly applied if fracture mechanics is considered.

The element splitting technique allows for these more freely defined fracture paths. Cracks can grow in any direction by splitting of the elements on the fracture path. Crack growth is thereby no longer constrained by the positions of the nodes. Although this method may present itself as very promising difficult implementation, such as local re-meshing requirements, prevent

practical implementation [1]. This specifically applies for 3D crack geometries. With the lack of a practical method to determine the SERR there are also two additional unknowns present: The crack growth direction and the crack growth extension value. These additional unknowns and practical difficulties make this method not commonly applied. No implementations were found in the context of composite materials. Its application is however similar to XFEM discussed later, which allows for similar features but does not explicitly create new elements.

Finally the element elimination technique and smeared crack model are considered. Both of these methods do not explicitly model a fracture plane but rather smear the damage of a crack either by completely removing the element or by selectively degrading material properties of the element close to zero [1, 36]. With again the lack of methods to determine the SERR this typically use stresses or strains to determine what elements should fail. Using the stresses in the element can however allow these methods to be characterized as a stress-strain based approach rather than a fracture mechanics based method. These models are similar to CDM implementations and are not further discussed as they do not create clearly defined fracture planes and have no physical basis.

2.3 Cohesive zone modelling

Different from the previously discussed methods described in the framework of LEFM, cohesive zone modelling assumes fracture to take place in a cohesive zone in front of the crack tip until final separation [1]. This method includes no unrealistic stress singularities, requiring the use of special FEM elements which allow for the $1/\sqrt{r}$ behaviour as previously discussed in the context of LEFM. Rather, cohesive elements are inserted in between the regular FEM elements. Cohesive zone models are particularly interesting for materials in which failure occurs over a narrow region [1]. A typical example for composites is the so called formation of crazes or cracks over which fibre-bridging occurs.

Initial formulation for cohesive zone models considered mode I cracks only [37]. The basic principles are discussed first considering only these mode I cracks. In Section 2.3.4 the extension for cracks including multiple fracture modes is made. In CZM the stress state at the crack tip, the progression the crack and the fracture criteria are all combined in the formulation of the cohesive element. The outline therefore differs from the methods discussed in the context of LEFM.

2.3.1 Traction-Separation laws

Unlike the methods discussed in the framework of LEFM, both fracture criterion and crack progression are integrated in the formulation of the traction-separation law. The separation law describes the behaviour of the cohesive zone. Figure 2.1 shows examples of these traction-separation laws. A maximum strength is defined as σ_u and final separation occurs at a displacement δ_c. The fracture toughness is given by the area under the traction-separation law.

A distinction is made between two different families of cohesive models [13, 38]. An initial

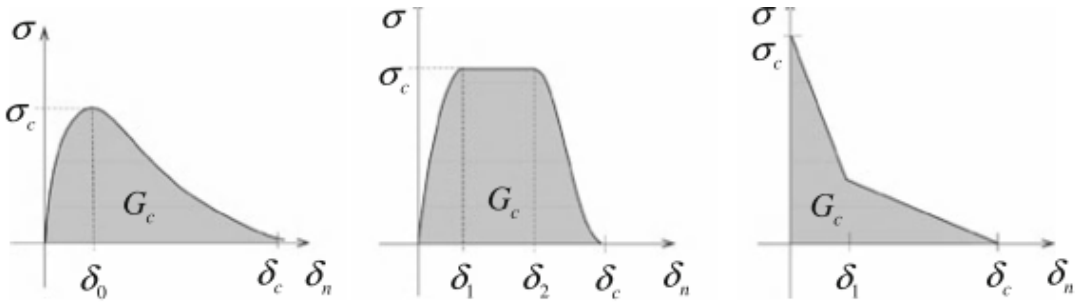

Figure 2.1: Overview of typical traction-separation laws [1]

rigid law, as illustrated by the third cohesive law in Figure 2.1 and laws with an initially elastic slope, as illustrated by the first two laws of Figure 2.1. These laws are also referred to as extrinsic and intrinsic respectively.

Intrinsic laws feature an initial increasing elastic traction up to the ultimate strengths. This increase is typically linear elastic thereby simpler than shown in Figure 2.1. Extrinsic traction-separation laws add cohesive elements to the model only as soon as the ultimate strength σ_u is reached. For both types, after the peak stress a softening function follows. In this softening part the properties are degraded using a softening function e.g. $f(\delta)$ until final separation at δ_c. The previously defined fracture toughness remains the standard for separation and follows from the softening part of the traction-separation curve via equation (2.4):

$$G_c = \int^{\delta_c} f(\delta) \mathrm{d}\delta \tag{2.4}$$

From the traction-separation laws the application of cohesive zone models requires the additional variables of an ultimate strength and the form of the cohesive law as illustrated by Figure 2.1. Although at first similar to the classical fracture criteria based solely on the SERR, the addition of these parameters can be seen as a clear downside of CZM. Moreover, even though the fracture toughness still defines fracture it is used in a distinctly different manner.

Both intrinsic laws and extrinsic laws have practical advantages and disadvantages. For extrinsic laws the interface elements are added as soon as fracture occurs which requires additional mesh updating as the crack progresses. Intrinsic laws do not have this problem but typically face one of either two other issues: (1) the slope (before fracture) of the cohesive law artificially changes the structural stiffness and is moreover strongly dependent on the mesh. This can be alleviated by using high stiffness cohesive elements, but this faces the issue (2) of an 'ill-conditioned stiffness matrix' [13, p.543]. Although cohesive elements can in principle be placed in between any regular FEM element, these issues prevent that in practice. Therefore, if intrinsic laws are used, this is only done for problems where there is a clearly defined fractured plane that is known a priori. For the composites this limits its application to delaminations [39].

2.3.2 Softening laws

The defining aspect of the traction-separation law is the softening part present in both the extrinsic and intrinsic formulations. The type of softening law applicable is a material property an must be determined using experimental tests. Linear softening laws are commonly applied [40, 41], most likely because of its simple form, as argumentation on the form of the softening law is not provided. There is however a wide range of other softening laws available [41]. More advanced softening laws will moreover require additional testing to determine the exact shape of the law, this testing is however not trivial. Linear softening behaviour may be easily defined but its physical meaning may not be really present and it additionally introduces a fixed coupling between the ultimate stress, failure displacement and fracture energy.

2.3.3 The cohesive interface

Numerically CZM is implemented by placement of special cohesive elements in between the regular FEM elements. The properties of these elements follow from the traction-separation laws, possibly combined for multiple modes, as subsequently discussed in Section 2.3.4. The cohesive elements themselves have in principle initially a zero thickness [40] Their function is merely to connect the interface using the traction-separation laws. In practice the interface is sometimes modelled using a very small thickness and properties of the interface [42]. The exact practice on how the interface is modelled is often not described and appears to be done pragmatically to deal with stability issues of CZM [43]. This again also relates to the use of intrinsic and extrinsic formulation of the cohesive zone.

It is noted that the directions a crack can follow is for CZM directly provided by the numerical implementation of the cohesive laws at the modelled interfaces. This clearly presents itself as one of the main advantages of CZM as the crack path does not need to be known beforehand, and no pre-crack is required as opposed to e.g. the commonly applied VCCT. This does require the addition of cohesive elements at the interface, which for cracks other than delaminations, may introduce a mesh dependency. Still, the generally less strict requirements on a mesh in that sense may be seen as an additional advantage of CZM. Moreover, FEM implementations of cohesive zones benefit from slightly random meshes [38], with a slight randomness increasing the convergence rate, thereby slightly lowering the mesh requirements.

In practice CZM is typically only used for the modelling of delaminations as noted previously. For delaminations not only the strong mesh dependency disappears, but the interface together with its properties can be relatively clearly defined by the matrix material in the resin rich layer. The practical aspects of mesh dependency for matrix cracks is solved by using XFEM in which CZM can still be applied as is further discussed in Section 2.4.

2.3.4 The cohesive element and combined loading

Incorporation of the previously discussed traction-separation laws at the interface requires a special class of cohesive elements. Rather than special CTEs, replacing the original elements for VCCT, CZM relies on the insertion of cohesive interface elements. The traction-separation laws of Section 5.1 dictate a direct coupling between the displacements and tractions.

Formulation for the cohesive element exists in both the continuum and discrete form. The latter of these is the most commonly applied and is derived using the potential energy and the combined multi mode traction-separation laws [44]. The cohesive element in its continuum form has the same topology as the surrounding, non-cohesive elements at the interface. An example complete formulation of the continuum form can be found at [44] or [45] for the discrete version.

The original formulation for the traction-separation law refers to cracks in mode I. Extensions have however been made to also include the effects of the other crack modes. In the most basic version this simply refers to the separate traction-separation laws for the different modes. They are however often also combined to allow for mixed mode behaviour. For practical purposes in such cases the traction-separation law is usually kept simple, typically with a linear softening functions. Implementation of CZM accounting for the other crack modes is provided by [40], [41] and [38]. In all these mixed mode cases an equivalent traction-separation law of a similar format is defined for the shear loadings. An intrinsic formulation is used, using all bi-linear traction-separation laws (i.e. initially linear elastic behaviour, and linear softening). Use is made of an effective separation combining all the displacements of the individual mode components. In any case the concept of mixed mode fracture criteria as given by e.g. the power law or BK criterion remain applicable. This is incorporated in the traction-separation law. As shear modes need to be combined any possible distinguishing between mode II and III shear cracks is now lost. Although typically used with linear softening laws, it has also been applied more recently in conjunction with a more advanced softening law [13].

2.4 Extended Finite Element Method

The regular finite element method is subject to a strong mesh dependency if cracks are involved. This applies specifically when special CTE elements are used to model the crack tip. To overcome these problems of a strong mesh dependency in 1999 the Extended Finite Element Method (XFEM) method was developed by Belytschko and Black [46]. If fracture is considered this allows for two important functions: The (1) possibility for mesh independent fracture planes and (2) the inclusion of singular expressions. The former of these allows cracks to follow any path and fracture planes therefore no longer have to be aligned with the mesh. This is especially useful if the fracture plane is not known a priori such as is the case for matrix cracks. The latter function prevents the use of special CTE to model the singular expressions at the crack tip. In a regular FEM formulation the displacement field is written as the sum of (continuous) basis functions. In the XFEM formulation these displacement fields are appended by a series discontinuous displacement functions and heavyside functions in a process known as enrichment. These discontinuous displacement functions allow for the inclusion of singular expressions and arbitrary fracture planes [47].

The relevance of XFEM to VCCT follows directly from its formulation. The classic VCCT formulation is no longer applicable and XFEM replaces VCCT. The solution is however based on similar principles from a LEFM point of view. XFEM alleviates the main disadvantages of the VCCT method which can be found in the strong mesh dependency. However the principle as to how to model the progression of cracks also disappears. Crucial descriptions

required for modelling the progression of a crack do not exist and XFEM is therefore more commonly applied in conjunction with CZM. As opposed to VCCT, XFEM and CZM append each other and are often used in conjunction with each other [13, 48]. This makes XFEM extremely relevant to CZM. In this aspect typically only the mesh-independent fracture planes are used. Cohesive zones are added in an extrinsic formulation after fracture occurs to model the progression of cracks.

The previous discussion on XFEM is extremely short and serves, similar to the models in the framework of LEFM and CZM, merely to highlight the most important aspects. No further details are provided at this point as the applicability of XFEM within this thesis is largely driven by the implementation provided in Abaqus, which is limited in its application e.g by excluding the singular expressions in progressive cracks [49].

2.5 Comparison and selection of methods

From the aforementioned discussion VCCT and CZM are presented as the most commonly applied methods for the modelling of cracks. Therefore this section will provide a direct comparison between both methods. For CZM an extension with XFEM is considered as well. Any other numerical method in the framework of LEFM such at VCE is not considered. The methods are compared on five different aspects:

- Type of failure modes;
- Mesh requirements;
- Accuracy;
- Historic implementations;
- Blending with stress-strain based methods.

The latter of these aspects combines the conclusion of former aspects and ultimately presents the choice for a method.

2.5.1 Type of failure modes

Both VCCT and CZM have shown to be, for practical purposes, limited to the modelling of delaminations. In the case of VCCT, LEFM was found to inadequately incorporate the fibre-matrix relations in, for one, the order of the singularity [21]. This shortcoming may however be of lesser importance when compared to CZM.

For CZM different issues exist with regards to matrix cracks. As matrix cracks can occur in any plane the intrinsic formulation is clearly the easiest. However, the placement of cohesive zones in between all elements causes either an artificial change in stiffness and/or, in the case of a high initial stiffness in the fully reversible portion of the cohesive law, an ill conditioned stiffness matrix [13, p.543] and possible convergence issues. Therefore the intrinsic formulation typically deals only with delaminations as the planes over which cracking can occur are limited. The extrinsic formulation does not have this restriction, but does require significant

mesh updating as the crack progresses. Moreover for CZM its applicability for matrix cracks is arguable.

The more freely defined crack paths in a combined CZM and XFEM model do not have these problems in such an extent. Moreover the fracture planes are more realistic as they do not automatically align with the base mesh, leading to a more physical representation of the cracks. Arguably one of the better examples is the combined CZM and XFEM implementations presented in [13] in which the intrinsic approach is used for delaminations and the extrinsic approach, with XFEM, for matrix cracking.

2.5.2 Mesh requirements

Mesh requirements can serve, in the absence of quantitative data, as a great indicator for computational effort. Considering again solely delaminations both methods have clear disadvantages in this aspect. For VCCT these disadvantages are the most clear. Firstly, cracks need to be explicitly included. Secondly the crack path these cracks can follow is subsequently completely determined by the mesh. The optional use of special CTE at the crack tip introduces additional difficulty as the mesh needs to be updated as the crack progresses to follow the crack tip. CZM is only affected by the second of these aspects. The fracture planes are strongly dependent on the mesh but, for delaminations this is no issue. Moreover, as for cohesive zones failure and progression of damage is embedded in the cohesive element formulation, the mesh needs not to be updated as a crack progresses. This does however introduce additional Degrees of Freedom (DoF)s to the system by the addition of the cohesive interface elements increasing the computational effort. From the perspective of blending methods this is seen as favourable as conflicts between both methods are less likely. The optional addition of XFEM does not introduce strict new requirements on the meshes itself and does allow for the inclusion of matrix cracks.

2.5.3 Accuracy

Arguably the most important issue for all methods is the accuracy of the acquired solution. This was up to now not touched upon in detail. For the purpose of this subsection a restriction is made to delaminations only. It is evident that an absence of matrix cracking in some methods presents a drawback.

VCCT has been the classic method to describe cracks. Arguments for the use of CZM most frequently include the more simplistic FEM implementation in terms of mesh and the state of the crack tip which is argued to consist of a cohesive zone (applicable to e.g. composites). In such statements typically no direct links are made comparing both methods in terms of accuracy.

A comparison for an implementation of both VCCT and CZM is presented in [50] using also experimental data of a DCB experiments. The results presented can be distinguished in two separate sections. The portion up to delamination growth, and the portion after delamination growth. In the former portion VCCT presents itself as superior having an almost exact fit with the experimental data. CZM present itself worse with somewhat significant deviations in this first, no crack growth, portion. This is however dominated by the length of the

inserted pre-crack. In the portion during delamination growth both VCCT and CZM present themselves equally good or bad. Similar studies [51, 52] for CZM with DCB experiments do not show a lack of accuracy, but do mention the requirement of a very fine mesh.

All these results do work with a clearly defined pre-crack to allow for fair comparison of results. This does however not guarantee anything about the accuracy if no pre-crack is inserted. This is an important note as VCCT, as opposed to CZM, requires a pre-crack and the research objective focusses around a high fidelity numerical tool.

2.5.4 Applications

Historic applications for a complete PDA framework are limited to CZM only. For VCCT no applications were found in which multiple types of damaged were combined. For simpler applications such as DCB and ENF test many references are available, but these do not provide a general framework. For CZM implementations are available but the total amount is still limited.

Vinay [15] combines a cohesive zone model for delamination with an intralaminar stress-strain based failure criteria (Hashin) for $[\pm 45/0_2]_{3s}$ laminates. An intrinsic formulation is used in which the cohesive elements are placed at regions with a high chance of forming delaminations. A discrete version of CZM is used in which the interface is modelled using springs. Mixed mode behaviour is modelled using effective tractions. As an additional parameter, the damage is not solely described by a single damage variable with traction-separation laws, but an additional damage variable is introduced to account for brittle failure, relevant if the specimen is loaded multiple times. The results appear to match experimental test results very well. The verification is however done using just a single experimental test set and more verification would be required to properly judge these results. Moreover the interaction between different failure modes make it difficult to properly judge the performance of CZM is this study.

A more extensive series of PDA was performed by Pinho [53]. Intralaminar failure was again considered as well as multiple stress-strain based failure theories. CZM was used to model the interlaminar delaminations. Using the intrinsic formulation a series of DCB and ENF tests was performed showing excellent agreement with experimental results. The validity hereof should however always be considered with some scepticism as the properties of the FEM model are often directly coupled to the experimental data.

Models which also combined XFEM for matrix cracking are presented by Van der Meer [14, 54] whom provides a complete numerical description and shows very promising results. This is currently among the best available reference works. More recently work presented by Viguaras [13] implemented a similar model with CZM for delaminations and CZM+XFEM for matrix cracking which also showed very promising results when compared to X-ray Computerized Tomography (CT) scans. The major criticism would be the size of the associated models, which could result in large solver times outside the parallel processing framework in which Vigueras works

2.5.5 Blending with stress-strain based methods

Arguably the most important aspect in the selection of methods for this thesis is their suitability in a blended framework for PDA. It is this aspect that sets both methods apart. For blending of stress-strain and fracture mechanics based methods all of the four previously discussed aspects are important to consider because they can either alleviate problems or create separate problems. Moreover their extendibility to a blended framework should be considered.

In terms of the failure modes VCCT and CZM can cover, the latter presents itself as superior. Even though both VCCT and CZM are mainly used for the modelling of delaminations, CZM is still seen as more versatile for two of reasons:

- CZM allows for multiple cracks to join.
- CZM does not exclude the possibility to model matrix cracks.

The option for multiple cracks to join, can be seen as an important aspect in the development a high fidelity numerical PDA tool. Specifically since the location of damage is in principle not known beforehand, hence such a tool, the usability would be greatly reduced. This can be seen as one of the main reasons not to use VCCT. It is therefore not seen as surprising that in Section 2.5.4 no full PDA implementations were found using VCCT. The option to model matrix cracks with CZM, specifically when combined with XFEM, is an additional asset for the cohesive model. Although delaminations are generally more important, the exclusion of failure modes and possible interactions is not seen as favourable for development of high fidelity PDA tool. This specifically holds if interactions drive final failure.

In the context of mesh requirements CZM clearly outperforms VCCT as well. The continuous updating of meshes in VCCT is in any case unfavourable. Moreover stress states can not directly be compared as the crack progresses, as there will be no direct correspondence between elements in different time increments if special CTE are used, with local mesh refinement around the crack tip. For CZM in an extrinsic formulation meshes are updated by the insertion of cohesive elements. The original elements are however always kept intact and CZM as such does not pose this issue. Most importantly however in the context of a blended stress-strain and fracture mechanics PDA method is the uncoupling of cohesive elements from the regular elements in terms of formulation. This poses the following advantages for CZM:

- No requirements on the adjacent, regular, mesh;
- Failure is defined in the cohesive element formulation.

With no requirements on the adjacent mesh any element formulation can be used. This guarantees compatibility with other stress-strain CDM PDA methods. Moreover as failure is completely defined in the formulation of the cohesive element and no information is required about the surrounding elements. VCCT does not have this advantage, as it would require knowledge of nodes adjacent to the fracture front in order to model the progression of a crack. It is however again noted that these advantages come at the cost of typically more refined meshes as compared to VCCT.

Finally the aspect of accuracy is considered. For modelling of simple delaminations no clear method can be described as preferable as comparisons on the accuracy are inconclusive. In a

blended framework the previous aspects drive the choice for CZM. Key herein is to incorporate all possible failure modes and their interactions. In this aspect, as noted in the context of failure modes and mesh requirements in a blended framework, CZM outperforms VCCT. When neither method presents itself as superior for the modelling of delaminations it is these aspects that drive the choice towards CZM.

2.6 Conclusion

This chapter described two main methods to model progression of damage from a fracture mechanics perspective. VCCT in the framework of LEFM is well founded analytically, and may have a stronger physical basis. This physical basis however reduces as the process zone in front of the crack tip increases shifting favourability towards CZM.

Suitability in a blended framework is however primarily driven by aspects regarding practical implementation of the methods, in which CZM yields superior. This is not unexpected considering also that VCCT more accurately models the crack tip and is able to provide full mode separation of the crack modes. CZM consider fracture more from a meso mechanical perspective and is far more practical in implementation, but is e.g. unable to provide a distinguishing between mode II and III shear cracks.

Practical implementation of CZM, typically with simple traction-separation laws, further reduces physical basis for the model. Still, it is a big steps forward if the more traditional, stress-strain continuum damage based models, in which all fracture is smeared is considered as the precursor. In this aspect CZM, in conjunction with (XFEM), does provide a significant increase in realism of crack modelling. Therefore, considering its shortcomings a combination CZM for delaminations and CZM+XFEM for matrix cracks is seen as the optimal solution for this thesis.

3 | FEM Model Implementation

This chapter describes the basic PDA model used for all results presented in this report. The previous chapter motivated the choice for a combination of CZM for delaminations and XFEM with CZM for matrix cracks. This chapter provides a more detailed description on the implementation of these damage models. Moreover it includes the CDM based damage models as part of the blended framework, and the implementation of the framework that supports this. The basis of the model presented here was therefore to some extent already shown by Van Dongen [2] in the context of continuum damage models. This is retained in the fibre damage model presented in Section 3.2.3. Delaminations are a new addition, and for matrix failure only the Puck failure initiation criterion is retained.

This chapter is divided into two parts. A model overview is provided in Section 3.1 and outlines how the model is generated, integrated and where each failure and damage model is implemented. This section is rather extensive, providing a detailed description of functionality and where it is implemented. This relates closely to the framework within Abaqus. As issues discussed later on are related to the use of Abaqus, this description is detailed on where implementations are defined. This allows limitations of the framework to be more apparent and makes it possible to judge the generality of the presented model. This chapter should provide the reader all the required building blocks to recreate the model in Abaqus.

The first section does not provide details on the final damage models. Section 3.2 will discuss the numerical aspects of these damage models considering delaminations, matrix failure and fibre failure both in terms of damage initiation and damage progression. Whereas the first section relates to how the complete model is generated, this section relates solely to the damage models and their numerical aspects. This follows from the selection of CZM for delaminations, XFEM with CZM for matrix cracks as discussed in the previous chapter and a CDM for fibre failure from Van Dongen [2].

3.1 Model overview and framework

The implementation of the PDA model can be separated in two parts: (1) Pre-processing and model preparation and (2) a nested analysis part. An overview of this set-up is presented in Figure 3.1 and is discussed further in the subsequent subsections. Unlike the User Defined Material (UMAT) implementation from [2] for CDMs an integral approach is required already during part generation to coherently combine all elements of the model. Part of this implementation was already used in the work presented by Van Dongen [2] and has in the

meantime been improved and further extended. Key aspect herein is generality for arbitrarily shaped laminates.

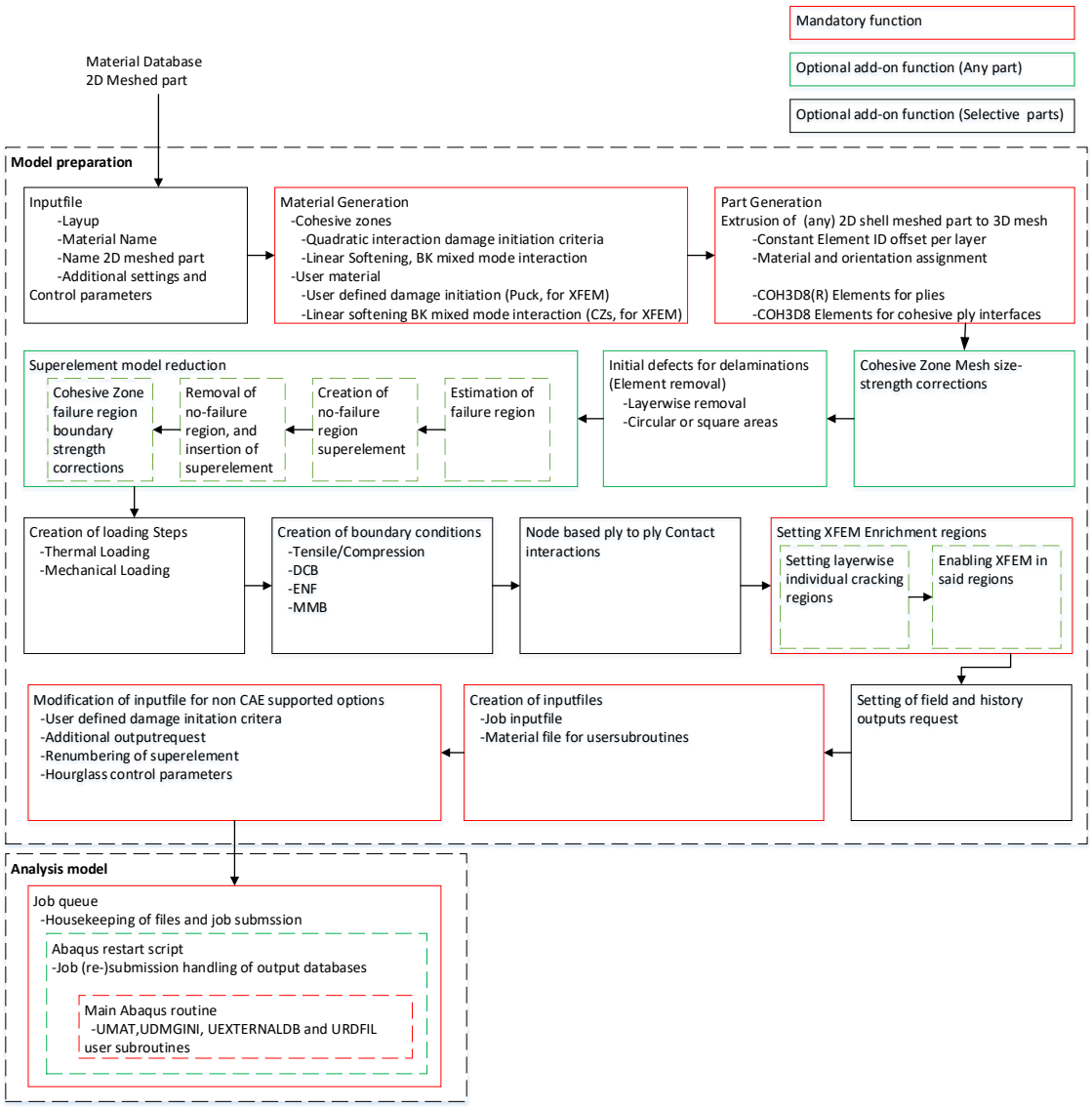

Figure 3.1: Flowchart of global model setup

Figure 3.1 distinguishes between three separate type of functions. Essential functions for working of the code are indicated in **red**. These functions are discussed in this chapter. Moreover a select number of **black** functions is included, which are model specific functions. Their implementation is not further detailed upon, other than their implication on the specific models as in Chapter 4. Finally a series of **green** add-on functions are included which are not part of the base model, but rather are improvements, which are also mostly bypassed in this chapter but are further detailed in Chapter 4. A more detailed overview as to where all these additional improvements are discussed is provided in Table 3.1.

All functions of Figure 3.1 are programmed in Python in partial conjunction with the Abaqus 6.14 scripting interface, apart from the Abaqus Subroutines in the analysis part which are written in Fortran.

Table 3.1: Overview of additional framework functions in thesis

Function	Location
Cohesive Zone mesh size corrections	Section 3.2.2 and 4.4.5
Initial Defects for delaminations	Not reported upon
Super Element Model Reduction	Section 4.4.7.3
XFEM Enrichment Regions	Section 3.1.1.3 and 4.5
Abaqus restart script	Section 4.4.1

3.1.1 Model preparation

The model preparation is an essential part of the PDA implementation. It defines the way the part is modelled and also creates a part that is compatible with the user subroutines of the FEM model. The way the part is built up is moreover an essential aspect in the constitutive behaviour of the laminate. This section covers the essential red blocks of Figure 3.1.

3.1.1.1 Material Generation

Material generation defines the materials and part of the failure related properties. Two basic materials are defined for each laminate. Default implementations are used if these suffice to not unnecessarily overcomplicate the model.

- A user material for the ply-constitutive behaviour
  - Defines fibre failure (Section 3.2.3)
  - Defines matrix failure (Section 3.2.2)
- A cohesive interface material
  - Defines delamination failure (Section 3.2.1)

For the user material the constitutive behaviour and the fibre failure are defined within a user subroutine. Initiation of the damage for matrix failure is also defined in a user subroutine as this provides some of the required control for XFEM, but damage evolution using cohesive zones is defined within the default material definition of Abaqus. For the delaminations, both initiation and damage evolution are defined within the material definition in Abaqus. Apart from the constitutive behaviour and damage models, orthotropic thermo-elastic behaviour is defined for all materials to allow the modelling of residual stresses appearing as the laminates cools down after curing. The damage models themselves are discussed in the next Section 3.2.

3.1.1.2 Part Generation

Part Generation is split into two main parts: part extrusion and element assignment:

Part Extrusion Part generation is based on either a pre-defined meshed 2D part or an automatically generated rectangular (open hole) 2D specimen. The nodal positions of this 2D part are copied to a 3D part, and extruded. Spacing is defined as function of the layer ply thickness and user defined cohesive zone thickness. Elements are placed layerwise, alternating elements assigned to the user material and cohesive material. No geometry is associated allowing the adjoinment of different element types and a user defined element numbering scheme:

- Each layer is defined with a element ID offset of 10000;
- Each element within this layer is defined a random ID within the local 10000 range.

The former allows each layer to be identified in the user subroutine. This offers distinct advantages in the modelling of a direct matrix failure-delamination coupling and for defining a layer-wise Crack Limiting Function (CLF). The latter point is again also an implementation required for a CLF. The random element numbering, which is apart from the 10000 offset, the same in each layer creates a random order in which failure is evaluated. This prevents clustering of matrix cracks for some CLFs as adjacent elements are now no longer likely to be processed in the same order within the Abaqus main routine. Both of these aspects are detailed upon further in Section 4.5.

Element Selection The basic model is built up using a combination of C3D8R and COH3D8 elements for the individual plies and cohesive interface respectively. This choice is not ideal but is driven by the limited compatible options that are possible within this model. A complete overview hereof is provided in Table 3.2. A driving aspect herein was the compatibility with XFEM in Abaqus which is for now limited to C3D8, C3D4 and C3D10 elements together with their reduced integration (R) variants.

Using the default Abaqus implementation for cohesive zones limits the selection to linear hex and quadratic tet elements [49]. The sharp increase of number of nodes and associated DoFs (order of magnitude 5) for an implementation with quadratic tet elements makes this option infeasible from the perspective of computational effort. This may not be the ideal option considering the complete numerical framework, but is dictated by the limited support for enrichment in Abaqus. Were this limitation not applicable the preferred option would most likely be a combination of C3D15(R) and COH3D6 elements for the following reasons

- Better through thickness behaviour due to the quadratic element formulation
- Limited increase in total DoFs
- A single quadratic wedge attaches to four linear wedge elements
  - Finer mesh in the cohesive zones, which drives mesh size requirements
  - Rougher mesh in plies possible due to quadratic formulation
- Meshes can be more random improving convergence for cohesive zones and matrix crack initiation

Alternatively a combination with continuum shell elements (CS8 and CS6) may would yield similarly favourable results, specifically in the through thickness behaviour, if supported by the Abaqus XFEM implementation. The use of continuum shell elements would however have as additional downside that non-zero fracture angles for matrix failure, specifically relevant for compressive failure [55], could not be supported. Moreover the out-of-plane stresses are

Table 3.2: Overview of possible FEM element types and their cross compatability

	Advantages	Disadvantages
CS8 (CS.HEX)	Good through thickness approximation of stresses	No out of plane stresses, not compatible with XFEM
CS6 (CS.WEDGE)	Good through thickness approximation of stresses	No out of plane stresses, not compatible with XFEM
C3D8(R) (L.HEX)	Simple interface with adjacent elements	Bad through thickness approximation of stresses
C3D6(R) (L.WEDGE)	Simple interface with adjacent elements	Overly stiff, not compatible with XFEM
C3D4(R) (L.TET)	None	Overly stiff, significant increase in DoFs
C3D20(R) (Q.HEX)	Good through thickness approximation of stresses	Bad interface to continuum cohesive zones, not compatible with XFEM
C3D15(R) (Q.WEDGE)	Good through thickness approximation of stresses	Not compatible with XFEM
C3D10(R) (Q.TET)	Good through thickness approximation of stresses	Very significant increase in DoFs, overly complex
SPRINGA (Disc.CZ)	Compatible with all interfaces, simple	No coupling to adjacent plies possible. Requires user defined constitutive behaviour
COH3D8 (Cont.CZ)	Can interface with C3D8(R) elements, Coupling to adjacent plies possible	Default Abaqus implementation available
COH3D6 (Cont.CZ)	Can interface with C3D6(R), C3D4(R), C3D15(R), C3D10(R) elements, Coupling adjacent plies possible for C3D6(R) and C3D15(R) elements	Default Abaqus implementation available, No coupling to adjacent plies possible for C3D4(R) and C3D10(R) elements

not adequately modelled.

For the cohesive zones a continuum approach is chosen over a discrete implementation. The former is primarily chosen as it is already implemented and verified in Abaqus. However, discrete cohesive zones may offer distinct advantages over continuum cohesive zones [45], specifically if convergence or computational effort is an issue.

For all the 3D solid elements a differentiation can be made between full and reduced integration elements, indicated by the (R). Previous implementation of the CDM by Van Dongen [2], or in generic CDMs, the use of full integration elements is favoured. CDMs are able to slightly more accurately predict the stresses within the elements. More importantly however, the additional number of integration points/ material points allows for a more gradual decrease in properties, at each integration point independently rather than solely at the elements centroid, preventing the requirement of very fine meshes for CDMs. This behaviour comes however at a cost. The full integration hex elements are roughly 8 times more costly to evaluate as compared to their reduced integration counterpart. Moreover their linear variants are susceptible to locking problems [56]. This is especially true for composites if they are modelled with one element through the ply thickness.

Reduced integration elements do not feature these disadvantages, but do suffer from so called zero energy hourglass modes. This problem can however easily be controlled by the use of an hourglass stiffness. For an orthotropic material, this stiffness can be based on the average shear stiffness, i.e. Equation (3.1):

$$G = \frac{G_{12} + G_{23} + G_{31}}{3} \tag{3.1}$$

The use of a more discrete modelling approach using XFEM, in which matrix cracks are no longer modelled using a CDM justifies the switch towards reduced integration elements. The additional integration points are no longer required for a more gradual degradation of properties as this is now taken into account by inserted cohesive zones (see also Section 3.2.2). Moreover the hourglass stiffness based on equation (3.1) is not updated as properties are degraded, increasing the relative stiffness introduced by hourglass control as damage progresses. With discrete XFEM cracks this is no longer an issue. Finally, matrix cracking does not benefit from additional integration points as XFEM in Abaqus averages for damage initiation over all the integration points [49]. For fibre failure a CDM framework is still used, but the impact hereof is smaller and poses no problem as is also confirmed in Chapter 4. Moreover fibre failure is more localized, which would possibly allow for selective full integration if deemed necessary.

An experimental comparison between full and reduced integration elements is provided in Section 4.4.7, considering both the aspects of computational efficiency and accuracy.

3.1.1.3 Setting XFEM enrichment regions

This functionality defines the enrichment regions for XFEM in Abaqus. It also provides one of the main distinctions between the single and multiple crack model which was already mentioned in the outline of the introduction and is further detailed in the next chapter. The

(green) additional functionality of Figure 3 is discussed in the context of the multiple crack model of Section 4.5. The basic functionality which applies for both models is highlighted here.

Enrichment regions refer to sets of elements in which XFEM is enabled. Elements are therefore required to be in an enriched region to allow for matrix cracks to occur. The process of enrichment refers to the additional types of shape functions that will be possible within these elements. This functional block enables enrichment for all ply elements.

Within Abaqus XFEM is implemented using the phantom node method with limitations. Practical limitations were already partly discussed in context of the elements which can use this functionality and further practical limitations are discussed in detail in the next chapter. Numerical limitations within Abaqus are the following [49]:

- No singular functions possible for progressive cracks;
- Progressive cracks always cover a full element (element-face to element-face).

Both these limitations strongly reduce the physical basis XFEM can provide, but are still of minor importance in relation to more apparent physical limitations also discussed in the previous chapter.

3.1.1.4 Input file generation

The function writes the main analysis input file and an analysis material file. A separate material, with different strengths, is written to the file corresponding to each layer of the laminate and its corresponding material name. This takes into account the adjusted strengths that may be required per ply to take the in-situ effects into account as discussed in Section 3.2.2.

3.1.1.5 Input file modification

A series of options which are not by default supported in the Abaqus CAE, are added in this step by new entries or modifying existing entries. Some of these entries are related to functionality discussed in Chapter 4, such as additional .fil and .dat output files and renumbering. The input file modifications themselves are not further detailed on.

3.1.2 Analysis Model

The analysis model is, different from the sequential part generation, embedded in a nested loop. In this block the actual analyses are performed. Four aspects can be considered herein, nested in the order as shown in Figure 3.1 or as follows:

1. Job Queue: Submission of multiple jobs either locally or to cluster machines, house keeping of the analysis files and support files
   - Abaqus model input file
   - Material File
   - Super Element Files (see Section 4.4.7.3)

    - Abaqus Restart script
    - Abaqus Exit script
2. Abaqus Restart script: Restarting Jobs after matrix crack completion
3. Main Abaqus routine with user subroutines:
    - UMAT
    - User Damage Imitation (UDMGINI)
    - User Read File (URDFIL)
    - User External Database (UEXTERNALDB)
4. Abaqus Exit script: Termination control of analysis based on observed load drops.

The Job Queue (1) functions merely as external shell to ease the process of job submission, especially for jobs to the cluster, by automatically copying and renaming all the required files. Its function is a non essential one, but it nests the other functions.

The Abaqus restart script (2) is an essential aspect of the PDA model. It deals with specific crashes found when using Abaqus in conjunction with XFEM. It makes small changes to the model resubmits restart jobs after these crashes occur. It is an essential part in modelling the behaviour up to and especially past the failure load. The script also combines the restart job Output DataBase (ODB) with the original ODB of the model. The use of the restart script is further discussed in Section 4.4.1.

The main Abaqus routine (3) is appended with user defined subroutines. The UMAT user subroutine is used to model the ply constitutive behaviour and fibre failure. It is further discussed in the context of CDMs by Van Dongen [2]. A UDMGINI user subroutine is used to define and control the initiation of matrix cracks in XFEM. The URDFIL subroutine is used to load the cohesive interface degradation factors for delaminations, to make them accessible for Matrix Failure-Delamination coupling in the UDMGINI subroutine. Finally, the UEXTERNALDB subroutine is used to clear and set common variables at the start of new increments. Moreover it calls the external Abaqus Exit script for possible termination of the analysis. The interaction of these subroutines is discussed in relation to Figure 3.2

The Abaqus Exit Script (4) is a final optional Python script which allows to terminate the analysis by more advanced termination criteria such as a 5% load drop. Termination is controlled by non-zero return codes and is discussed further in Section 4.4.7.

The main Abaqus routine (3) consists of four main routines nested as in Figure 3.2. Herein a simplified version of the UMAT subroutine is shown, using only the fibre failure model and constitutive modelling. Compatibility with the CDMs of [2] still exists, and is incorporated in this routine as well, but is not explicitly shown.

3.2 Damage Models

This section discusses the individual damage models. Only the numerical aspects of the damage models are discussed. The support for these damage models follows primarily from the previous chapter, the CDM implementation by Van Dongen, or is discussed separately if not yet supported. The numerical implementations of the damage models, together with the previously discussed framework, is what defines the complete PDA model. Similarly to

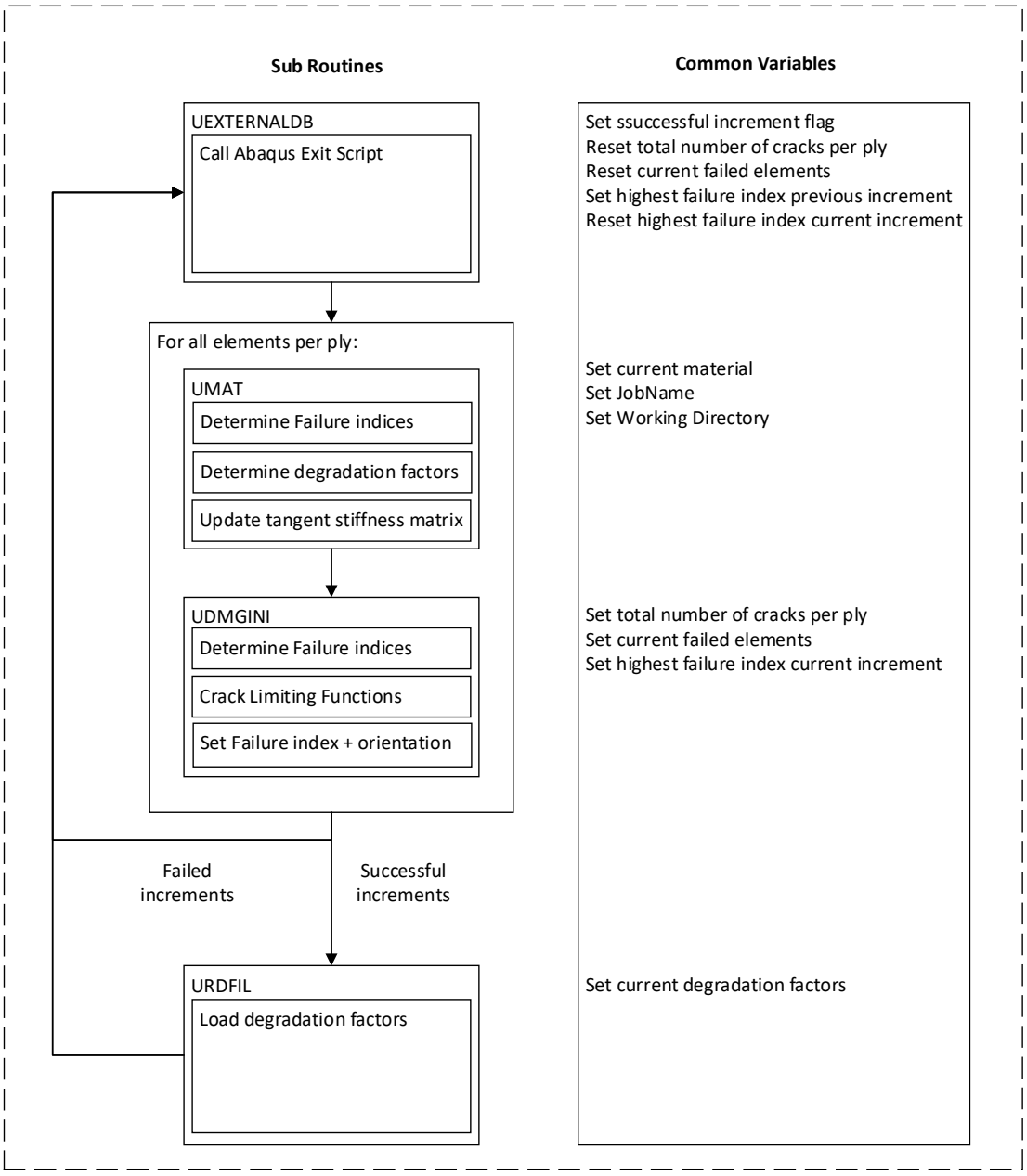

Figure 3.2: Flowchart of main Abaqus routine

the framework, a description of each model is provided to allow for discussion of issues and limitations later on.

For an overview as to where these damage models are implemented in the complete framework reference is made to Table 3.3.

Table 3.3: Implementation location of the different failure mechanisms

	Initiation	Evolution
Fibre Failure	Analysis model (UMAT User Subroutine)	Analysis model (UMAT User Subroutine)
Matrix Failure	Analysis model (UDMGINI User Subroutine)	Model preparation/Main Routine
Delaminations	Model preparation/Main Routine	Model preparation/Main Routine

3.2.1 Delamination failure - CZs

Delamination failure is modelled with an intrinsic cohesive zone model, with cohesive elements inserted between all plies. Initiation of delaminations is determined by a quadratic criterion as in equation (3.2). Most delamination criterion, such as in [57–59] are based on such a form of interaction. Consideration of such a form is however not supported by a (strong) physical basis.

$$\frac{\sigma}{\sigma_c} + \frac{\tau_1}{\tau_c} + \frac{\tau_2}{\tau_c} \geq 1 \tag{3.2}$$

The softening part of the cohesive zone model is dictated by a linear softening law. Argumentation for this choice is twofold: implementation of such behaviour is simple, supported by the large amount of times such behaviour is implemented [13, 40, 41]. Moreover, there is no consistent argumentation to support different softening behaviour, and a material dependency is involved as well [41]. The strong lack of a physical basis for the cohesive zone model is seen as the main downside of using the cohesive zone model. This mostly relates to not knowing what all the relevant parameters are, as also highlighted in the previous chapter.

The mixed mode behaviour has similar lack of physical basis as the form of the softening law [27]. For the tested materials a BK-criterion [19] (equation (3.2.1)) was most applicable and was thus used.

$$\frac{G_I + G_{II} + G_{III}}{G_{Ic} + (G_{IIc} - G_{Ic})(\frac{G_{II}+G_{II}}{G_I+G_{II}+G_{III}})^\eta + (G_{IIIc} - G_{Ic})(\frac{G_{II}+G_{III}}{G_I+G_{II}+G_{III}})^\eta} \geq 1 \tag{3.3}$$

An in-plane stiffness value, belonging to the linear elastic part, prior to failure of the cohesive zone, is assigned based the nominal ply properties and is given by equation (3.4).

$$k = \alpha \frac{t_{cz}}{t_{ply}} E_3 \tag{3.4}$$

Unless otherwise specified the value for α is taken as 50, which is a commonly used value [60].

The dimensions of the cohesive zone are split in two parts. The thickness of the cohesive zone, and the in-plane dimensions. For the former any small number suffices, and the models presented in this report have used values in the order of 0.5% or less of the cohesive zone thickness. The constitutive behaviour of the cohesive zone is not taken into account, and thickness values are only assigned to prevent numerical issues. Any small value which no longer effects the global constitutive behaviour is therefore sufficient.

The in-plane dimensions are dictated by size constraints following from the Mode I behaviour. A threshold for the size of the cohesive zone is provided by a form of equation (3.5) with m ranging between 0.21 and 1 depending on the author [60].

$$l_{cz} = m\frac{EG_c}{\tau_c^2} \tag{3.5}$$

As these element sizes may be quite small a strength correction factor is required for successful application in rougher meshes [60, 61]. This was recognized at early stages of model verification and is therefore discussed here. A concept based on a minimal required “process zone" is used as was proposed by Turon et. al. [60]. The reduced inter-facial strength is given by equation (3.6):

$$\bar{\tau_c} = \sqrt{\frac{9\pi EG_c}{32N_{cz}l_{cz}}} \tag{3.6}$$

The effective strength is consequently given by equation (3.7):

$$\tau_c = max(\bar{\tau_c}, \tau_c) \tag{3.7}$$

Although this strength reduction has effectively been applied in practice in the subsequent chapters, it also highlights again the shortcomings of cohesive zone models. If the cohesive zone model is argued to represent a true physical process than this argumentation cannot be maintained. Such strength based corrections can never guarantee that the cohesive behaviour is a consistent model as both the failure strength, fracture toughness, failure displacement and softening behaviour are coupled and one of these can not be changed independent of the other parameters.

Verification of the delamination model was done on a set of DCB, ENF and MMB specimens but is not further discussed, with this thesis focussing on the complete PDA implementation.

3.2.2 Matrix failure - XFEM

Matrix failure is initiated using the Puck Failure criterion [55] which performed relatively favourably compared to other failure theories, as e.g. shown in the recent World Wide Failure Exercise (WWFE) [12, 62], and was selected from the precursor thesis focusing on stress-strain based models [2]. The Puck failure criterion is based on the Mohr-Coulomb theory [63] and differentiates between different types of matrix failure. Moreover a fracture angle is

explicitly found and used. The non-zero fracture angle for compressive fracture, enabling the strong matrix failure-delamination interaction, can in such a way be incorporated as well by using this non-zero fracture angle and a contact interaction between the fractured surfaces. Although fully incorporated, this will not be further discussed as a restriction was made to tensile loading. The underlying equations of the Puck failure theory are shortly summarized below in equation (3.8) to (3.19).

For a tensile crack loading, $\sigma_n > 0$ failure is determined by equation (3.8).

$$\sqrt{\left[(\frac{1}{R_{\perp}^{(+)A}} - \frac{p_{\perp\psi}^{(+)}}{R_{\perp\psi}^{A}})\sigma_n(\theta)\right]^2 + \left(\frac{\tau_{nt}(\theta)}{R_{\perp\perp}^{A}}\right)^2 + \left(\frac{\tau_{nl}(\theta)}{R_{\perp\parallel}^{A}}\right)^2} + \frac{p_{\perp\psi}^{(+)}}{R_{\perp\psi}^{A}}\sigma_n(\theta) \geq 1 \tag{3.8}$$

Or, for compressive crack loading, $\sigma_n < 0$ failure is determined by equation (3.9).

$$\sqrt{\left(\frac{\tau_{nt}(\theta)}{R_{\perp\perp}^{A}}\right)^2 + \left(\frac{\tau_{nl}(\theta)}{R_{\perp\parallel}^{A}}\right)^2 + \left[\frac{p_{\perp\psi}^{(-)}}{R_{\perp\psi}^{A}}\sigma_n(\theta)\right]^2} + \frac{p_{\perp\psi}^{(-)}}{R_{\perp\psi}^{A}}\sigma_n(\theta) \geq 1 \tag{3.9}$$

In either case the values for $\sigma_n, \tau_{nt}, \tau_{nl}$, the normal and shear forces on the crack surface, are given by equations (3.10) to (3.12).

$$\sigma_n(\theta) = \sigma_2 \cos^2(\theta) + \sigma_3 \sin^2(\theta) + 2\tau_{23}(\cos(\theta)\sin(\theta)) \tag{3.10}$$

$$\tau_{nt}(\theta) = (\sigma_3 - \sigma_2)\cos(glssym : theta)\sin(\theta) + \tau_{23}(\cos^2(\theta) - \sin^2(\theta)) \tag{3.11}$$

$$\tau_{nl}(\theta) = \tau_{31}\sin\theta + \tau_{21}\cos\theta \tag{3.12}$$

The actual initiation of failure is determined by the fracture angle at which the inequality is first satisfied. This is a function of the fracture angle θ and no closed form solution exists, but rather this angle has to be found implicitly. The parameters ψ is also implicitly dependent on this angle and is given by equation (3.13) and (3.13).

$$\cos^2(\psi) = \frac{\tau_{nt}^2}{\tau_{nt}^2 + \tau_{nl}^2} \tag{3.13}$$

$$\sin^2(\psi) = \frac{\tau_{nl}^2}{\tau_{nt}^2 + \tau_{nl}^2} \tag{3.14}$$

Furthermore, the following ratios as per equation (3.15) and (3.16) are defined.

$$\frac{p_{\perp\psi}^{(+)}}{R_{\perp\psi}^{A}} = \frac{p_{\perp\perp}^{(+)}}{R_{\perp\perp}^{A}}\cos^2(\psi) + \frac{p_{\perp\parallel}^{(+)}}{R_{\perp\parallel}^{A}}\sin^2(\psi) \tag{3.15}$$

$$\frac{p_{\perp\psi}^{(-)}}{R_{\perp\psi}^{A}} = \frac{p_{\perp\perp}^{(-)}}{R_{\perp\perp}^{A}}\cos^2(\psi) + \frac{p_{\perp\parallel}^{(-)}}{R_{\perp\parallel}^{A}}\sin^2(\psi) \tag{3.16}$$

This is finally related to the ply strengths Y_T, Y_C and S_{21} as per equations (3.17) to (3.19):

$$R_{\perp}^{(+)A} = Y_T \tag{3.17}$$

$$R_{\perp\parallel}^{A} = S_{21} \tag{3.18}$$

$$R_{\perp\perp}^{A} = \frac{Y_C}{2(1 + p_{\perp\perp}^{(-)})} \tag{3.19}$$

The post initiation softening behaviour is again controlled using cohesive zones, this time in an extrinsic formulation. Similarly to the cohesive zones for delaminations a linear softening law is used with the BK-Criterion. The same fracture toughness and BK-value is used as for delaminations unless otherwise specified. It is highly unlikely that the matrix fracture and delamination process differ merely in initiation strengths, as two different types of fracture processes take place at different types of interfaces. These assumptions should therefore be considered with some critical note, even without considering the real applicability of cohesive zones in general. There is however some support for at least the fracture toughness values to be of a similar order [64], with for a select set of relevant composite materials interply fracture toughness values ranging between 0.82 and 2.83 of the intraply value.

The strengths used in the modelling of matrix failure is important in both the initiation criterion (equations (3.17) to (3.19)) and the post-initiation softening behaviour, as the failure displacement is linearly related to the failure strength for constant fracture toughness and linear softening behaviour. The failure displacement is important to consider as well, as this can prevent the triggering of inter-facial delaminations.

The concept of in-situ strengths is a recognized phenomena [65, 66] for composite laminates. The embedding of plies locally constraints the materials, hindering the initiation of matrix cracks, thereby increasing the strengths and decreasing the susceptibility to matrix cracking. The magnitude hereof depending on ply thickness, whether plies are fully embedded and the stacking sequence or existence of ply-blocks among others.

The concept of in-situ strengths is an important aspect both for predicting the correct failure patterns and rate of damage progression as will be further discussed in Chapter 4. A model proposed by Camanho [65] et al. was used to estimate these parameters.

The in-situ strengths are computed from fracture mechanical analysis of embedded cracks, distinguishing between three different cases: Thin outside plies, thin embedded plies and thick embedded plies. Similarly to the Puck initiation criterion the equations defining this model are shown for completeness.

The in-situ strength S_{is} is given for all three cases by the general equation (3.20) [65].

$$S_{is} = \sqrt{\frac{\sqrt{1 + \beta\Phi G_{12}^2} - 1}{3\beta G_{12}}} \tag{3.20}$$

The value for ϕ depends on the case at hand and is given by the relevant of equations (3.21) to (3.23) [65].

For a thin outer ply this is given by equation (3.21):

$$\Phi = \frac{24 G_{II}}{\pi t} \tag{3.21}$$

For a thin embedded ply by equation (3.22):

$$\Phi = \frac{48 G_{II}}{\pi t} \tag{3.22}$$

And thick embedded ply by equation (3.23):

$$\Phi = \frac{12 S_{12}^2}{G_{12}} + \frac{72}{4}\beta S_{12}^4 \tag{3.23}$$

For the strength Y_T the modified in-situ strength is given by equations (3.24) to (3.27) [65]. For a thin outer ply this is given by equation (3.24) [67] :

$$Y_{is} = 1.79\sqrt{\frac{G_I}{\pi t \Lambda_{22}^0}} \tag{3.24}$$

For a thin embedded ply by equation (3.25):

$$Y_{is} = \sqrt{\frac{8 G_I}{\pi t \Lambda_{22}^0}} \tag{3.25}$$

For which in both cases the parameter Λ_{22}^0 is function of the ply material properties and given by equation (3.26):

$$\Lambda_{22}^0 = 2\left(\frac{1}{E_2} - \frac{\nu_{21}}{E_2}\right) \tag{3.26}$$

For a thick embedded ply by equation (3.27):

$$Y_{is} = 1.12\sqrt{2} Y_T \tag{3.27}$$

In all cases the thickness value t relates to the effective ply thickness, taking the effect of ply blocks with similar orientation into account as a single thickness. For the case of a thick outer ply, no concept exists. It is however reasonable to assume that the in-situ strength will

not drop below the nominal ply strength values, used as input for equations (3.21) to (3.27). Therefore a lower limit is established based on these strengths. The necessity of this limit was confirmed in Chapter 4. A example of the complete in-situ strength behaviour is provided in Figure 3.3 for a IM7/8552 composite.

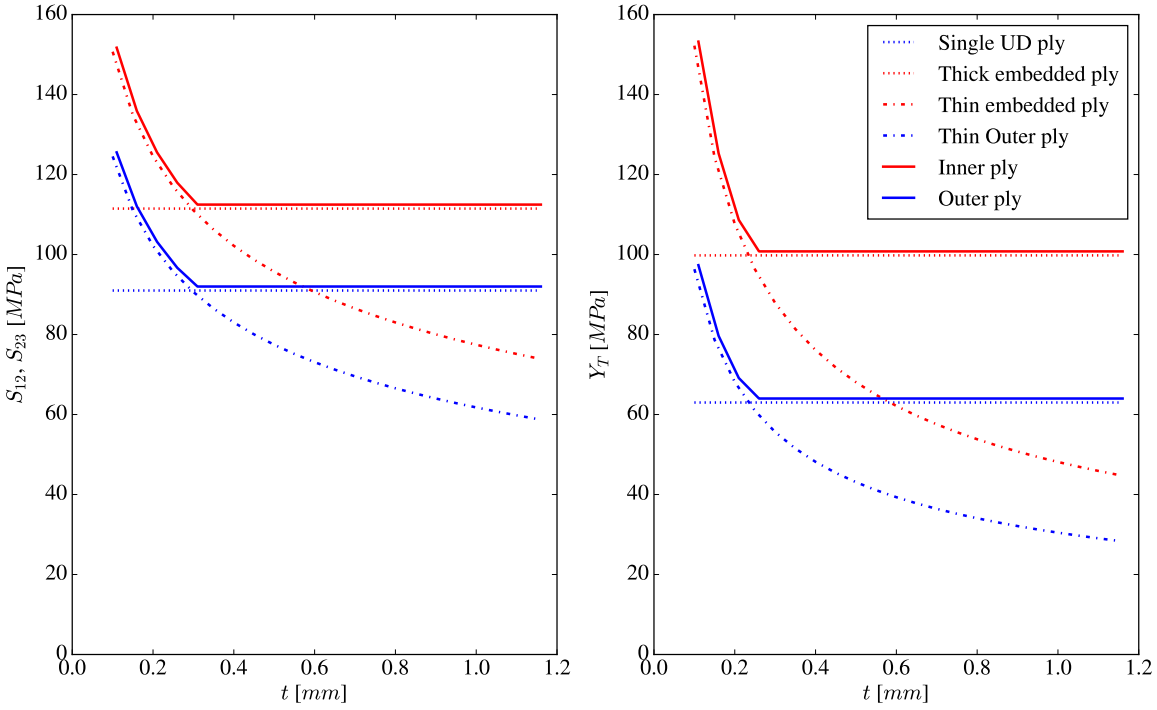

Figure 3.3: In-situ strength effects with varying ply thickness

A clear ambiguity remains when Figure 3.3 is considered in terms of strengths. The concept of in-situ strengths is defined for constrained plies. This is a state that is clearly defined for undamaged specimens, but is no longer clear as damage initiates and evolves. Specific reference is made to delaminations which causes a separation of the plies. Keeping aside the damage delaminations may do to the plies at the interface, the separation itself also causes a clear issue. For a complete delamination at either one or two of the interfaces, plies can no longer be considered as embedded. Rather they can at best be considered as an outer ply, or even as a single UD ply. In such a sense the strengths are also a function of the damage state in the laminate. This issue is partly considered in Section 4.5 in which a coupling to the degradation factor of the cohesive interface for delaminations is made.

In a more general sense it is considered highly unlikely that the model parameters remain the same as the strength changes. Notably the cohesive zones no longer behave the same as with equal fracture toughness either the failure displacement changes, or with an equal failure displacement, the fracture toughness would change as was previously also noted for delaminations. Keeping both the same would require a different softening behaviour. These effects and the applicability of cohesive zones are not further considered, but do highlight a shortcoming and clear lack of physical understanding. The cohesive zone model is implemented with these shortcomings accepted and traded for generality and computational efficiency. The switch to a discrete cohesive zone model would not require this strength

correction and may therefore be favoured. It does however require a user defined element and was left outside the scope of this thesis as the modelling of delaminations is not the driving issue.

3.2.3 Fibre Failure - CDM

The fibre failure model follows from the previous implementations by Van Dongen [2]. A cross compatibility with all the CDM models implemented here is maintained. This allows fibre failure to be modelled by either the Puck [55], Cuntze [68] or LaRC05 [69] criterion. For the results presented in this report only the LaRC05 initiation criterion has been used following from the CDM results presented by Van Dongen [2]. As a restriction was made in this research to focus on tensile load cases, the compressive failure criteria and their implementation is left out. Details on this implementation can be found in [2]. The fibre failure criteria here is stated merely for completeness, and is in the case of tensile loading no different than a simple maximum stress criteria for $\sigma_1 > 0$ as equation (3.28):

$$\frac{\sigma_1}{X_T} \geq 1 \tag{3.28}$$

Damage evolution is modelled using a linear softening function, much like the cohesive zone model, with a fracture energy defining the extend of the softening behaviour. Linear softening aids the convergence behaviour, and the model was found to work best for CDMs [2]. The physical meaning of this is however very arguable.

Selected properties are degraded to mimic the behaviour of the failing fibres. Properties are degraded as proposed by Matzenmiller et. al. [70], which in the case of merely tensile fibre failure is just a gradual reduction in the stiffness E_1. For more details on the specifics of the implementation of fibre failure reference is again made to [2] or the original implementations [71].

It is highlighted that CDMs lack a true physical representation of damage as was also previously highlighted by Van Dongen [2]. Besides the possibly excessive smearing of damage, relatively large residual stiffness's may exist past final failure to aid convergence.

3.3 Conclusions

The framework built around the commercial FEM software Abaqus was discussed in this chapter, together with the damage models for delamination, matrix failure and fibre failure.

The established framework provides generality for arbitrary laminates and a desired level of expandability. However, it is strongly built around the part generation requiring a large number of naming and modelling conventions for it to work, thereby reducing the general applicability. This applies specifically when compared to the CDM implementation [2] which required in the framework only the naming convention of materials. This cost is a significant driver for the more common use of CDMs which remain far easier to use. Still all of the

desired flexibility can be provided, with the exception of XFEM, which is almost completely controlled by the way it is implemented in Abaqus.

The damage models, and where they are implemented, is strongly nested in this framework. Cohesive zones for delaminations are fully controlled by the Abaqus implementation as all the required control can be provided. The first main issue with the current model for delaminations is the linear traction-separation behaviour for which no solid argumentation can be provided other than its simple numerical implementation. Moreover the strength correction, although shown to be required and verified for large element sizes, is dubious in relation to this simple traction separation behaviour.

Matrix cracks, using XFEM, are implemented in two parts. In Abaqus the progression is defined whereas the damage initiation, using the Puck failure criterion, is controlled in the UDMGINI user subroutine to allow for some control of the cracking behaviour. Other than this very limited control is possible. The main issue with the presented model is the lack of this control in the cracking behaviour. Similar to the delaminations main issues relate again the unsupported linear softening behaviour combined with, in this case, a uncertainty in the in-situ strengths.

Fibre failure is finally, under the limitation of tensile loading, defined with a simple maximum strength criteria with gradual softening behaviour. The more advanced Larc05 criteria for compressive failure is also implemented [2] but not relevant in the scope of this thesis. Prime possible issue for the failure model would be its residual stiffness, which is a essential element of CDMs, that can never truly represent the damage state of fully broken fibres.

4 | Model verification

This chapter discusses model verification using the Nixon-Pearson experimental investigation [3, 72] on damage patterns in CFRP OHT specimens. The laminates are based on a large set of sub-laminate and ply-level scaled laminates [5], with additional selective X-Ray CT scans [3] allowing to check not only the observed failure loads, but more importantly the corresponding failure patterns. Previously reported preliminary results for the model presented in this thesis have already been used as part of the parallel research effort [2].

This chapter first discusses the setup of the Nixon-Pearson verification case and the basic FEM implementation. Hereafter the shortcomings of a previously implemented preliminary model are discussed and final failure is defined in Section 4.3. Subsequently two main models are described in Section 4.4 and 4.5. The first of these sections evolves around the single crack model in which each ply is modelled with at most one matrix crack per side (two total). This model has a significant shortcoming with regards to the damage it can describe, as it is limiting the total amount of damage. An attempt to at least partially tackle this issue a new model is presented in Section 4.5 which describes the multiple crack model. It discusses solutions to overcome these problems for as much as is possible within the framework with Abaqus and presents a limited set of new results. Finally Section 4.6 discuses the most important conclusions for both models.

4.1 Test set-up description

The laminates in the Nixon-Pearson case are made of IM7/8552 composite prepreg with a nominal ply thickness of $0.125[mm]$. The layup differs between the sub-laminate scaled and ply-level scaled laminates, but in all cases consist of combination of $[45/90/-45/0]$ plies. For the sub-laminate specimens a $[45/0/-45/90]_{ns}$ layup is used. For the ply-level scaled specimens a $[45_n/90_n/-45_n/0_n]_s$ layup is considered. Focus is put on the ply-level scaled specimens, as these feature the widest variation as to how and when final failure occurs. Laminates with $n = 1$ are fibre failure dominated, whereas for $n > 1$ the ply blocking of similar ply orientations causes larger inter-facial stiffness differences yielding more delamination dominated failure mechanisms. An overview of the material properties used is provided in Table 4.1.

The properties as shown in Table 4.1 are the properties as taken directly from literature. Corrections for mesh size or the in-situ effects are not yet taken into account and the tabulated properties are used as raw input.

Table 4.1: Material properties Nixon-Pearson verification tests [4–6]

.

E_1	171.42	GPa	X_T	2323.5	MPa
ν_{12}, ν_{13}	0.32	$-$	X_C	1200	MPa
G_{12}, G_{13}	5.29	GPa	Z_T	60.3	MPa
E_2, E_3	9.08	GPa	Z_C	185	MPa
ν_{23}	0.4	$-$	Y_T	60.3	MPa
G_{23}	3.249	GPa	Y_C	199.8	MPa
β	$3 \cdot 10^{-10}$	MPa^{-3}	S_{12}	92.3	MPa
CTE_1	0	mm/deg			
CTE_2, CTE_3	0.00003	mm/deg	$G_{FF}^{(+)}$	$81.5 \cdot 10^3$	J
			$G_{FF}^{(-)}$	$106.3 \cdot 10^3$	J
G_{IC}	200	J			
G_{IIC}, G_{IIIC}	1000	J	$p_{\perp\perp}^{(-)}$	0.225	$-$
σ_1	60	Mpa	$p_{\perp\perp}^{(+)}$	0.225	$-$
σ_2, σ_3	90	MPa	$p_{\parallel\perp}^{(-)}$	0.25	$-$
$BK\ Value$	4.71	$-$	$p_{\parallel\perp}^{(+)}$	0.3	$-$

4.2 FEM implementation

The model is created as outlined in Chapter 3. A description of the test set-up is provided in Figure 4.1. Only half the specimen is modelled, and no cohesive interface is considered at the symmetry plane. The specimen is first loaded in a thermal loading step, to take cooldown residual stresses into account, using a temperature difference of 160 degrees. Material shear non-linearity (β) is not taken into account for the constitutive behaviour as this can cause severe convergence issues at the cohesive interfaces and moreover may take some damage into account in multiple ways as is further discussed in Section 4.4.7.5. Material shear-non linearity is taken into account however for the computation of in-situ strengths. A strength reduction for the cohesive zones is applied using a process zone of 5 elements (see also Section 3.2.1).

A displacement controlled loading is applied using a dynamic implicit analysis (with quasi static application). Time incrementation is controlled automatically, with a maximum time step of 0.01 and a minimum time step of $1 \cdot 10^{-15}$.

The results of the FEM implementation are split into two sections. The single crack model of Section 4.4 and the multiple crack model of Section 4.5. The single crack model, presented first, models at most one crack per ply, per side. It is used as the main model for sensitivity studies and model validation. The model is however limited and cannot be extended in a more general framework. For this purpose the multiple crack model is presented, which does not have this limitation, but has more troublesome convergence. To introduce the necessity of both these models, results of a preliminary model are first shortly discussed in the subsequent section.

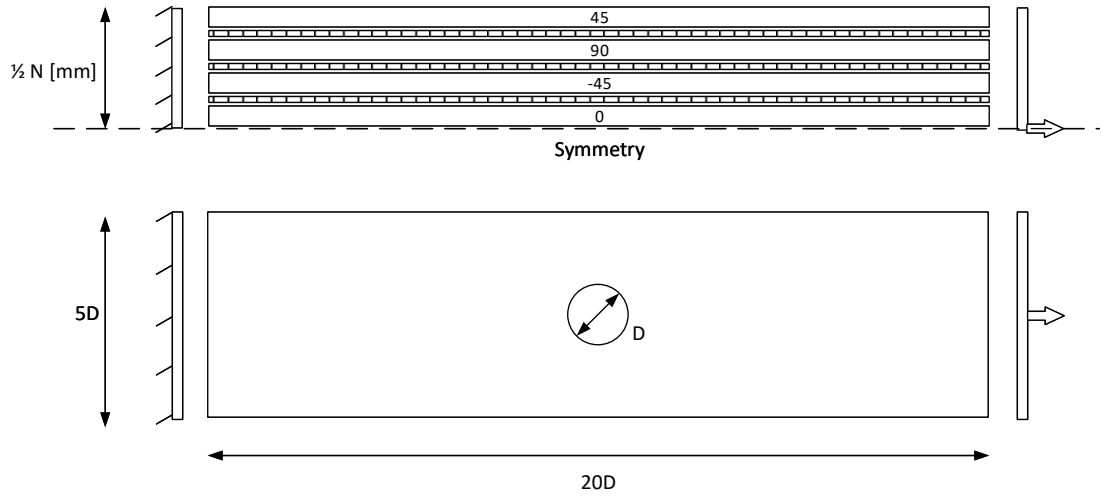

Figure 4.1: Basic setup Nixon-Pearson OHT tests

4.3 Preliminary model

The blend of the fracture mechanics and stress-strain based model implemented the cohesive zone model for delaminations and the XFEM matrix crack model of this thesis with the fibre damage CDM and initiation criterion implemented by Van Dongen [2]. This chapter presents the continuation of the work on which was previously collaborated and tackles the issues that were still apparent in the preliminary model that was already presented by Van Dongen [2]. The main issues being:

1. The model was unable to converge/crashed before showing at least some load drop for most cases (75 to 95% of the time, depending on the used settings);
2. Some cases could never converge/complete;
3. If load drops were observed, these were typically very small $< 5\%$ and could not guarantee that final failure had occurred;
4. The model was computationally very slow;
5. The model did not work for any slight asymmetry, making it unsuited for more generic problems other than the open hole tests or not even for open hole test if asymmetries in mesh, material values etc. are present;
6. The combination of convergence issues and computational cost made sensitivity studies infeasible and presented a huge amount of model uncertainty in the obtained results.

In the end a load drop was observed for only two of the four considered cases of the Nixon-Pearson verification tests [2]. These load drops were however small, and still required artificial changes to the matrix fracture toughness to aid convergence. The other two cases never showed load drops and merely wishful thinking, combined with the observed failure patterns,

could be employed that the crashes were a forerunner of final failure. Something that was later disproven in this thesis.

The importance of clear load drops can not be stressed enough. For a generic open hole specimen, as discussed in this chapter, increased loading presents damage in both the increasing and decreasing part of the load displacement curve. The decreasing part of the load displacement curve represents unstable damage growth and an inability to sustain any further increase in load. It is therefore easy to see any negative gradient in the load-displacement behaviour as final failure as was done previously [2]. A more robust definition would be a full decrease in the load, but residual stiffness in the CDM make this practically impossible (see also Section 3.2.3). Moreover it presents another difficulty as load drops may only be partial, meaning there is some form of unstable damage growth, but this is only temporary. Such cases are relatively frequent for small load drops of only a few fractions of a percent (for the cases at hand). This can however not be defined as final failure. Using a definition for final failure which incorporates a negative gradient to define the failure load is therefore very dangerous as this may happen before a significant load drop is observed, thereby underestimating the failure load. For this thesis therefore a minimum load drop of 5 % is required to define final failure in line with previous models for the same test set[5]. It is therefore important to capture not only the peak load, but also the post peak load behaviour, to determine whether this 5% threshold has been met. Even in such a case, multiple load drops may still be present for which a distinction is made between final failure and ultimate failure, with the latter referring to a complete load drop.

Still, with this key issue present, it was very clear that the model showed great potential if these problems could be solved, especially in the context of observed failure patterns:

1. The failure patterns and observed damage states towards final failure were in line with experimental results, and;
2. The failure patterns of the more conventional implemented CDMs were at the same time unrealistic and unphysical.

4.4 Single crack model

The single crack model refers to the matrix cracking which is modelled with a single crack per side, per ply. In this model enrichment [1] is enabled on a ply to ply basis. The XFEM implementation by Abaqus allows for only one crack to initiate per time increment, per enrichment region [49]. Simultaneously, no cracks can initiate at all while previously cracks are still growing. Multiple cracks per enrichment region are only possible if they initiate one after each other, allowing each previously initiated crack to complete first. Alternatively multiple cracks can grow at the same time, but only if they initiated in the same time increment.

This latter aspect was used in the single crack model to allow for one crack per side of the hole. It is however clear that such behaviour cannot be repeated by even the slightest randomness, causing an asymmetry in the ply, or for more generic loading conditions. Moreover it gives rise to the "Sudden Cracking Problem".

[1] Enriched elements/regions allow for imitation and progression of XFEM cracks

This section is subdivided into seven subsections. First the Abaqus restart control is explained, which greatly reduced the amount of crashes in the preliminary model, and forms the basis for the single crack model of this section. Subsequently a set of baseline results are presented for the four main cases. Hereafter for one of the cases a direct comparison with experimental CT data is made. The subsequent three sections show the most important sensitivity studies. This relates to the effect of mesh size, the effect of not using in-situ strengths, and the effect of not including temperature loading for residual stresses. All of these have a significant influence on the interactions and are a driving aspect of the model. The final subsection of the single crack model deals with the computational efficiency. In this subsection a wide variety of implementations and model parameters is discussed which are driving in the efficiency of the model.

4.4.1 Abaqus restart control - The Sudden Cracking Problem

The limitations in crack initiation and growth in XFEM for Abaqus gave rise to the problem that from now on is called the “Sudden Cracking Problem". The sudden cracking problem does not relate to a physical event in the laminates, but rather to the crack initiation limitations imposed by XFEM in Abaqus.

As initiation of new cracks is prohibited while previously initiated cracks are not yet complete [49], there is a possibility that not all cracks that want to grow are actually modelled, but rather only the cracks that initiated first. If these cracks, or damage elsewhere in the laminate, at the same time does not provide enough load relieve the failure indices in other elements in the same ply may continue to rise above 1. As however no new cracks can be initiated at these elements, they also cannot provide any load relieve. This spreads the problem to adjacent elements. As the first initiated cracks ultimately grow outside the enrichment region’s boundary, crack initiation is again computed for the whole enrichment region giving rise to the sudden cracking problem. Suddenly cracks can initiate everywhere in the ply again leading to sudden widespread initiation of new cracks. An example hereof is shown in Figure 4.2.

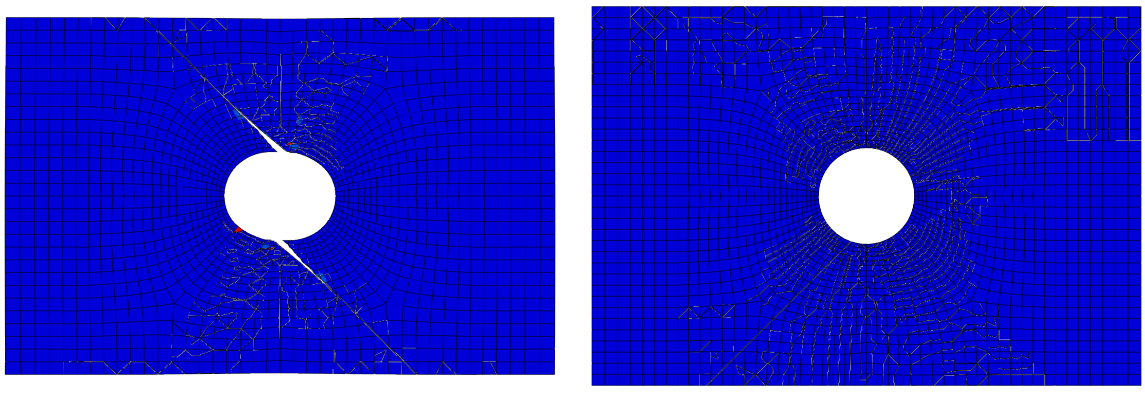

Figure 4.2: Example of the sudden cracking problem for two different plies

The phenomenon of sudden cracking is an unphyscial phenomenon by both the unconstrained

total amount of cracks, but primarily in the direction these cracks take. As cracks initiate, Abaqus attempts to join multiple cracks into a single crack. The user defined fracture plane in the UDMGINI subroutine is herein bypassed, leading to parallel cracks that are joined. Consequently fracture planes may no longer be aligned with the fibre direction, but rather are cutting the fibres. This creates a fracture process as shown in Figure 4.2. Only in the next increment cracks again attempt to propagate, but are unable to do so as their fracture path is obstructed by the fibre cutting cracks created in the previous increment. This behaviour leads to a hard crash of Abaqus with the following type of error message:

> ***error: the system error in std_findcutshape3d8_xfem – nodal level set values might not be correct for element 123

The Abaqus restart script is created to tackle this issue by selectively disabling the enrichment region and the formation of new cracks. The Abaqus restart script reads the associated element ID from the error message, finds the element sets in which this ID is found, and finally finds the enrichment region which uses one of these element sets. Consequently a restart analysis is prepared based on the original input file. The new input file differs primarily in the disabling of the previously found enrichment region, preventing new cracks to initiate, but allowing previously initiated cracks to complete [2].

As the cutshape error happens one increment after the sudden cracks have been initiated a restart analysis needs to go back at least two increments in time. For the models in this report it has been observed that a restart frequency of 5 is enough to achieve this [3], allowing the single crack to fully propagate to the boundary of the enrichment region before the initiation of new cracks is disabled. Larger values may not guarantee this, while smaller values can create excessive amounts of restart data. All results using the single crack model are produced using the restart control. Other than the creation of restart data, the restart control had no influence of any significance on the individual analysis, or the total required computational effort.

4.4.2 Baseline results

This subsection presents the baseline results. It is split into two parts: final failure, which considers load displacement behaviour compared to experimental results and also compared to more conventional CDM implementation provided as part of the parallel research. The next subsection considers damage progression of the individual failure modes. The baseline results presented here are presented not only to set a baseline for the results, but also to highlight some of the present issues and provide an introduction for the subsequent sections and chapter. Specifically the multiple crack model of Section 4.5.

4.4.2.1 Final failure

For the single crack model four prime verification cases are considered. These are all specimens with a hole diameter $D = 3.175[mm]$, but with varying ply thickness with n in the stacking

[2] Initiation refers to insertion of cohesive zones, completion refers to a degradation factor of 1 for the cohesive zone, indicating full separation of the fracture plane

[3] This indicates that restart information is written every 5 increments

sequence being either 1, 2, 4 or 8. These are also referred to as the 1t, 2t, 4t and 8t cases. Following the above described implementation the results as shown in Figure 4.3 are obtained for the load displacement behaviour. The sudden cracking problem described in the previous section is illustrated with vertical dotted lines. Each of them indicating a cutshape error in one of the layers and a subsequent restart of the analysis. As can be observed in Figure 4.3 a very good correspondence with experimental results appears. Note that for the 2t, 4t and 8t cases the specimens from [5] showed two failure loads. One corresponding to delamination failure, and one corresponding to fibre failure as ultimate failure. The first delamination failure is taken in this report as final failure, unless mentioned otherwise.

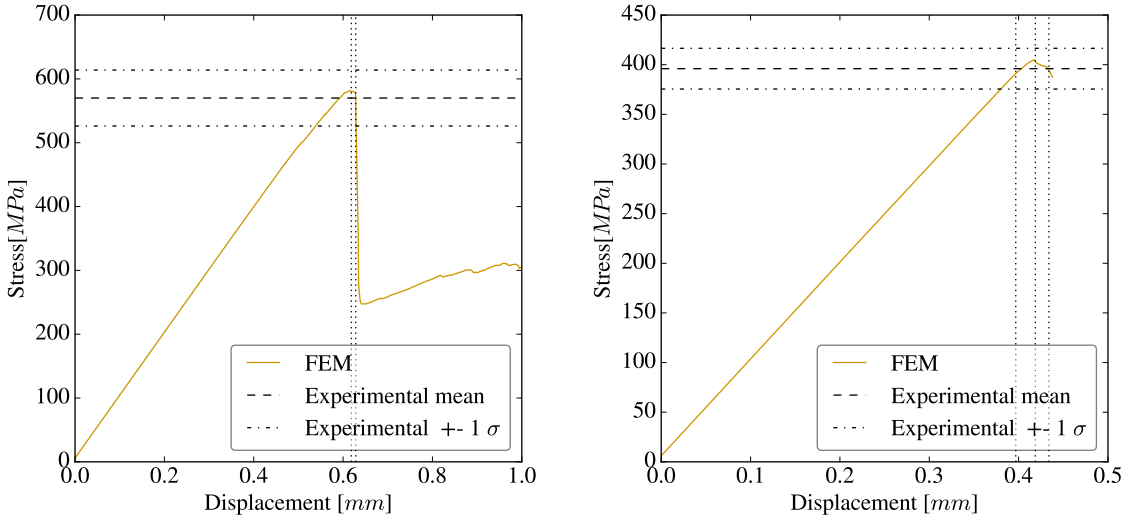

(a) 1t Case

(b) 2t Case

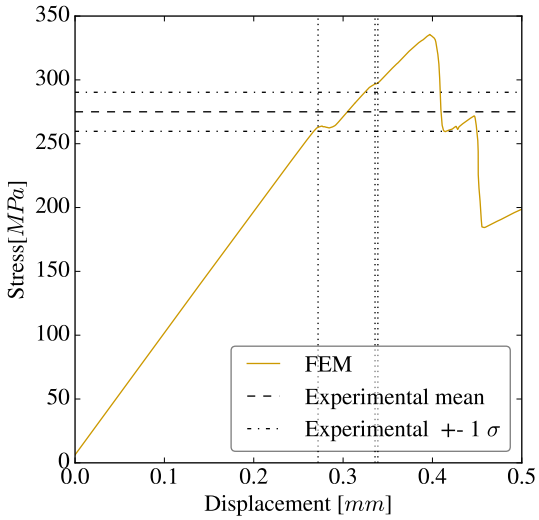

(c) 4t Case

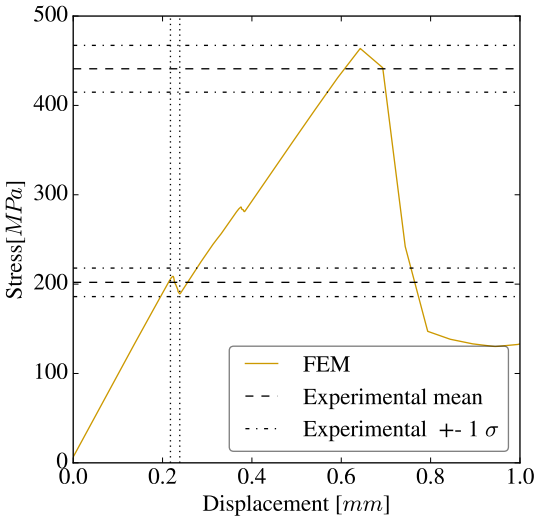

(d) 8t Case

Figure 4.3: Load displacement behaviour

The baseline results can also be compared to the more conventional CDM implementation which were previously reported upon as part of the parallel research. Figure 4.4 shows the ply level scaling for the four baseline cases as well as the previously obtained results with a CDM. The single crack model clearly shows the trend which is also observed in the experimental data, with all predictions within the experimental scatter. A preliminary model, on which was participated with Van Dongen, was only able to predict failure for two of the four cases as mentioned in at the start of this chapter for the preliminary model.

The two stress-strain based CDMs show predictions significantly less in line with experimental results. CDM in this case refers to a model in which both fibre failure and matrix failure are modelled using selective stiffness reductions. The addition of cohesive zones for delaminations from this thesis is denoted as the CDM+CZs model. It is clear that both these models are insufficient even with the addition of delaminations, driving the need for fracture mechanics based methods which are discussed in this thesis. Although the CDM implementation which included delaminations follows from the framework and delamination model of this thesis, it is not further discussed. Similar to the simplified DCB, ENF and MMB verification tests for the delaminations these results are of lesser interest and focus is put on the complete integrated framework as discussed in the previous chapter.

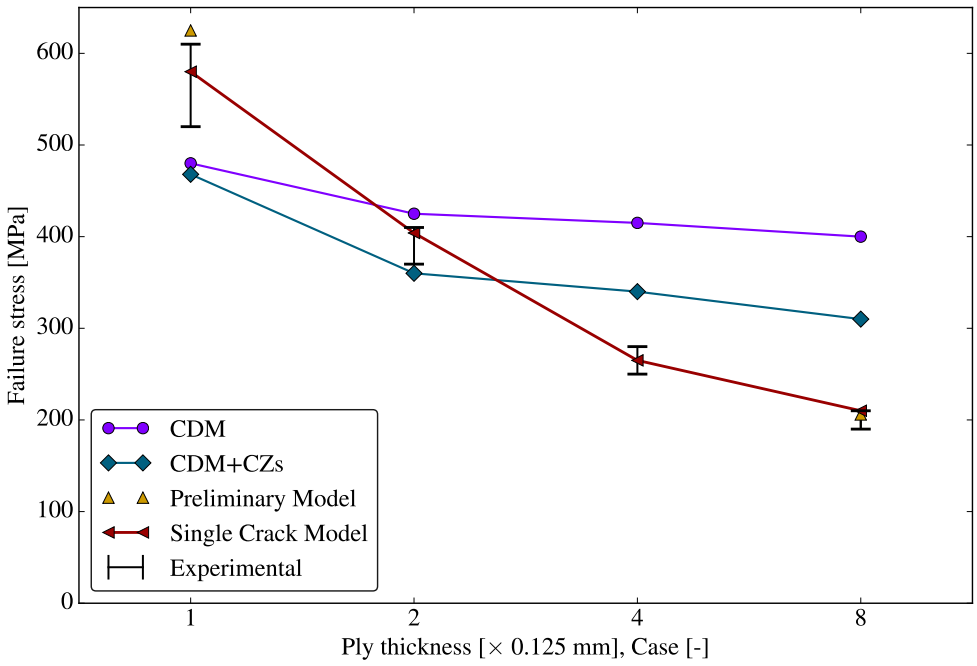

Figure 4.4: Ply level scaling and comparison with CDM [2] methods

4.4.2.2 Damage progression

Although the correspondence to the observed failure loads is good, arguably a much more important consideration than the load displacement behaviour are the observed failure patterns as these relate more closely to the physical process. To set a baseline, two sets of failure patterns are provided for each of the specimens. One failure pattern is provided at 95% of the final failure load, and one failure pattern at the end of the observed load drop. Each of these sets of figures consists of two parts: the ply damage and the interface damage. For the plies fibre damage is shown as red, whereas matrix cracks can be observed as a discontinuity. The interface damage shows the mixed mode ratio of the delaminations. Red indicates mode II/III (shear) delaminations. Green corresponds to mode I (out of plane) delaminations. Note that this may not mean that an element is yet fully delaminated, especially at the edges the delamination region elements may still be somewhere in the softening part of the traction separation law indicated by the degradation factor (excluded here). The mixed mode ratio is shown as it can provide more information on how the damage is evolving (Mode I or Mode II/III). On a macro/meso level the mixed mode ratio may have no meaning and the local degradation factor is more applicable as this presents the actual (current) damage state. All these figures show only the damaged part of the specimen, with the left and right side of the figures trimmed. Loading is applied along this axis, elongating the specimens horizontally, as also shown in Figure 4.1. For figures at the 95% load level displacements may be scaled slightly to enhance visibility of the matrix cracks.

At the same time, for all cases a figure showing the progression of matrix cracking and delaminations for each ply and ply interface separately is shown. Individual damage states at certain load levels provide very little information on how the damage developed, specifically if sequencing is considered. For this purpose the fractured area is shown for both matrix failure and delaminations. For delaminations this follows simply from the area of the connecting element faces. For matrix cracks some simplifications are made. The area follows from the element/ply thickness combined with an average crack length over the ply interfaces, taking also the local ply orientation into account. The local degradation factor of the cohesive zones is taken into account by considering an element to be fully fractured only if the local degradation factor equals 1. Otherwise the fractured area is locally scaled with the degradation factor. Means are provided, which average the results of all plies/interfaces respectively. Tensile damage progression is not shown for two reason:

- CDMs have no physical damage parameter that can be measured, fracture in CDMs occurs over volumes rather than areas
- Focus is laid on matrix failure and delaminations, with only the 1t case considering fibre failure.

1t Case Figure 4.6 shows the damage state at the plies at 95% of the failure load for the 1t case. Figure 4.7 does the same but at the ply interfaces. Similarly Figure 4.8 and 4.9 show the damage after the peak load. The cumulative damage development over the whole displacement is shown in Figure 4.5 for both matrix failure and delaminations. For the 1t case final failure occurs due to fibre failure, as is confirmed by the damage patterns. This is in line with experimental results [5]. Figure 4.6d and 4.8d show a clear crack band leading up

to fibre failure. At the same time, no matrix cracking or delaminations appear to be driving this failure, with no sharp increases observed in Figure 4.5 at the point of the peak load. The extensive damage shown in Figure 4.9 is merely a result of the previous fibre failure.

Past the final failure load the matrix and delamination based failure mechanism appear to become significant. This happens gradually indicating this was not the cause for final failure and only had a limited contribution towards the final failure load. This is confirmed by sensitivity tests indicating that the fibre failure dominated load cases are relatively insensitive to other failure modes (see also Sections 4.4.5 and 4.4.6 concerning in-situ strength and temperature effects). It is therefore also important to keep in mind that even though the results here provide a good match with the experimental results, the relative insensitivity to other failure modes does not guarantee in any way that these results are correct. Only the non-fibre failure dominated load cases can indirectly provide some of this confidence.

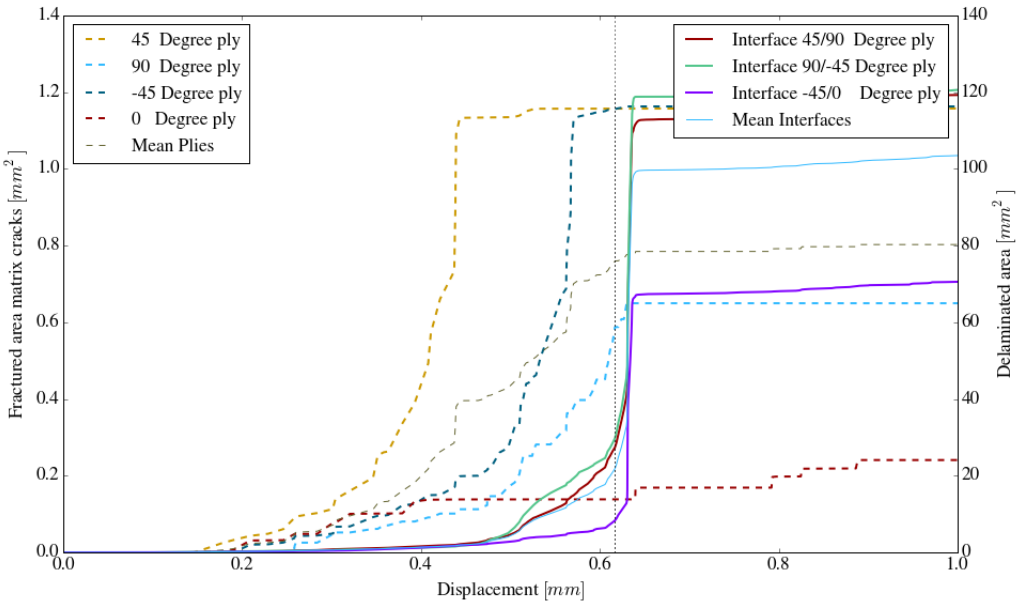

Figure 4.5: Evolution of delamination and matrix failure growth for the 1t case

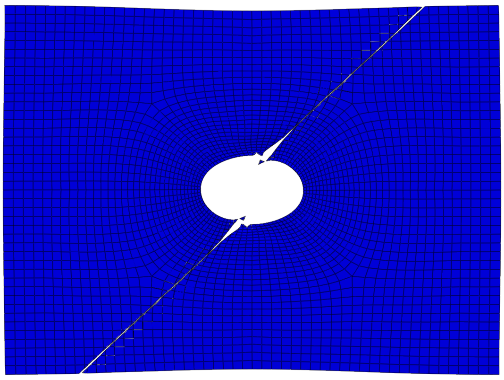

(a) 45 Degree layer

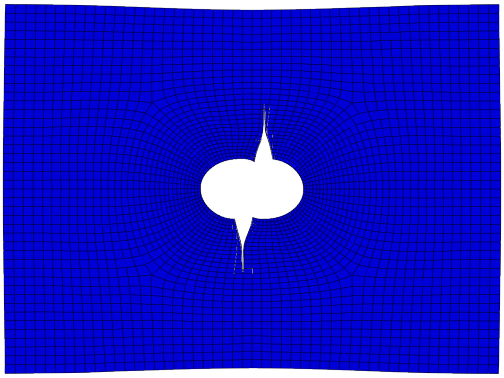

(b) 90 Degree layer

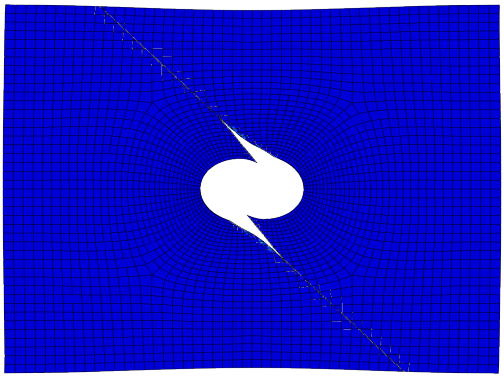

(c) -45 Degree layer

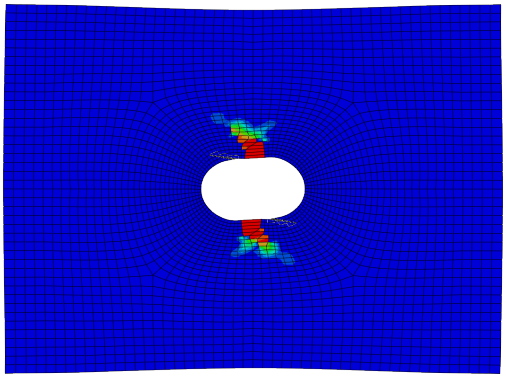

(d) 0 Degree layer

Figure 4.6: Ply damage patterns, fibre failure and matrix failure at 95% of failure load for 1t case

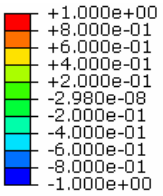

Fibre damage, mixed mode ratio. Negative values denote undamaged elements.

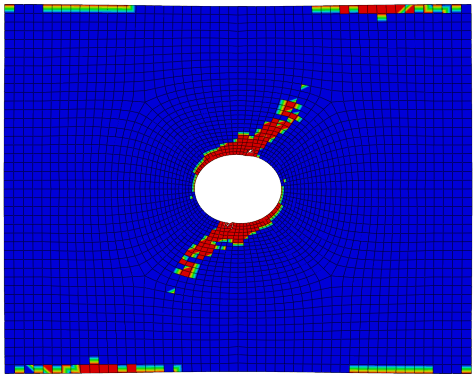

(a) 45/90 Degree interface

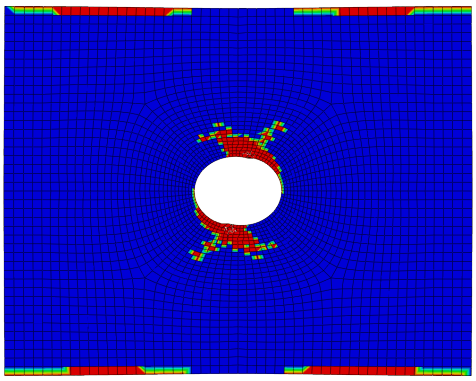

(b) 90/-45 Degree interface

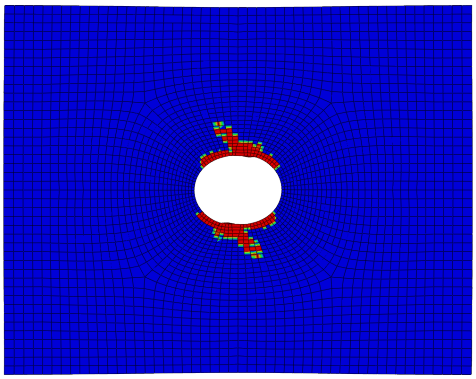

(c) -45/0 Degree interface

Figure 4.7: Interface damage patterns, delamination mixed mode ratio at 95% of failure load for 1t case

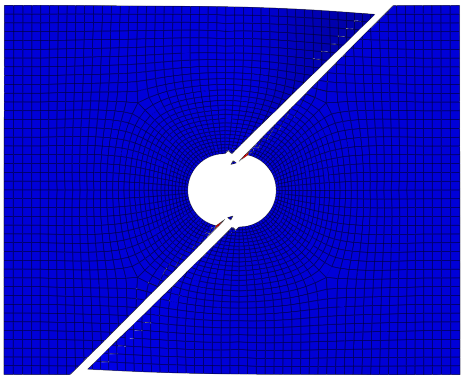

(a) 45 Degree layer

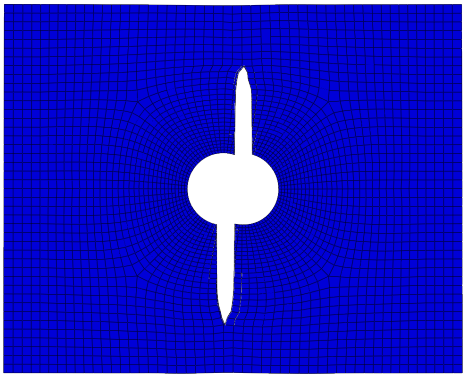

(b) 90 Degree layer

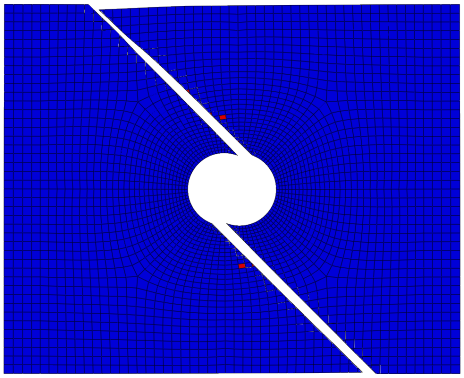

(c) -45 Degree layer

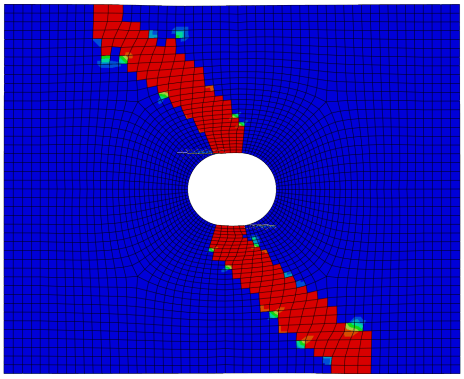

(d) 0 Degree layer

Figure 4.8: Ply damage patterns, fibre failure and matrix failure after failure load for 1t case

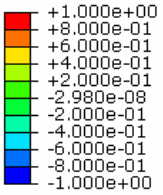

Fibre damage, mixed mode ratio. Negative values denote undamaged elements.

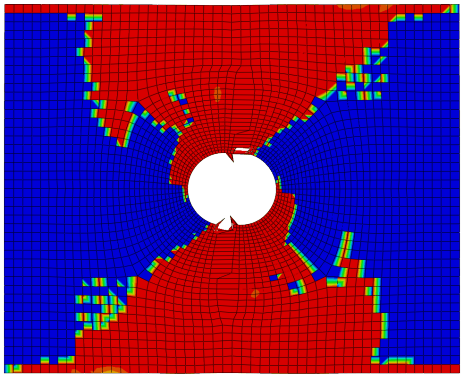

(a) 45/90 Degree interface

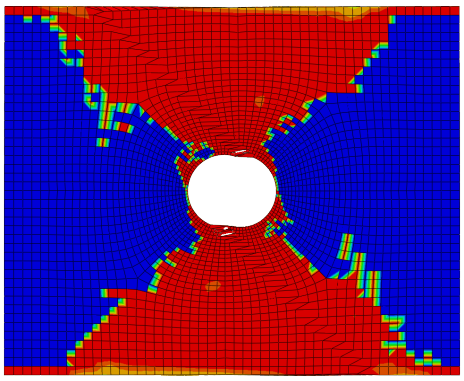

(b) 90/-45 Degree interface

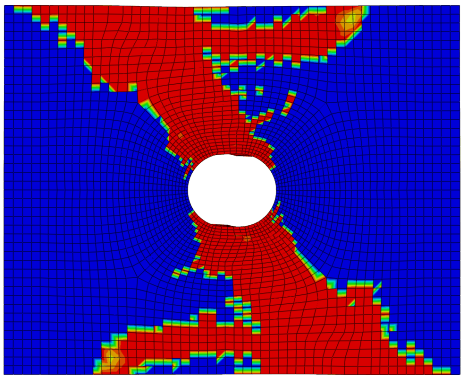

(c) -45/0 Degree interface

Figure 4.9: Interface damage patterns, delamination mixed mode ratio after failure load for 1t case

2t Case Figures 4.10 to 4.14 provide a similar set of results as for the 1t case, but now for the 2t case. The 2t case is a delamination dominated load case in the experimental campaign, with however some specimens failing in fibre failure [5]. These results are clearly matched with a sharp increase in delaminations at the -45/0 interface as shown in Figure 4.10. Unlike the other specimens the baseline model did not show a complete load drop, but crashed just after the start of a sharp decrease in load. Models in later sensitivity studies did complete and a full load drop was found for this case.

The delamination patterns show the expected triangular failure patterns as reported in [3]. As can be observed in Figure 4.10 this model shows very high levels of interaction between the failure modes. It was together with the 4t case, one of the two cases that was previously unable to converge due to XFEM crashes in Abaqus, related to the then unsolved problem of "Sudden Cracking Problem" as discussed in section 4.4.1. Previous attempts to improve convergence increased the fracture toughness of the matrix by a factor 1.5 [2], which was not fully justifiable to the extent performed for this material [64, 73]. This fix worked, for the 8t case as the sudden cracking problem was effectively delayed. However, with the restart control of section 4.4.1 the analysis could now also continue for the 2t and 4t cases, and they showed significant errors using the artificial increase in fracture toughness. The high interaction, and clustering of failure modes, shifted all failure to a higher load causing a significant error (+20 to 30%), typically leading to final failure being fibre failure dominated.

The increase of (matrix) fracture toughness to aid convergence is therefore not seen as justifiable. Slightly better results can be obtained if the in-situ strength effect is at the same time not taken into account. This has however two main issues:

- The in-situ strength concept is required for realistic failure patterns (see also section 4.4.5);
- The traction-separation behaviour is severely altered by both the increase in fracture toughness and reduction in strength.

For this case a direct comparison is also made with CT scans which is discussed separately in Section 4.4.3.

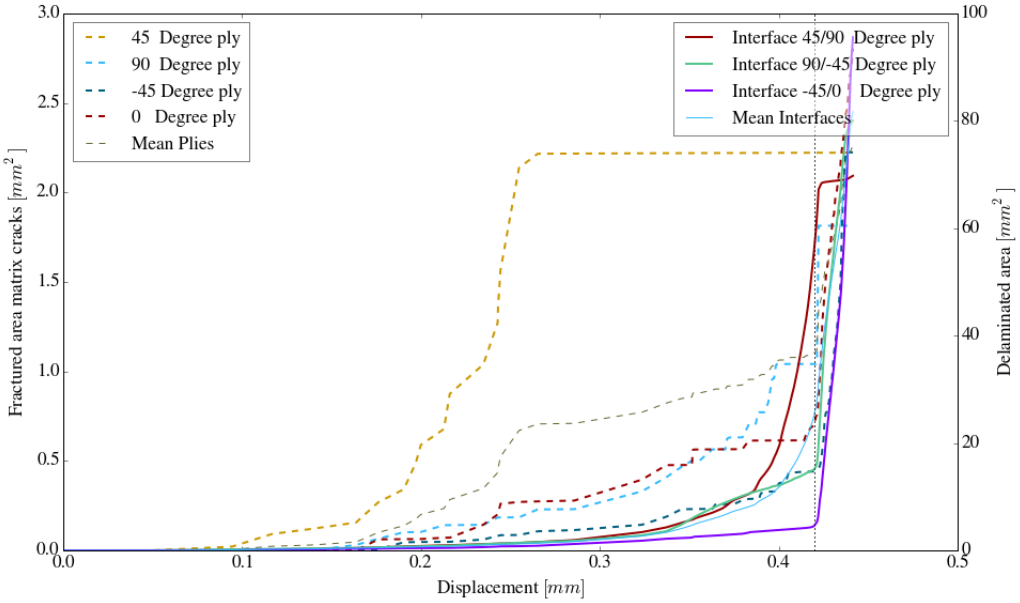

Figure 4.10: Evolution of delamination and matrix failure growth for the 2t case

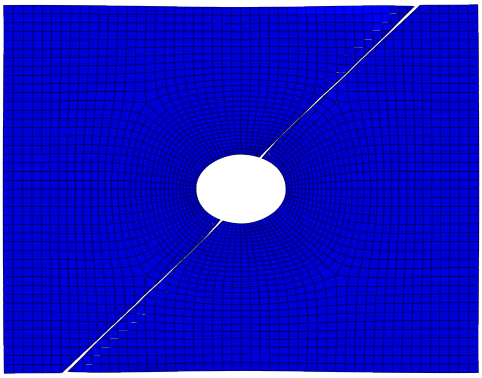

(a) 45 Degree layer

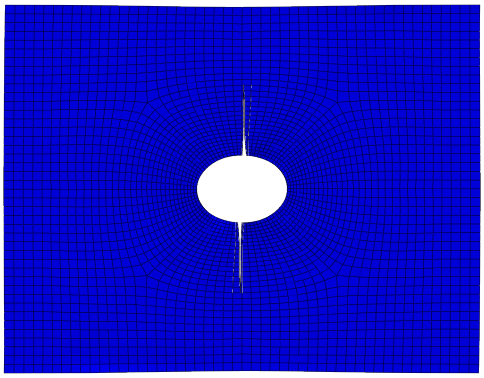

(b) 90 Degree layer

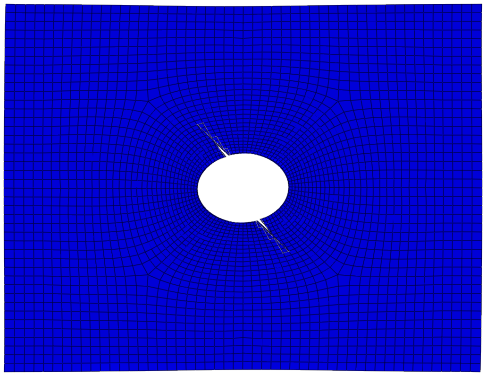

(c) -45 Degree layer

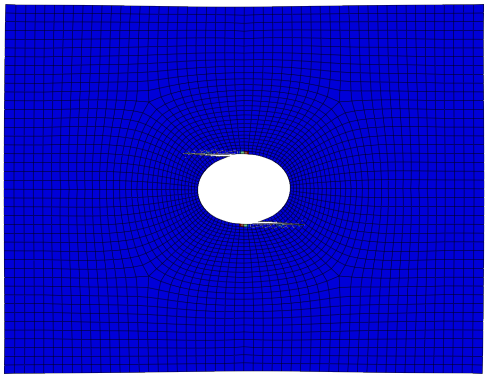

(d) 0 Degree layer

Figure 4.11: Ply damage patterns, fibre failure and matrix failure at 95% of failure load for 2t case

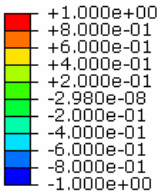

Fibre damage, mixed mode ratio. Negative values denote undamaged elements.

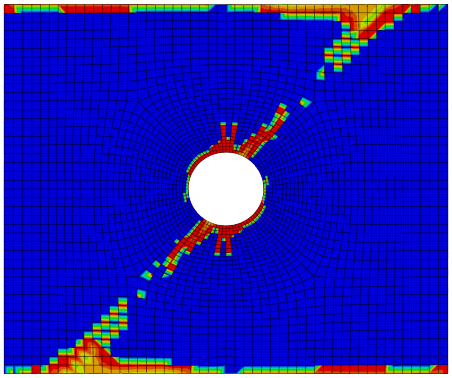

(a) 45/90 Degree interface

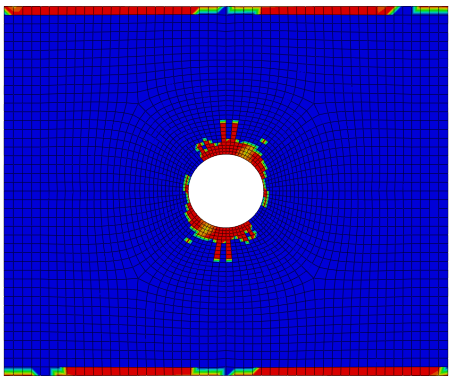

(b) 90/-45 Degree interface

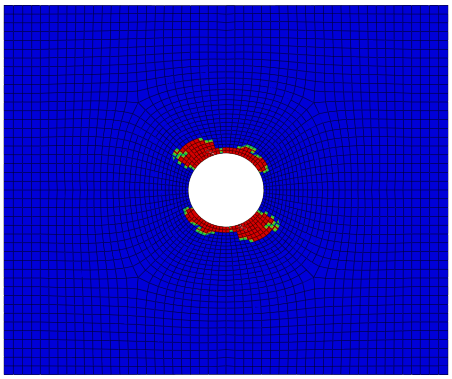

(c) -45/0 Degree interface

Figure 4.12: Interface damage patterns, delamination mixed mode ratio at 95% of failure load for 2t case

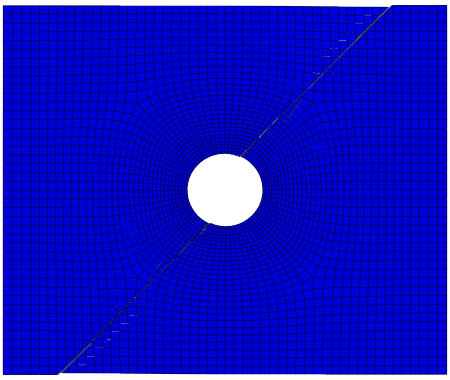

(a) 45 Degree layer

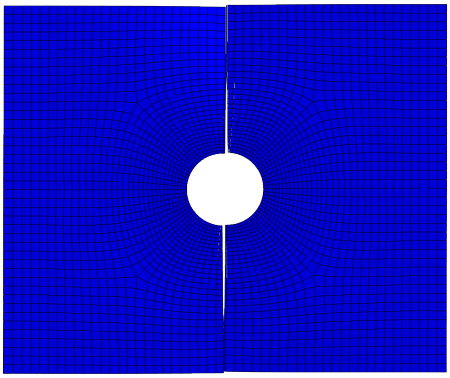

(b) 90 Degree layer

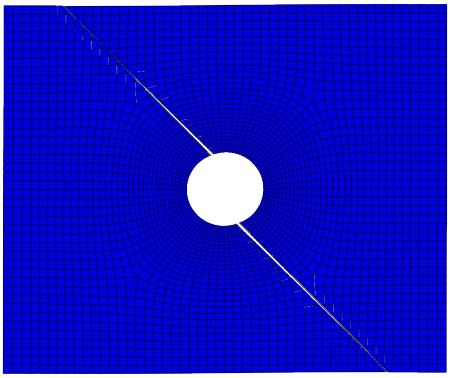

(c) -45 Degree layer

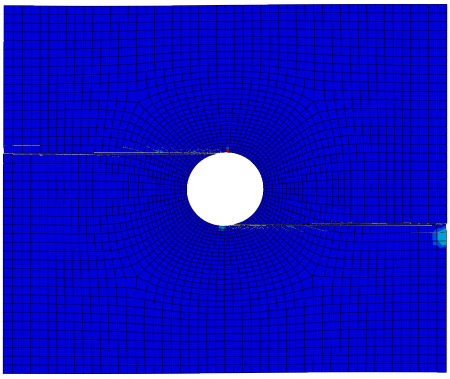

(d) 0 Degree layer

Figure 4.13: Ply damage patterns, fibre failure and matrix failure after failure load for 2t case

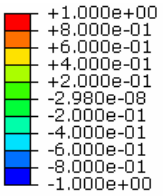

Fibre damage, mixed mode ratio. Negative values denote undamaged elements.

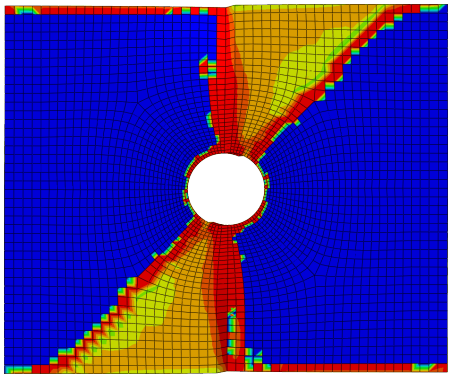

(a) 45/90 Degree interface

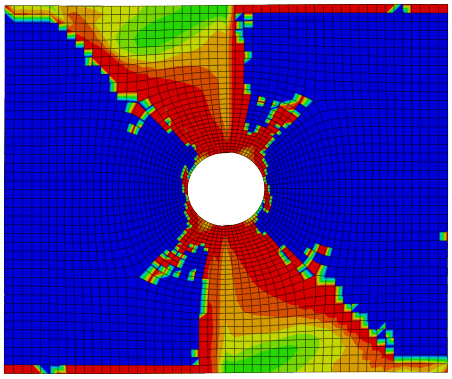

(b) 90/-45 Degree interface

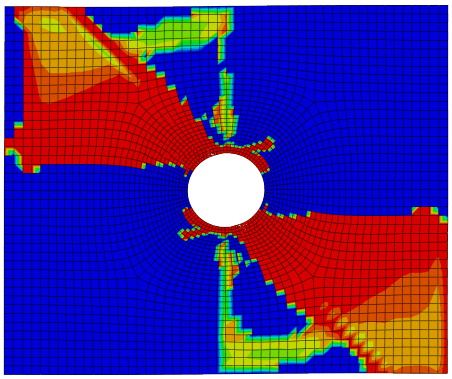

(c) -45/0 Degree interface

Figure 4.14: Interface damage patterns, delamination mixed mode ratio after failure load for 2t case

4t Case Results for the baseline 4t case are shown in Figure 4.15 to 4.19 taking the same set-up as the previous two cases. The 4t case is in many ways very similar to the 2t case, with the 4t case however never failing due to fibre failure. Of the four focus cases under consideration the 4t case has the most troublesome convergence. This is primarily due to two reasons:

- Failure occurs due to strong interactions
- The single crack model is inadequate

The former issue was already discussed previously in the 2t case and can again be observed for this case as well in Figure 4.15. The latter issue manifests itself in a number of ways. First, no significant load drop is observed as can be seen in the load displacement curves of Figure 4.3. Rather, the load displacement curve flattens for a significant portion of the displacement. At the same time the observed failure patterns are also not in line with experimental observations. The delaminations of Figure 4.19 show a clear asymmetry. This asymmetry can however already be traced down to a point quite early in the failure process and is best explained using Figure 4.16c.

In the 90 degree layer six cracks are originally initiated. Four of these cracks, two on each side, consequently join, leaving only one crack per side. However Abaqus automatically forces one of these cracks to grow away from the other cracks, to prevent a collision with a fracture surface that it cannot join. This is the case for the upper crack that grows at an angle with respect to the fibre direction. By doing so it overrides the user defined fracture plane and starts cutting fibres, similar as observed in the sudden cracking problem. As the offset is created Abaqus does not correct itself and the crack continues to grow away from its user defined fracture plane. This issue is further discussed in Section 4.5 dealing with the multiple crack model.

As the matrix crack in the 90 degree layer does not develop in a physical way, the failure patterns are also off. On the lower side the expected triangular delamination patterns are formed. On the upper side however, these do not form due to the absence of the crack in the 90 degree layer. Delamination at the interfaces consequently develops very slow as can be observed in Figure 4.15, and no sharp load drop is observed as this failure develops to slowly. Rather, only the flattening behaviour of Figure 4.3 is observed.

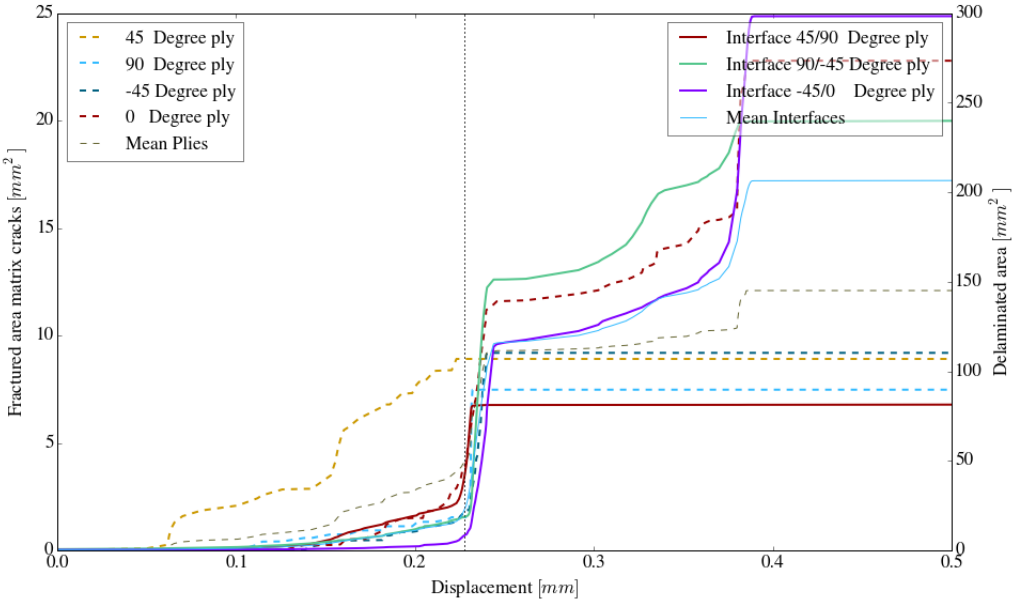

Figure 4.15: Evolution of delamination and matrix failure growth for the 4t case

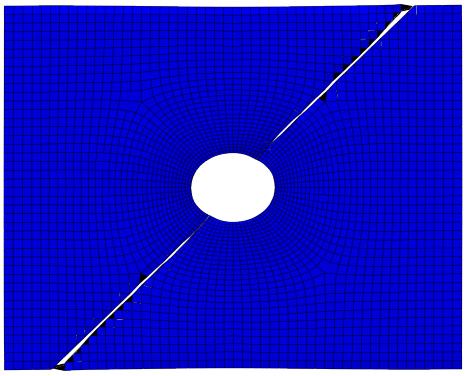

(a) 45 Degree layer

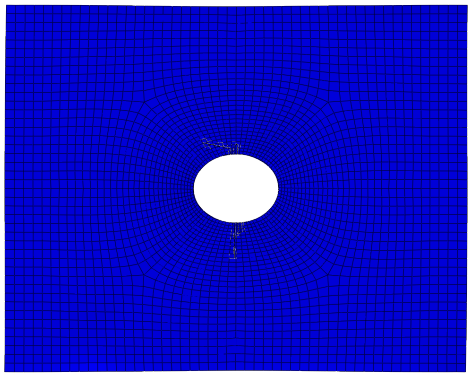

(b) 90 Degree layer

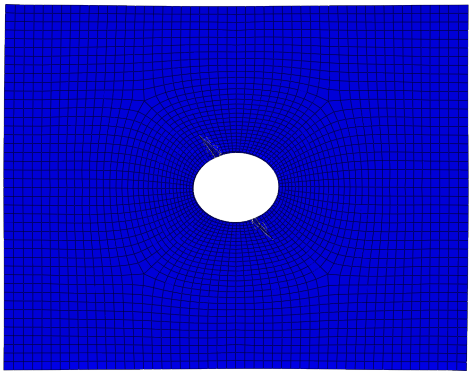

(c) -45 Degree layer

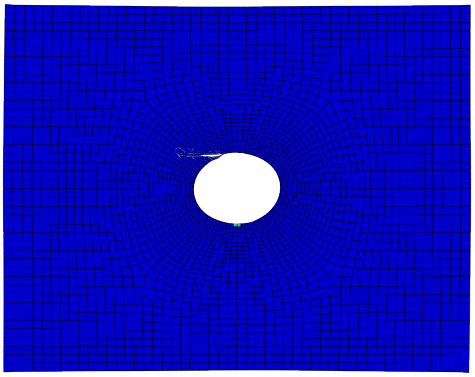

(d) 0 Degree layer

Figure 4.16: Ply damage patterns, fibre failure and matrix failure at 95% of failure load for 4t case

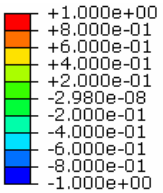

Fibre damage, mixed mode ratio. Negative values denote undamaged elements.

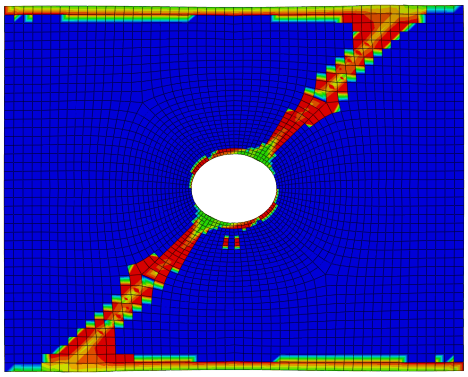

(a) 45/90 Degree interface

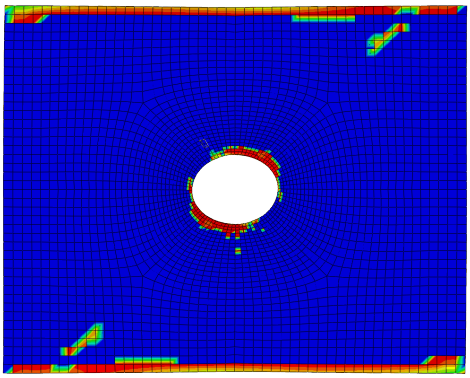

(b) 90/-45 Degree interface

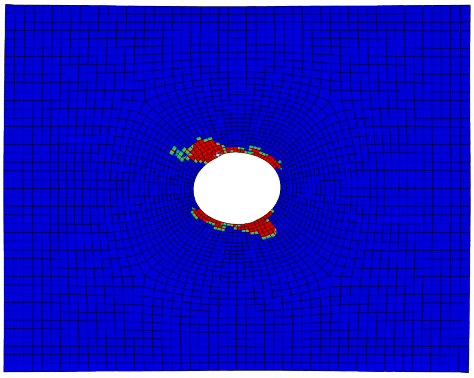

(c) -45/0 Degree interface

Figure 4.17: Interface damage patterns, delamination mixed mode ratio at 95% of failure load for 4t case

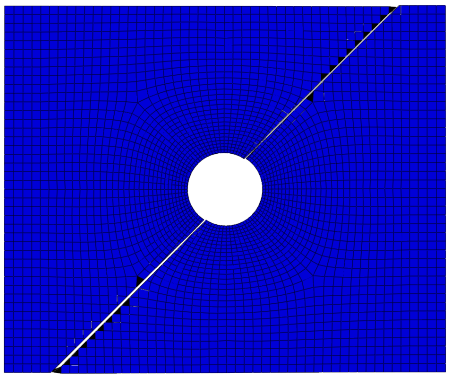

(a) 45 Degree layer

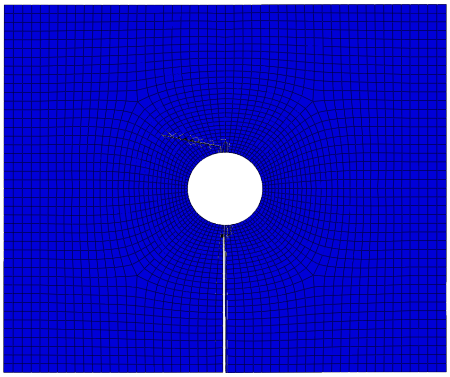

(b) 90 Degree layer

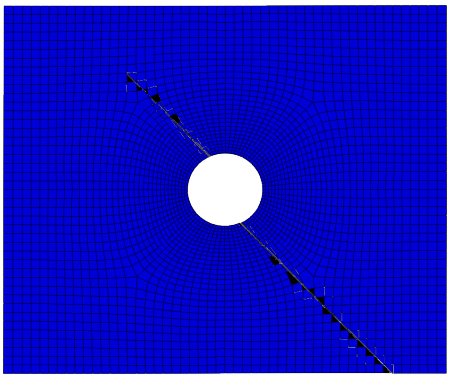

(c) -45 Degree layer

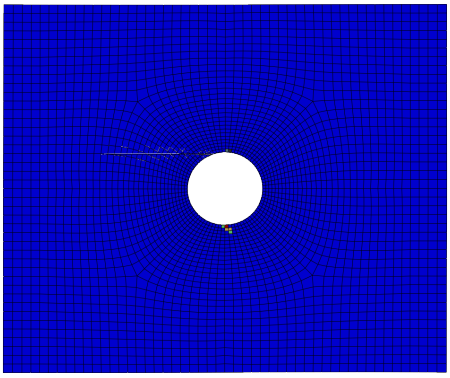

(d) 0 Degree layer

Figure 4.18: Ply damage patterns, fibre failure and matrix failure after failure load for 4t case

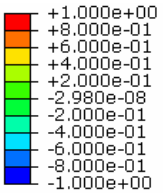

Fibre damage, mixed mode ratio. Negative values denote undamaged elements.

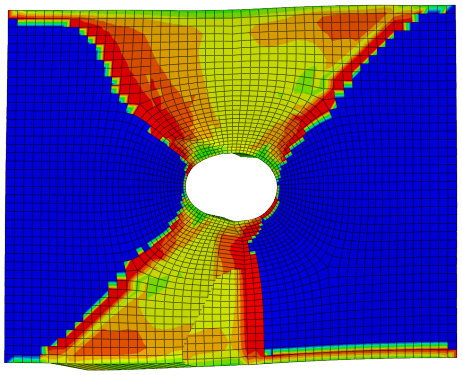

(a) 45/90 Degree interface

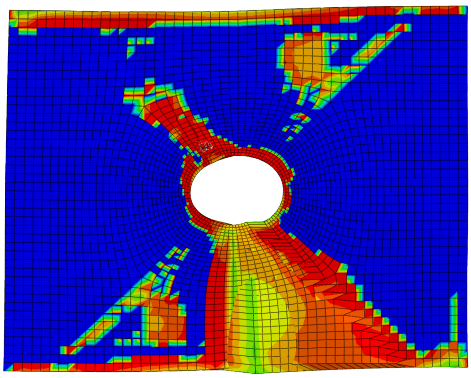

(b) 90/-45 Degree interface

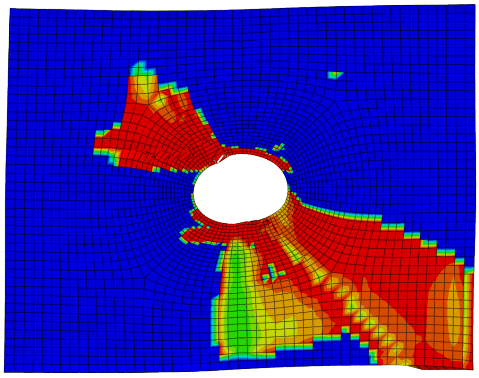

(c) -45/0 Degree interface

Figure 4.19: Interface damage patterns, delamination mixed mode ratio after failure load for 4t case

8t Case Failure in the 8t case, as in Figure 4.20 to 4.24, suffers from relatively little convergence issues. Delamination failure is mostly driven by mode I making the previous convergence issues less prominent. The previously employed fracture toughness corrections [2] did therefore hardly cause any overshoot as in mode I delaminations there is less interaction with the matrix cracks. This was a significant issue for the 2t and 4t cases.

However from Figure 4.20 it can be noted that delamination growth is slow, specifically at the -45/0 interface. After a sharp increase, just after the final failure load, further growth is slow. This is not in line with the experimental results as reported in [5], which reported an almost instantaneous delamination of the complete -45/0 interface. This can also be observed in Figure 4.24c which only shows a partially delaminated interface after the first load drop. The absence of this instantaneous delamination growth is however a deliberate choice in which failure is only modelled for a limited region within the laminate. This region corresponds to the areas shown in the failure patterns. This has no effect on the observed failure loads, but it does influence the behaviour post final failure. The results are therefore as expected. This limitation is optional, and is implemented to improve the computational efficiency. It is further discussed in Section 4.4.7.

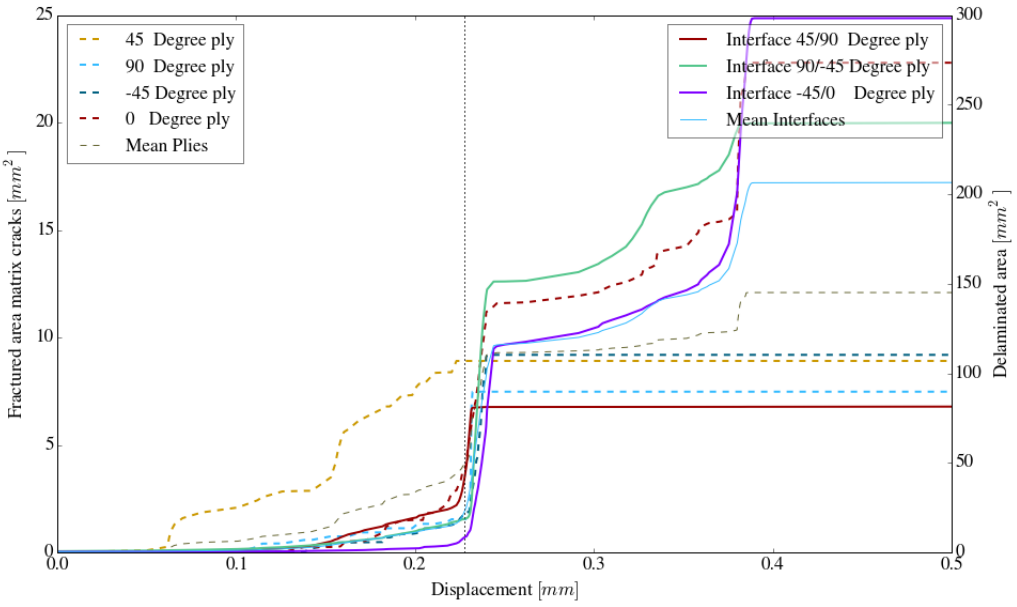

Figure 4.20: Evolution of delamination and matrix failure growth for the 8t case

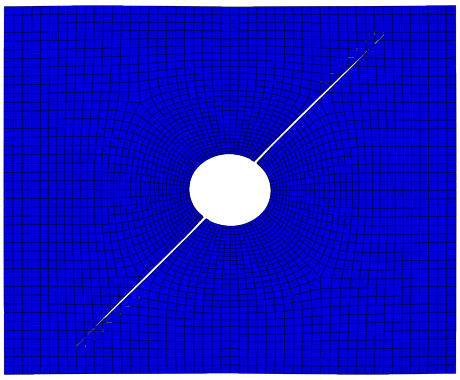

(a) 45 Degree layer

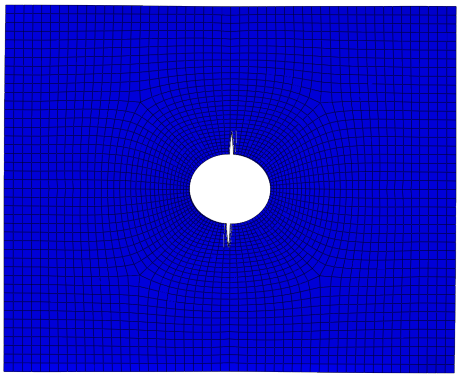

(b) 90 Degree layer

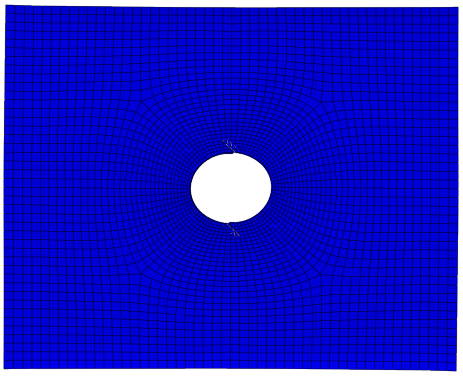

(c) -45 Degree layer

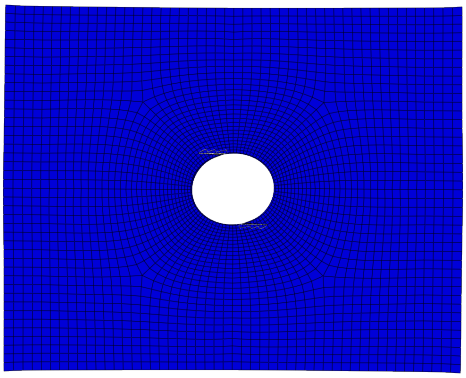

(d) 0 Degree layer

Figure 4.21: Ply damage patterns, fibre failure and matrix failure at 95% of failure load for 8t case

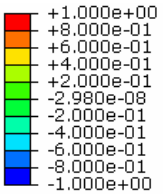

Fibre damage, mixed mode ratio. Negative values denote undamaged elements.

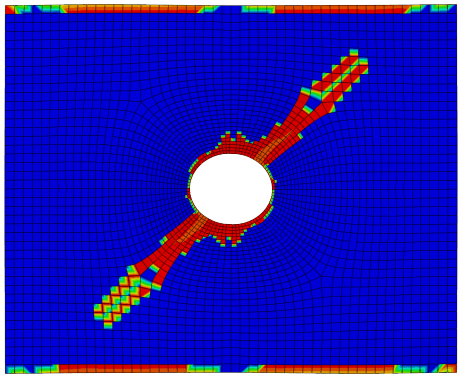

(a) 45/90 Degree interface

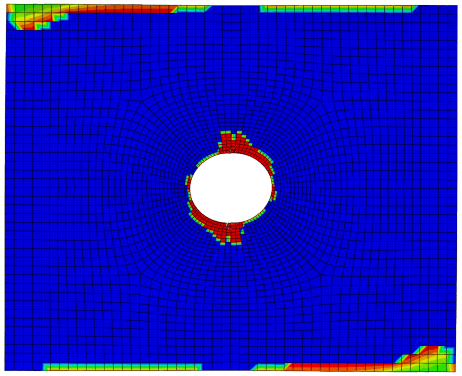

(b) 90/-45 Degree interface

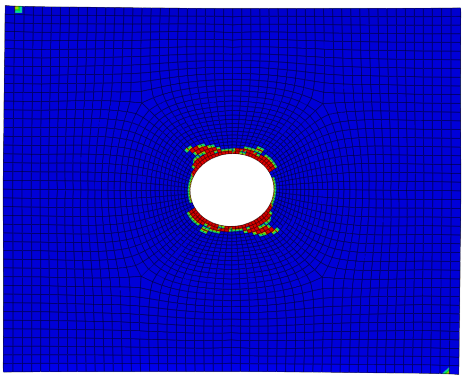

(c) -45/0 Degree interface

Figure 4.22: Interface damage patterns, delamination mixed mode ratio at 95% of failure load for 8t case

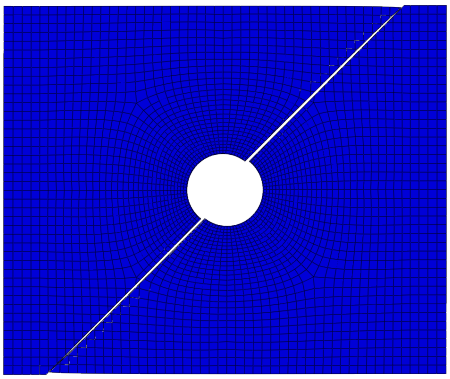

(a) 45 Degree layer

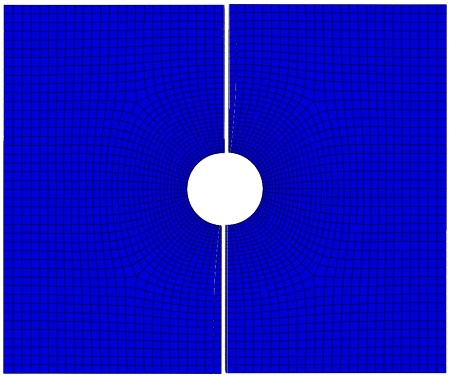

(b) 90 Degree layer

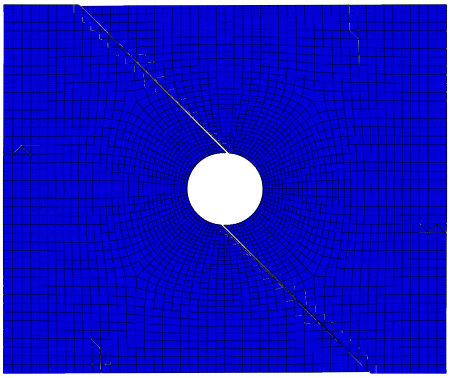

(c) -45 Degree layer

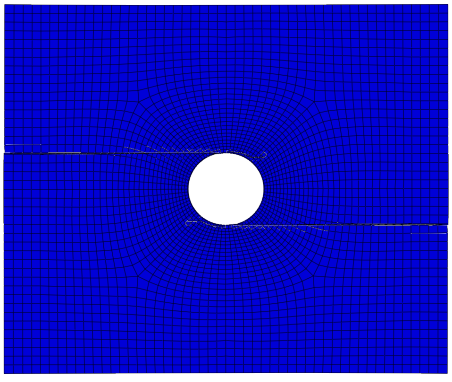

(d) 0 Degree layer

Figure 4.23: Ply damage patterns, fibre failure and matrix failure after failure load for 8t case

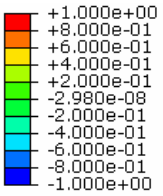

Fibre damage, mixed mode ratio. Negative values denote undamaged elements.

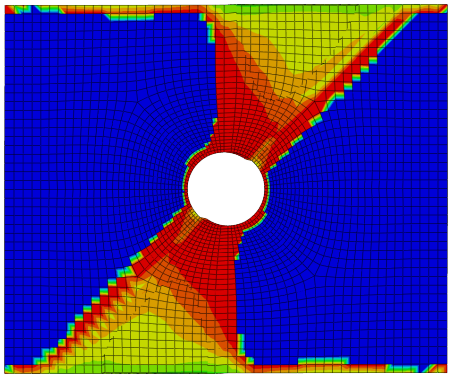

(a) 45/90 Degree interface

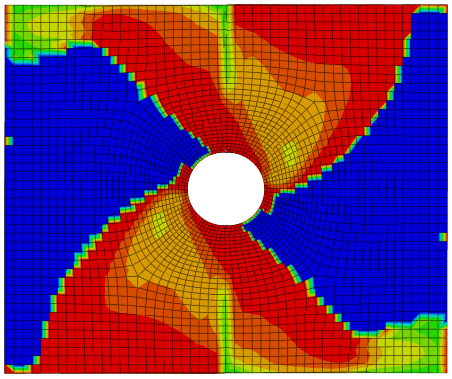

(b) 90/-45 Degree interface

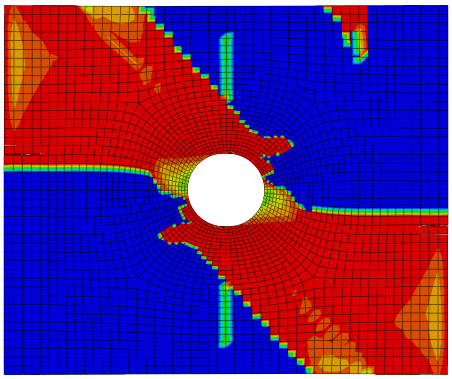

(c) -45/0 Degree interface

Figure 4.24: Interface damage patterns, delamination mixed mode ratio after failure load for 8t case

4.4.3 Comparison with experimental CT scans

For the 2t Case experimental CT testing is available that shows the damage patterns in the individual layers at 60 and 80 % load levels [3]. Experimental CT delamination patterns are not available, and delaminations are omitted from this section in its entirety. A comparison of the experimental results (Figure 4.25) at 60% of the failure load shows relatively good agreement in damage initiation locations and progression. Some notes must however be made:

- The matrix crack in the 45 degree layer appear to be severely overestimated. The 60% load level is however just after a sharp increase in fractured area as can be observed in Figure 4.10, justifying this error.
- Multiple cracks appear to be initiating, something the single crack model cannot capture.

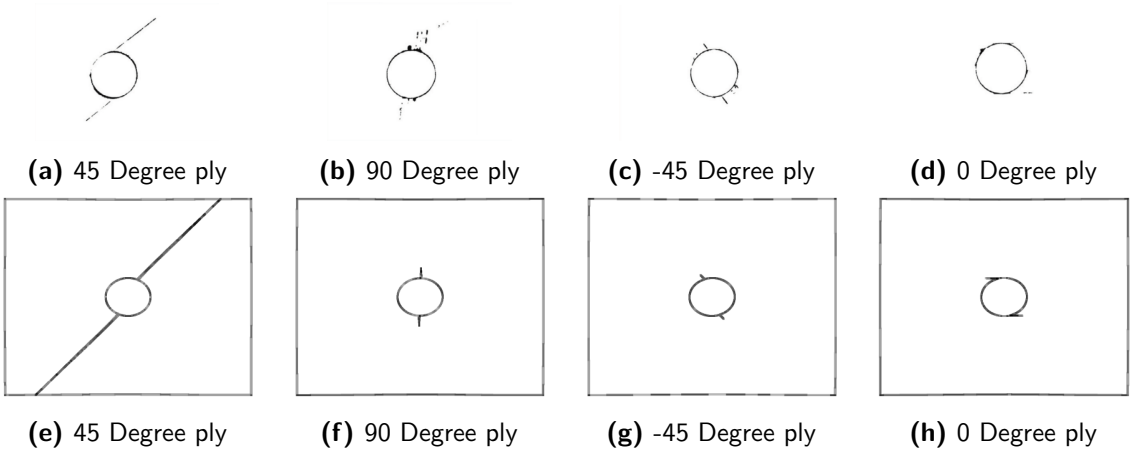

(a) 45 Degree ply **(b)** 90 Degree ply **(c)** -45 Degree ply **(d)** 0 Degree ply

(e) 45 Degree ply **(f)** 90 Degree ply **(g)** -45 Degree ply **(h)** 0 Degree ply

Figure 4.25: Matrix failure damage patterns at 60% of the failure load compared to experimental results [3]. Experimental top, model bottom.

Similarly to 60% load level, another static interrupted test was performed at 80% of the failure load level. Figure 4.26 shows that the model results are in relatively well agreement with the experimental results. An important shortcoming is however still the limitations imposed by using the single crack model. For the 90 degree layer this is most obvious and it is clear that the current model underestimates the matrix damage to some extent. Also the matrix damage in the 0 degree layers appear to be underestimated, with moreover only two cracks per side. The exact consequence hereof is unknown and among the main drivers for the multiple crack model.

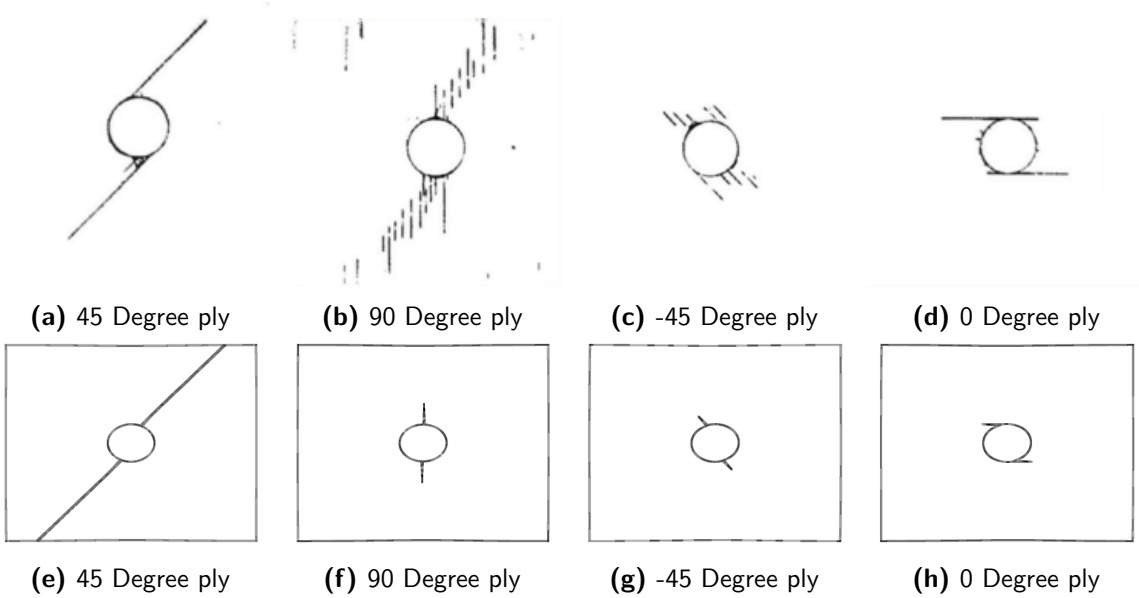

(a) 45 Degree ply **(b)** 90 Degree ply **(c)** -45 Degree ply **(d)** 0 Degree ply

(e) 45 Degree ply **(f)** 90 Degree ply **(g)** -45 Degree ply **(h)** 0 Degree ply

Figure 4.26: Matrix failure damage patterns at 80% of the failure load compared to experimental results [3]. Experimental top, model bottom.

4.4.4 Mesh Size effects

The aspect of mesh size is considered to show the effects of size requirements on damage progression. Mesh convergence in the context of realistic stress gradients around the hole is not explicitly considered as it is subordinate to mesh size requirements for realistic damage progression. Several other aspects are however considered in this context:

- Scaling with total number of elements with a constant hole size
- Scaling with increasing hole size with a constant number of elements

The first of these aspects focusses primarily on the effects of matrix and fibre damage in relation to stress gradient around the hole. This considers the element size required to effectively capture the damage state. The latter aspect considers the requirements of mesh size in relation to the physical input quantities. This relates primarily to the cohesive zone strength reduction equation (3.6). As a rough subdivision it can be said that the first aspect focusses on fibre and matrix damage and the latter aspect focusses on delaminations. Apart from the scaling of element size, the ply level scaling is also taken into account by considering all of the ply level scaled test cases. Table 4.2 shows the convergence study results. Each specimen has a range of mesh sizes. The lower value refers to the element size at the hole, and the larger value refers to the element size at the edge of the specimen. All the ply level scaled tests from the experimental campaign in [5] have been repeated. The results for a hole diameter of $3.75[mm]$ have already been reported upon in the previous sections. The tests with a larger hole diameter have a constant number of elements and thereby an increasing element size with hole diameter. For the 1t and 2t case also a smaller number of elements is considered by increasing the mesh size with respect to the base mesh. The 1t case herein failing due to fibre failure, and the 2t case due to matrix failure.

Table 4.2: Mesh size effects. The * denotes that final (delamination) failure was obtained in two smaller load drops at the reported load levels

		Mesh Size [mm] (Strength Corrected)				(Uncorrected)
		0.25-0.75	0.5-1.5	1.0-3.0	2.0-6.0	0.25-0.75
Mesh	Ply Thickness [mm]	Hole diameter [mm] 3.175	6.35	12.7	25.4	3.175
Mesh Size x2.0	1	-5%				-6%
Mesh Size x1.5		1%				2%
Reference Mesh		**2%**				-9%
Mesh Size x2.0	2	15%				30%
Mesh Size x1.5		11%				22%
Reference Mesh		**2%**	**-6%**			3%
Reference Mesh	4	**-4%**	**6%**	**2%**	**-20%**	36%
Reference Mesh	8	**4%**			**37%**	35% *

The results of Table 4.2 show relativity good agreement for the most important cases. For scaling with the hole diameter only for the largest considered hole diameter (of 25.4[mm]) the results are getting rather off. However, this is with a constant number of elements employing the cohesive zone strength correction. Mesh sizes are now in between 2.0 and 6.0[mm] whereas, without the strength correction a mesh size of roughly 0.15[mm] would be required. At the same time, for the hole diameter of 3.175[mm] without the strength correction the results are already significantly off for the delamination dominated load cases. For the 2t case the error remains small as delamination failure switches to fibre failure. For the 4t case no real load drop is found and for the 8t case the sequencing is very much affected. The delamination failure happens in two stages of very small load drops in the 8t Case. Only at +35% of the reported failure load a similar damage state is obtained.

For the 1t, fibre failure dominated, load case the solution appears to have converged for the used mesh size, with all errors within a reasonable range considering also the experimental scatter. For the 2t case this cannot directly be said. The larger mesh size shows a clear overshoot. This result is not very surprising considering the 2t case is driven by large amount of interactions as opposed to the 1t case as can also be seen in Figures 4.5 and 4.10. For this case with the rougher meshes of 1 time and 1.5 times the base mesh the observed delamination failure is partly delayed. This causes final failure to be driven by fibre failure rather than delamination failure. This is not per-se a bad result as this was also observed for some of the specimens of the test campaign [5].

4.4.5 The case for In-situ strengths

The concept of in-situ strengths was previously introduced in Section 3.2.2 of the previous chapter. This subsection reviews the effects of using in-situ strengths.

To show the necessity of using in-situ cracks -at least in the context of the single crack

model- the four prime verification cases have been re-run without using in-situ strengths. Two sets of results are considered. The observed failure loads as shown in Table 4.3 and more importantly the observed failure patterns as shown in Figure 4.27 and 4.28. As using the in-situ strength also changes the ratio of strengths ($\frac{Y_T}{S_{12}}$), even in the absence of other damage, crack patterns will differ. Not merely in crack length, but also in initiation positions. This effect is highlighted in Figure 4.29.

Merely the switch to in-situ strengths has little influence on the observed failure loads as provided in Table 4.3. The errors without using the In-Situ strengths become slightly larger, but they remain small enough considering again the experimental scatter as well. Considering only the failure loads not one model can be considered superior.

Table 4.3: Effect of in-situ strengths on observed failure loads

	1t Case	2t Case	4t Case	8t Case
With in-situ Strengths (Baseline)	2%	2%	-4%	4%
Without in-situ Strengths	2%	-4%	-6%	7%

The failure patterns show a very different story. Matrix crack initiation and growth is severely accelerated. Figure 4.27 shows again the comparison with experimental results at 60% of the final failure load level. Already at this load level all matrix cracks have completed in all layers but the 0 degree ply. For the 90 degree ply an unphysical crack developed, which was typically found to only delay damage growth, making the overestimation even worse. Only for the 0 degree ply the cracks appear to match the experimental results slightly better both at the 60% and 80% load levels. This difference is however only slight and does not justify the overestimation of the crack growth in the other layers.

The unphysical cracking was previously mentioned for the baseline 4t case and is also further discussed in Section 4.5. It will not be discussed here.

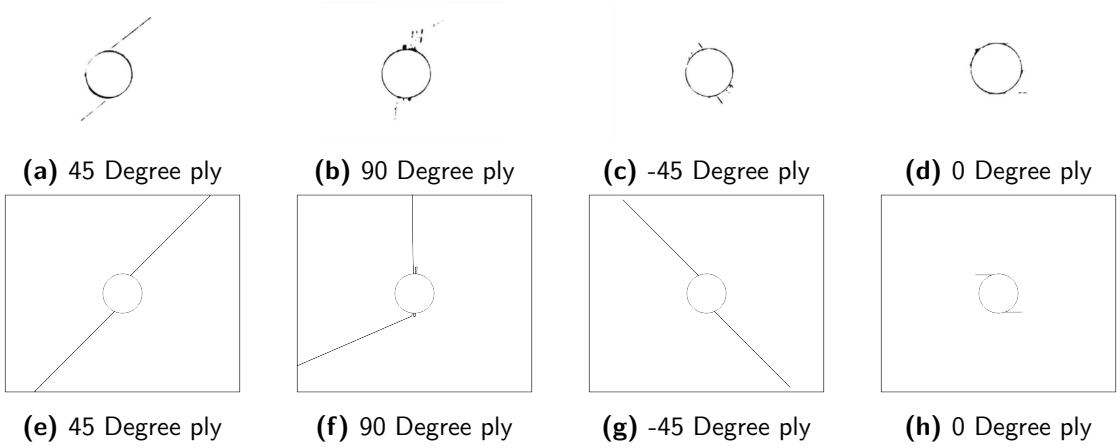

(a) 45 Degree ply **(b)** 90 Degree ply **(c)** -45 Degree ply **(d)** 0 Degree ply

(e) 45 Degree ply **(f)** 90 Degree ply **(g)** -45 Degree ply **(h)** 0 Degree ply

Figure 4.27: Matrix failure damage patterns at 60% of the failure load compared to experimental results [3]. Experimental top, model bottom.

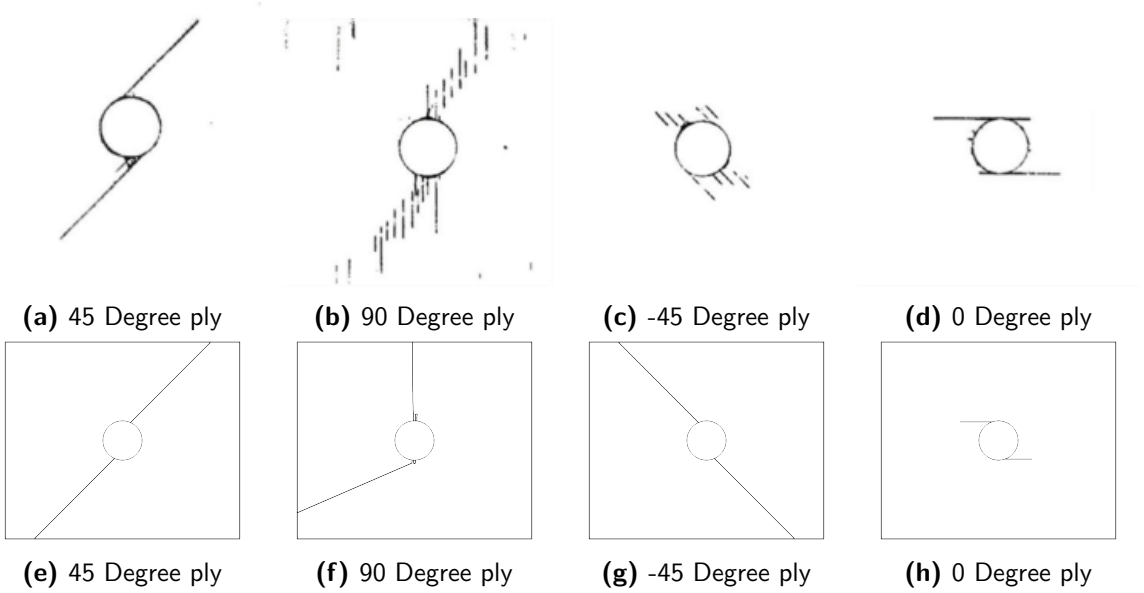

Figure 4.28: Matrix failure damage patterns at 80% of the failure load without usign in-situ strengths compared to experimental results [3]. Experimental top, model bottom.

Next to the accelerated crack growth, the use of in-situ strengths also changes the location where cracks first initiate. This is specifically relevant for the single crack model. Figure 4.29 shows how these cracks move with increasing and decreasing strengths. The observed effects in the numerical model are most prominent for the strongly ply blocked laminates such as the 4t and 8t case. The effect of not using the in-situ strengths results in cracks creating increasingly large angles with respect to the hole. The effect is most prominent for the cracks in the 0 degree ply. For this ply cracks at both sides of the hole join, creating a single crack at the middle of the laminate in the 4t and 8t case. For the 45 and -45 degree plies, the initiated crack has already moved away quite significantly from its position parallel to the hole. Not using the in-situ strength worsens this effect further. Both these issues are not in line with reported experimental results [5, 72, 74].

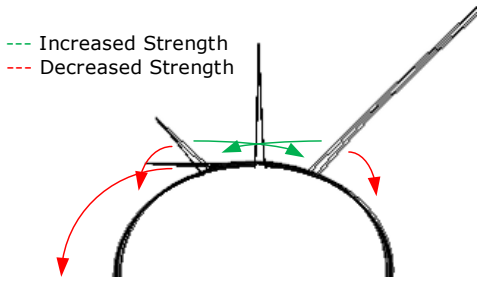

Figure 4.29: Effects of in-situ strengths on matrix fracture damage patterns

4.4.6 The case for Temperature cooldown effects

Similar to in-situ strengths the inclusion temperature effects is seen as very important in order to accurately predict the failure patterns. Although temperature is a variable in almost all parameters, the only influence considered in this thesis is residual stresses due to cool down effects.

This subsection shortly highlights the importance of including these cooldown effects, specifically for delamination driven load cases. It also highlights again the insensitivity of the fibre failure dominated load cases. Table 4.4 shows the effects of including thermo-elastic cooldown effects. The models in which these thermal effects are excluded show large errors for all the delamination dominated load cases. The results are as expected, with increased ply blocking creating larger stiffness differences. The orthotropic thermal expansion behaviour translates this into increased stresses at the interfaces between the plies.

Within the model it is assumed that the residual stresses are merely a consequence of the curing temperature and the thermoelastic properties. Herein stress relieve is disregarded and moreover the stress free state is assumed to be exactly at the curing temperature. Both of these effects appear to be valid assumptions for this specific laminate. Care must however be taken to extract this model to other laminates as these effects can be more significant [75, 76]. Specifically considering the strong possible influence these temperature effects can have as observed in Table 4.4.

Table 4.4: Effect of thermal loading on observed failure loads

	1t Case	2t Case	4t Case	8t Case
With Thermal Effects (Baseline)	2%	2%	-4%	4%
Without Thermal Effects	-3%	18%	26%	29%

4.4.7 Improving the computational efficiency

A large effort within this thesis was not only to make a model which can (relatively) accurately predict damage progression, but also to make a model and framework which is at the same time computationally efficient. This is important to consider if switches are made to either larger specimens, or more complicated loading conditions such as fatigue. Moreover this is important to consider if the model is to compete against the more traditional CDM implementations. This section considers five main aspects which have been used to improve the computational efficiency. An overview hereof is provided in Table 4.10.

4.4.7.1 Cohesive zone strength reduction

The cohesive zone strength reduction has already been mentioned multiple times, most prominently in Section 4.4.4, but is reconsidered here. From Section 4.4.4 it can be noted that the cohesive zone mesh size is one of the main drivers of the mesh size for the whole model. If the uncorrected minimum required element size of $0.15[mm]$ is again considered, to achieve

the same accurate results up to $1.0 - 3.0[mm]$ in the strength corrected model, elements need to be 20 times as small. This results in up to $20^2 = 400$ times less elements.

For the models at hand the computational expense is to a large degree driven by the evaluation of the subroutines and the numerical integration of the elements, resulting in an almost linear scaling with number of elements. However, at a larger number of DoFs solver time is likely to become the significant factor, making the scaling with number of elements go towards a quadratic rather than linear scaling, worsening the effect further.

4.4.7.2 Reduced integration elements

The use of reduced integration elements was previously explained in Section 3.1.1.2. Reduced integration elements are roughly a factor 8 cheaper to evaluate, making them very appealing to use. Justification for using reduced integration elements was previously provided. This section confirms this justification based on experimental (FEM) results.

Table 4.5 provides an comparison in observed failure loads between models using full integration elements and reduced integration elements. Both models perform similarly for the baseline cases. However for smaller element sizes the full integration model performs distinctly worse.

Table 4.5: Effect on error of using full integration elements

	1t Case			2t Case			4t Case	8t Case
	Mesh Size x2	Mesh Size x1.5		Mesh Size x2	Mesh Size x1.5			
Reduced integration (Baseline)	-5%	1 %	2%	15%	11%	2%	-4%	4%
Full integration	-10%	-15%	-6%	27%	22%	4%	-4%	2%

These larger differences are mostly likely attributed to locking effects in the full integration elements. These problems worsen with increasing aspect ratio, making them the most prominent in the 1t Case with two times the base mesh. Locking of elements causes additional stresses at the interface, increasing the amount of delaminations. This is exactly what was observed for the 1t case with two times the base mesh. Figure 4.30 shows the damage progression for both reduced and full integration models for the 1t case. As expected, the model with full integration elements shows a significant increase in delamination growth.

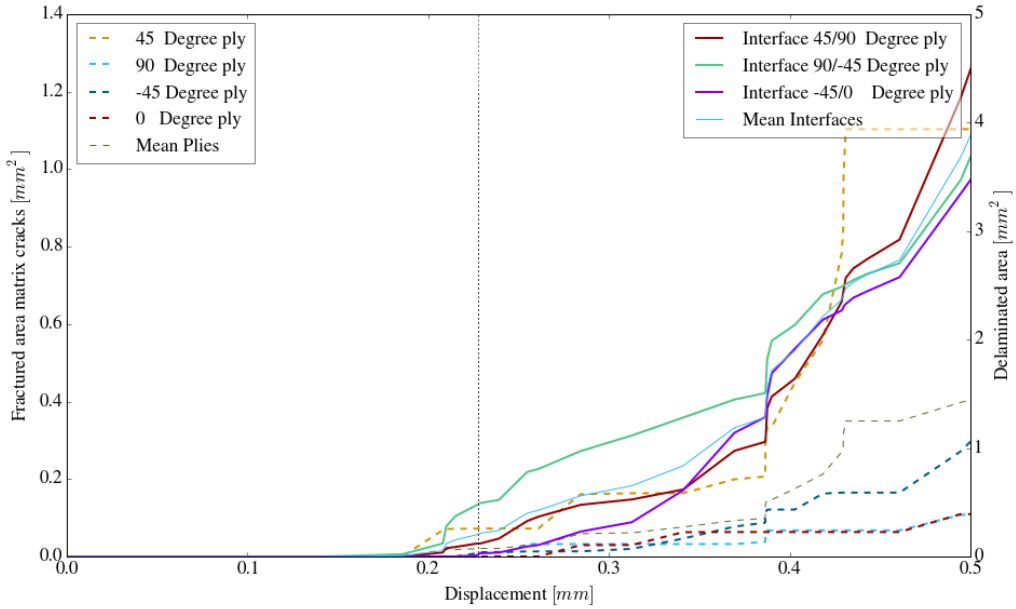

(a) Reduced intergation model

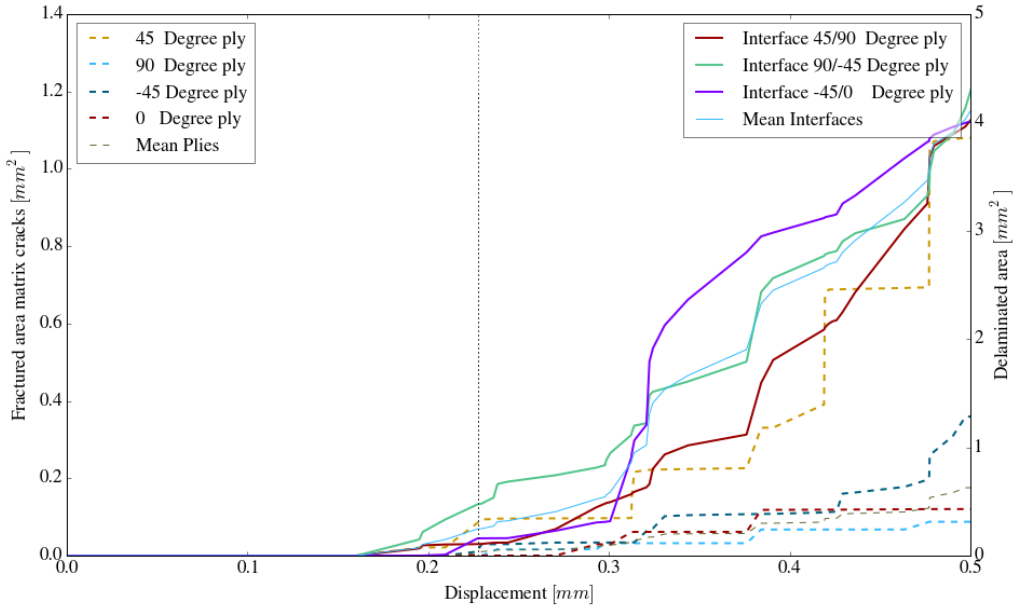

(b) Full integration model

Figure 4.30: Damage progression at 2x the baseline element size for the 1t Case

For models in which elements have a better aspect ratio by a increased total number of elements these locking effects appear to be no longer present. For these models the

displacement field is approximated slightly more accurate, leading to delamination being more mode I dominated. The effect is however only very small, and is only really clearly visible for the 8t case at the 45/90 interface for the focus cases under consideration, which is shown in Figure 4.31. For all other interfaces and cases this issue is not present.

Meanwhile the reduced integration elements provided a significant speed improvement. With the computational time of the models under consideration being dominated by the element evaluation and integration, this increase is roughly a factor 8 for reduced integration elements. FEM results show a total speed increase between roughly 2.5 and 4. This is in line with expectations as only just over half the elements are adjusted, leaving the cohesive zones untouched. Moreover the solving of the system, although of relatively small influence does still contribute in the total computational effort.

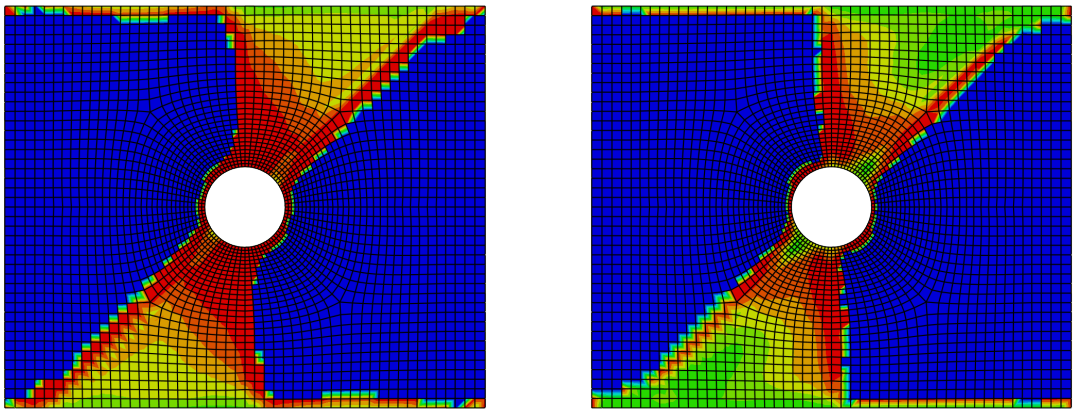

(a) Reduced intergation model **(b)** Full integration model

Figure 4.31: Mixed mode ratio for 45/90 interface in the the 8t Case

4.4.7.3 Failure region identification

The modelling of composites with one through thickness element per ply is an extremely inefficient way to model composite material if no failure occurs. This effect worsens when cohesive zones are also used in between the plies. At the same time it is hard to provide a realistic interface between efficient shell elements and a solid 3D model which incorporates the damage models. Therefore an automatic integration using super elements/ Abaqus substructures was implemented to help improve the computational efficiency and scalability. These super elements are created with a one time run during part generation (Chapter 3). This has two primary effects:

- Reducing the damage to a limited region
- Prevent recalculation of undamaged regions

The former is convenient as it prevents damage in unrealistic regions. A typical example hereof are simplified constraints at the boundaries. The latter is the main aid in improving the computational efficiency. Implementation is done automatically based on a user defined failure region. For the OHT case at hand three configurations have been compared. One full

model, without the use of super elements, one intermediate model and one model with a very small failure region. These models are also shown in Figure 4.32.

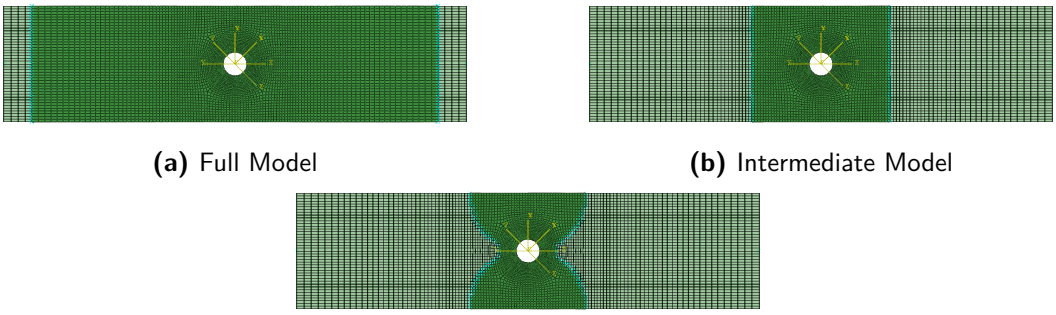

(a) Full Model **(b)** Intermediate Model

(c) Small Model

Figure 4.32: Overview reduced models

The full model is only used for reference and has never been used in this report. The intermediate model was used for all results presented in this report, and does not pose a loss in accuracy up to final failure (it does for the progression after final failure). The small model was accurate as well, but only for the fibre failure dominated load cases in which no damage reaches the boundary prior to final failure. The relative speed improvements for these models are summarized in Table 4.6. Scaling is roughly linear with the number of elements in the failure region, which is in line with expectations, considering the model computational time is not dominated by solving the system. Relative speed improvements may appear small, but are well scalable to larger models considering also that the open hole specimen is one of the more “simple" configurations.

Table 4.6: Speed improvement by failure region identification

	Full	Intermediate	Small
Relative Speed improvement	1	1.56	1.72

Some considerations must be made when using this model reduction, primarily in terms of accuracy. If the following aspects are considered there is in principle no loss of accuracy:

- Failure region is sufficiently large to capture all damage and allow thermal stresses to even out;
- No non-linear effects of any type are present within the super element region.

Results for the super element are maintained by using recovery options, but exclude any damage.

4.4.7.4 Viscosity

The use of artificial viscosity is a necessity in effectively, and computationally efficiently modelling failure if cohesive zones are involved. Without the use of viscosity none of the

models would be able to converge and its use is therefore seen as a necessity as long as implicit analysis are involved. Table 4.7 compares the effects of computational effort and accuracy for the 8t case. As the 8t case is the most delamination dominated load case, the effects are most pronounced here, be it only little more than in the 2t and 4t cases. Viscosity refers to the viscosity of the cohesive zones for delaminations and the viscosity of the extrinsic cohesive zones for the matrix cracks. The same value has been used for both. As the viscosity can also affect the point at which final failure occurs, a comparison is made at three different load levels. For final failure in the model with a decreased viscosity no speed improvement is reported as final failure is missed altogether.

Table 4.7: Effect of viscosity on accuracy and computational efficiency for the 8t Case

	Error [%]	Relative speed improvement [−]		
	Final Failure	Final Failure	30000[N]	Ultimate Failure
Viscosity $5 \cdot 10^{-4}$	98	-	0.28	1.46
Viscosity $5 \cdot 10^{-4}$ (Baseline)	4	1	1	1
Viscosity $5 \cdot 10^{-4}$	2	1.41	1.17	1.40

The results from Table 4.7 are in line with expectations that after a certain viscosity level accuracy is hardly effected, whereas computational efficiency sharply decreases. This was also found for simplified DCB and ENF test not further reported upon in this thesis. As viscosity is seen as necessity no improvement factor is taken into account for Table 4.10.

4.4.7.5 Shear-nonlinearity

Shear non-linearity (β) has been excluded from the analysis for two reasons. It is not known to what extent the implemented damage models describe the same damage processes and it moreover has a significant effect on the computation cost. Shear non-linearity is a material non-linearity that is the consequence of an accumulation of damage. It is whether that damage is also captured by the matrix failure and delamination failure models, with most likely the truth being somewhere in between. No further distinction can be made as the implemented shear non-linearity model [2] is based on a phenomenological model, such that any physical distinction of damage modes is absent. For practical implementation the main reason to exclude this effect was however computational efficiency. A test case using the baseline model with and without shear non-linearity has been run to compare differences in terms of final failure load. The results are tabulated in Table 4.8. For the 1t case no results are reported as the analysis was terminated prematurely by exceeding the maximum allowed number of iterations for the analysis.

Table 4.8: Effect on error of shear-nonlinearity on observed Failure loads

	1t Case	2t Case	4t Case	8t Case
Without Shear-nonlinearity (Baseline)	2%	2%	-4%	4%
With Shear-nonlinearity	-	3%	33 %	15%

The model including shear non-linearity yields significantly different results in the 4t and 8t case, which are more off. This is not entirely unexpected as the shear non-linearity changes the stiffness differences between the plies in similar way as delaminations do. In this case it could well be possible that material shear-non-linearity is for a large part already captured by the degradation of the interracial stiffness with delaminations. Including shear non-linearity, thereby unloads the cohesive interfaces reducing the delamination growth. Moreover this interaction with cohesive zones has dire effects on the computational efficiency for the implementation discussed in this thesis. Table 4.9 compares the speed improvements when shear non-linearity is disabled by comparing the total amount of steps required up to final failure. It can be noted that shear non-linearity severely effects the convergence rate. For this author it can not be argued that any of the models is by definition more true than the other model. The implemented effect of shear non-linearity has been excluded in the baseline model from the perspective of computational efficiency.

Table 4.9: Speed improvement by excluding material shear-nonlinearity

	1t Case	2t Case	4t Case	8t Case
Relative Speed improvement	5.75+	3.22	3.03	1.18

4.4.7.6 Termination Control

The improved convergence framework, with the restart control, allows analysis to continue past the final failure load. As a consequence an analysis may continue for a significant portion of time after this failure load was reached. This is specifically relevant in combination with the previously discussed failure region identification, possibly also invalidating results far past this failure load. A UEXTERNALDB user subroutine calls an external Python termination script after each successful increment. A termination signal is send whenever a 5% load drop is observed at the control node. Based on the baseline model this results in speed improvements is in between 1 (in the 2t case) and 3 (in the 1t case).

Note that the termination script was only used for sensitivity studies in which only the final failure loads are reported.

4.4.7.7 Overview

Table 4.10 provides a rough overview of the improvements in computational effort that can be achieved with the previously mentioned implementations. Although they should only be considered as rough indicators, they prove an important point. A baseline model with 55000 nodes, for which all of these speed improvements are applicable, runs in roughly eight hours. This is achieved using a single core on a 2.6 GHz Intel(R) Xeon(R) E5-2660 cluster machine with 128GB of ram. Further improvements in computational efficiency could only be achieved in two prime ways for this model. Moving to parallel processing, something which is not supported within this framework due to the extensive sharing of common variables (see also Figure 3.2), but could yield significant speed improvements as shown by Vigueras

et al. [13]. Alternatively for this framework other, user defined, cohesive elements could be implemented, which is currently the main source of cutback iterations.

Table 4.10: Overview typical speed improvements

	Typical improvement
Cohesive Zone Strength reduction	1-400
Reduced Integration	2.5-4
Failure Region Identification/Super Elements	1-2
Viscosity	1
No Shear-nonlinearity	1-5
Termination Control	1-3
Total Speed Improvement	2.5-48000

4.5 Multiple crack model

The multiple crack model is an attempt to deal with the limitations imposed by the single crack model. This deals both with expandability to a more general framework, as well as tackling the issues that are apparent for (relatively) simple OHT tests. It should be noted that fundamental solutions can not be provided as the behaviour of Abaqus with XFEM is hardly documented and only allows for very limited control. For more and better control the switch to a more general framework is proposed, moving away from commercial software. This control would most likely directly reduce practical applicability, for which this thesis attempted to provide a framework. In this section an attempt is made to move away from the heuristic method of Section 4.4.1 to tackle the sudden cracking problem and move to as much of a general framework as possible, while still adhering to the limitations imposed by Abaqus. Section 4.4.1, which discusses the sudden cracking problem, provides a great introduction for the problems discussed here.

This section, discussing the multiple crack model, will first again highlight the shortcomings and limitations of the single crack model discussed previously. Four aspects which can control this behaviour are consequently discussed: Selection of the enrichment regions in Section 4.5.2, the Crack Limiting Function (CLF) in Section 4.5.3, a matrix-failure delamination coupling in Section 4.5.4 and mesh requirements in section 4.5.5. A single set of results is finally presented in Section 4.5.6, which is again also compared to X-Ray CT scans.

4.5.1 Limitations of the single crack model

Limitations in the single crack model can be subdivided into two parts: Limitations that are apparent for the single crack model in the application of OHT tests, and more extensive limitations that prevent application in a more general framework in which damage initiation is not limited to a single confined region. A simple example of this would be a specimen with two holes instead of one. For the former case the main limitations would be:

- Only one crack can grow at a time per ply;
  - Total damage is limited;
  - Unable to deal with asymmetries;
- Sudden cracking after completion of cracks ("Sudden cracking problem" of Section 4.4.1);
- Parallel cracks attempt to join (Baseline 4t case of Section 4.4.2.1).

Moreover, for the framework with multiple damage initiation locations, the following additional limitations are apparent:

- Cracks can initiate only at one of these damage locations;
- Matrix cracks from multiple initiation regions cannot combine;
- Limited total amount of initiation regions.

As multiple cracks cannot grow per enrichment region, a single enrichment region per ply would limit the damage to a single location. Subdividing a ply in multiple enrichment regions would cover this problem, but the matrix cracks would be limited to those enrichment regions and could not join with cracks from neighbouring regions. Moreover there is a constraint on the total amount of enrichment regions of 20 per model [49]. Specifically if through thickness symmetry is not applicable this constraint is quickly met.

4.5.2 Enrichment regions

All the limitations of XFEM in Abaqus, apart from the limit of 20, are restrictions per individual enrichment region. It is therefore that control of these regions also to a very large extent controls the behaviour of the matrix cracks. Previously a single enrichment region was employed per ply, making the problems the most apparent. Two methods in which the single enrichment regions are split into multiple enrichment regions are discussed here, both with their respective advantages and downsides.

4.5.2.1 Crack splitting

Crack splitting is employed to tackle the problem of asymmetric cracking. The application is for now limited to open hole specimens, or other specimens for which some pre-existing knowledge on where damage will initiate is present.

Experimental observation from the Nixon-Pearson case and the experimental campaign of the next chapter shows typical damage initiation patterns for open hole specimens in regards to matrix cracking: Cracks grow along the fibre direction and typically initiate tangent to the hole or normal to the hole, as for e.g. cracks in the 90 degree layer of the test cases as extreme cases. For generic open hole specimens therefore only four extreme damage initiation locations need to be considered, as indicted in Figure 4.34a for a generic fibre orientation. This division in four enrichment regions for this verification case is provided in Figure 4.33. Alternatively, to limit the total amount of enrichment regions, the division cutting through the fibres may be left out keeping only the division parallel to the fibres.

Still, with these divisions, new issues arise. Damage can only initiate at the holes, with a single crack per enrichment region. Moreover a significant amount of enrichment regions may be required which can not be combined with the Abaqus imposed constraint limiting this number to 20 in total. In practical application the set-up is effective in solving the asymmetric cracking problem, but has a troublesome practical implementation. Within the Part Generation outlined in Chapter 3 functionality was build in to do so around a circular hole in laminates with arbitrary ply orientations. An example is shown in Figure 4.33.

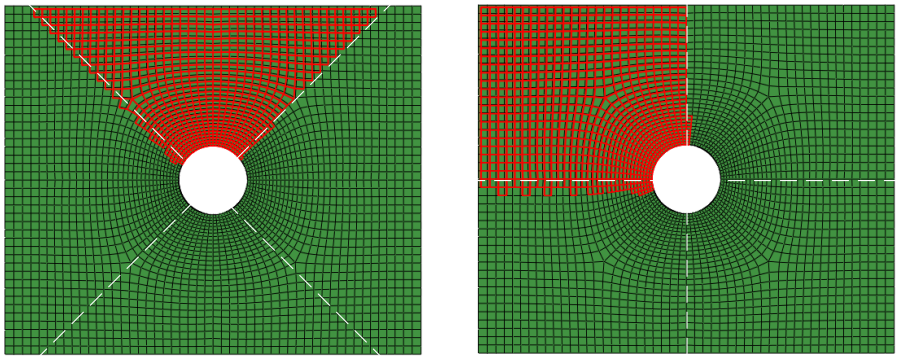

Figure 4.33: Crack splitting for 45/-45 and 0/90 degree layers

As can be noted from Figure 4.33, right at the boundaries of the division region, elements cannot adequately be mapped to either one of the regions. It is ensured that all elements are enriched, but the resulting boundaries are not smooth. This can partially be attributed to a heuristic approach to create this mapping. More importantly however, a true smooth boundary requires the mesh to be aligned with the fibre orientation. This approach works well if the matrix cracks initiate were expected as shown in Figure 4.34a. However, specifically for the ply blocked laminates there is tendency to sometimes move away from these locations as was also shown in Figure 4.29. Alternatively problems exist for cracks which initiate normal to the hole, such as in the 90 degree layer of the test case. If cracks move towards, or are at the boundaries of the enrichment regions, the rough edges may cause cracks to prematurely reach the boundary of the enrichment region. Consequent behaviour for XFEM in Abaqus is undocumented, but practical implementation has found the following to hold:

- Cracks can pass through enrichment regions into adjacent enrichment regions;
  - This holds also if the cracks were already initiated in the previous enrichment region;
  - If the crack progresses into a neighbouring enrichment region no new crack can initiate in this new enrichment region;
- Fracture is recomputed for the whole adjacent enrichment region as the crack progresses into the new region;
  - Fracture is also recomputed for the whole of the original enrichment region if the crack reaching the boundary was the only crack in that enrichment region as all

cracks in the enrichment region have now completed [4];

– Fracture is not recomputed for the original enrichment region if uncompleted cracks are still present in the enrichment region.

In practice the above results in frequent re-computations of crack initiation if a crack progresses around the boundary of the enrichment region, such as for cracks in the 90 degree layers of the test case. This frequent re-computation is therefore very likely to trigger a reduced form of the "Sudden Cracking Problem" of Section 4.4.1. In order to complete the analysis enrichment can again be disabled but this may lead to cracks that are unable to complete up to the edge of a specimen altogether. This problem may be circumvented by ensuring smooth boundaries at the enrichment regions. However, this would require a mesh that is strongly dependent on the fibre orientation, such that elements can be aligned. Moreover the cohesive interface between the plies becomes troublesome in such cases. In practice the advantages of using XFEM in such a case is no longer present. Rather, to solve these problems a series of CLFs are introduced in Section 4.5.3.

4.5.2.2 Damage imitation regions

The concept of damage initiation regions is based on the re-computation of fracture when cracks move through enrichment regions, discussed in the previous subsection. Two regions are defined: a crack initiation region, just around the hole or any region where damage initiation is found to be likely, and a crack growth region past the initiation region as shown in Figure 4.34b. The basic idea is as follows: cracks will initiate in the initiation region and will consequently propagate a short distance up to the boundary of this region. Here the crack will cross the boundary, and will continue in the damage growth region. As the crack in the initiation region is now complete, new cracks can initiate and grow again up to the boundary of the initiation region, repeating the procedure. In principle this approach should be able to solve close to all problems previously mentioned for the single crack model:

- Multiple cracks are possible at the same time;
- Sudden cracking is reduced as multiple cracks can now coexist providing load relief preventing additional cracks to initiate;
- Multiple crack initiation positions are possible.

However primarily the following issue still remains:

- Parallel cracks attempt to join;
- Limited total amount of initiation regions.

The latter issue can also be partially circumvented by combining enrichment regions of multiple layers. As an example the concept would also work with one growth region for all plies combined with a separate initiation region for all of the individual plies.

In practice the concept relies heavily on the idea that damage initiates in the enrichment region and continues to grow after this. For small initiation regions in the test case this is

[4] Completion requires a degradation factor of 1 for the inserted cohesive zones as well

true, however cracks consequently join right after entering the growth region. Therefore a sufficiently large initiation region must be considered. Moreover, as matrix cracks are still added discretely per element, a minimum number of elements is required in the initiation region introducing the mesh size dependency of the form given by equation (4.1).

$$R_{init} = max(f(R_{hole}), n \cdot l_{elem}) \tag{4.1}$$

A practical value is given by mesh size requirements discussed subsequently in Section 4.5.5 and is not driven by the physics of the problem. Mostly this is determined by the CLFs that are applied.

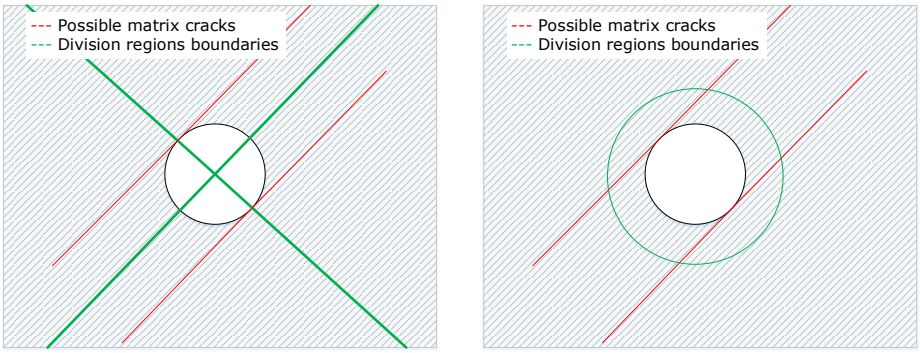

(a) Crack splitting enrichment regions **(b)** Damage imitation enrichment regions

Figure 4.34: Division of enrichment regions

4.5.3 Crack limiting functions

The introduction of the multiple crack model requires the introduction of CLFs mostly to prevent the sudden cracking problem of Section 4.4.1. The full disabling of XFEM for a given enrichment region is no longer feasible, as this prevents the essence of the multiple crack model. Therefore a more fundamental solution is sought after, within the limitations of the Abaqus framework. The baseline for this is the Crack Limiting Function (CLF). The previously discussed sudden cracking problem follows from insufficient step-size control within Abaqus. As the sudden cracking problem is a true “sudden" problem, cutbacks in the time steps do not work. Cutbacks are used to reduce the highest failure indices to within a tolerance margin of 1-1.05. As step-size control is unable to do so, after a fixed number of (5) unsuccessful increments the analysis is continued with failure indices still above the upper threshold value of 1.05. This causes a large amount of cracks to initiate in the same time increment.

It is argued that this is unphysical process as normally some cracks would have already initiated, but are constrained to do so by the XFEM implementation in Abaqus. If these cracks did however initiate they are likely to provide some form of load relieve, preventing the initiation of additional cracks. The CLFs are introduced to constrain this behaviour allowing some cracks to provide this load relieve.

User control of XFEM can only be provided within the UDMGINI subroutine by controlling the failure indices that are passed through. There is however only a very limited amount of information passed through to the subroutine. The use of some CLFs therefore requires careful model preparation as discussed in Chapter 3. Moreover additional subroutines are required to extend the information, using a set of common variables to pass this information, as was shown in Figure 3.2. Some CLFs are therefore based on random numbers to reduce these dependencies, arguing that the prime importance is to provide load relieve to prevent other cracks from initiating. All random numbers in the subroutines are always seeded using a combination of either element ID and/or the time increment to allow for repeatability. It is important to note that the UDMGINI subroutine is not evaluated once for all elements at every time increment. If no crack is present this holds, but as soon as cracks grow only elements around the crack tip are analysed posing a significant limitation for most CLFs.

Load history During analysis a loading history is recorded for the five last successful increments. Subsequently an adjusted failure index is given by equation (4.2).

$$FI = \frac{W_0 R_0 FI_n + W_1 R_1 FI_{n-1} + W_3 2 R_2 FI_{n-2} + W_3 R_3 FI_{n-3} + W_4 R_4 FI_{n-4}}{W_0 R_0 + W_1 R_1 + W_3 2 R_2 + W_3 R_3 + W_4 R_4} \tag{4.2}$$

In equation (4.2) the value R_i refers to randomly generated numbers between 0-1 whereas W_i are associated weights within the loading history. The use of this CLF is relatively simple in its implementation and provides some of the desired functionality. If the failure index is a monotonic rising function then failure is only delayed by at most 5 time increments, providing in some sense similar effects as the viscosity already used for fibre failure and the cohesive zones. This CLF significantly reduces the chance of sudden fracture, but does have some associated problems:

- Previously recorded failure indices FI_i are typically not from the past four increments;
- Significant weight is required on previous time increments;
- Randomization with loading history conflicts with automatic time control.

All of these points also conflict with each other. As historic failure indices are typically from prior to the initiation of the first crack, this delay is often significant. Moreover around the crack tip failure was evaluated later, with less delay, making clustering of cracks likely. As previously recorded failure indices are typically very old, a significant weight is put on these, which does not represent the current loading state. Finally, this randomization interacts strongly with the automatic time control of Abaqus. Either a linear or second order extrapolation of the failure indices is used in Abaqus to determine the required time step. As the failure indices are now a random function of time, the extrapolated function is no longer smooth and convergence rates are reduced.

Total amount of imitated cracks As a more robust alternative, a limitation on the total amount of cracks that can initiate at any given time increment is proposed and implemented. It is assumed that fracture occurs whenever a failure index above 1 is recorded. Failure indices

above 1 are reduced to 0.99 as soon as a critical threshold value for the total amount of cracks is reached. The limitation is implemented on a ply to ply basis. The part generation of Chapter 3 is therefore essential as it allows layers to be identified by their associated element IDs. As meshes are generated in a structured manner, it is likely that cracks will cluster as the UDMGINI subroutine is called for consecutive element numbers. In general, elements with similar element numbers are positioned close to each other. To overcome this problem, also during part generation, the element numbers for each ply are randomly shuffled and reassigned such that clustering of cracks cannot occur.

It is noted that this method does not limit the total amount of cracks, but only the amount of cracks that can initiate during a given time increment. In practice, on rare occasions problems can occur as a failure index above 1 may not always mean that a crack initiates. Previously evaluated elements with a crack may be re-evaluated if a new crack is in the proximity. A new crack can however not initiate at this element as a crack is already present. These problems are always momentary of nature. Either a large amount cracks should be allowed as a threshold value, which undermines its function, or additional measures need to be taken to prevent an analysis from getting stuck, such as random element evaluation.

Maximum failure index A maximum failure index based CLF is employed specifically for the sudden cracking problem. As regular time incrementation after the completion of a crack is not always able to reduce all the failure indices to within the threshold range of $1 - 1.05$ an additional control parameter is introduced. Failure indices are normalized by the maximum value to reduce the number of cracks initiating, as given by Equation (4.3). As the maximum value requires all elements to be evaluated before the normalizing value can be determined a one time increment delay is introduced.

Similarly to the limitation on the total amount of cracks, normalization may cause an analysis to get stuck. Slightly lower normalizing values can be employed or a form of random element evaluation is again considered.

$$FI = \frac{1.05FI_n}{max(FI_{n-1})} \tag{4.3}$$

Random element evaluation Random element evaluation is used as an additional control variable to prevent analysis from getting stuck. It can be used as a CLF as well, but performs less well than the other CLFs in this aspect. For each time increment only a select number of elements are allowed to have a failure index above 1. The unevaluated elements have in this case a maximum possible failure index of 0.99, preventing them from failing. The elements that are evaluated are based on an increment based random seed. If a large enough percentage of evaluated elements is taken it does not effect the solution, but does allow a stuck analysis to continue after some time increments.

4.5.4 Matrix Failure-Delamination coupling

The introduction of multiple matrix cracks per layer causes new cracks to initiate continuously during the loading of the specimen. These new cracks are much more influenced by the

damage created by previously initiated matrix cracks and other failure modes as they initiate at higher load levels. As the CLFs, such as the CLF based on the maximum failure index, use a prioritization this updated damage state needs to be taken into account. In general this is done implicitly by the updated constitutive behaviour of the laminate. However, specifically for matrix failure, previously assumptions were made for in-situ strengths in Section 3.2.2. Delaminations, which at the increased load levels may become apparent, can cause a reduction in strengths. Without a local strength reduction, matrix failure is more and more likely to initiate away from the hole. This can cause problems with the concept of the damage initiation (enrichment) region, and can also be argued to be unphysical. To remove this effect a coupling to the local delamination degradation factor of the adjacent cohesive interfaces is introduced.

Using the URDFIL and POSFILL subroutines, after each successful increment the degradation factor of the interface elements are retrieved. These degradation factors are accessible as common variable within the UDMGINI subroutine as also shown in Figure 3.2. Interface elements are identified with a $+-10000$ offset in element ID compared to the ply elements. Both interfaces are able to provide a 50 % reduction towards the non in-situ, UD, ply strengths. A linear coupling is implemented, such that the strengths are a smooth function of the degradation factor.

4.5.5 Mesh requirements

Although the use of XFEM is supposed to alleviate strong mesh requirements, current implementation allows this to only truly hold for the development of initial cracks, such as in the single crack model. In the multiple crack model, mesh requirement become apparent as a sufficiently large spacing is required for parallel cracks to develop. The requirements are best explained using Figure 4.35. In Figure 4.35 a damage imitation region corresponding to one row of elements has been used, indicated by the green (semi)-circle. This, in theory, would allow for the fast succession of subsequent cracks. In practice, miss-alignment with the mesh quickly halts this.

In Figure 4.35 three cracks are shown labelled 1 to 3, corresponding their initiation order. Crack one initiates first without problem, similar as to what would happen in the single crack model. Subsequently, for crack two, initiation is determined but the crack is unable to grow in the desired direction as the crack tip would reach an element which was already fractured. To prevent this problem the crack is automatically forced to grow away from this element face, overriding the user defined fracture angle and effectively cutting the fibres. There is no way to control this behaviour as a user with the XFEM implementation of Abaqus. Crack three subsequently faces a similar problem but rather than forcing the crack to grow away it is joined with crack number two.

This is a process that is frequently observed, specifically in the multiple crack model, but was also observed previously in the single crack model. Examples are provided in Figure 4.16 and 4.18 for the 4t case of the baseline model and Figures 4.27 and 4.28 for the 2t case without in-situ strengths.

A practical solution for this problem is not at hand, making it among the main limiting factors for the multiple crack model. The problems are to a large extent driven by the use

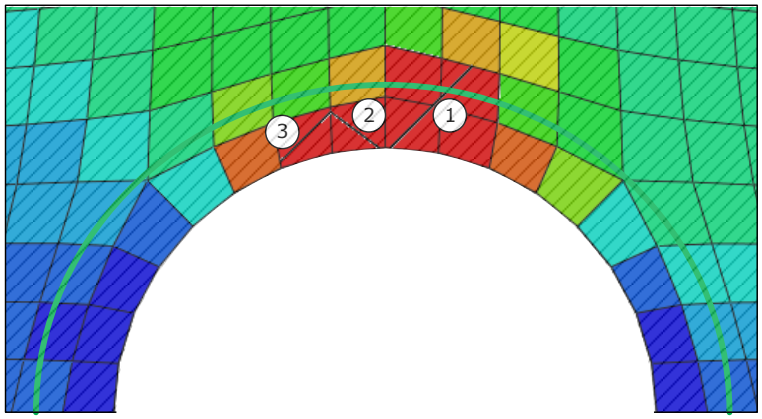

Figure 4.35: Development of parralel cracks

of hexahedral elements. The problem could be greatly reduced if elements with triangular faces were to be employed. This option is however in the current framework not feasible as was explained in relation to Table 3.2. Tetrahedral elements are unfavourable from the consideration of computational efficiency and continuum shell or wedge elements are unavailable for use with XFEM. Tria elements are available with XFEM but would result in a significant loss of accuracy and versatility.

Within the current framework, when using damage initiation regions, the only practical solution is to use a large initiation region. This prevents cracks joining just after the initiation region. Moreover, as these cracks develop, it is likely that the damage state in the laminate changes thereby also increasing the likelihood that new cracks develop in a different region. This specifically applies if the matrix failure-delamination coupling is used. Although the application of a large initiation region is limiting the initiation of damage, it is the best that can be achieved within the current framework with Abaqus.

Mesh size requirements are also apparent for the possible crack spacing. Current stability of the multiple crack model makes it however impossible to investigate this. Previous work by Van der Meer on the same specimens did however show that this was something that needs to be controlled [61].

4.5.6 Results

One set of results is provided for all the baseline test cases. For this purpose a combination of the previously described CLFs is used in conjunction with a special mesh and enrichment regions. These settings provided the best relative result if all test cases are considered.

As CLFs the load history is taken into account only very marginally as this may otherwise significantly effect the convergence rate with $W_0 = 1$ and $W_1 = 0.1$. The total amount of cracks was limited, but the limit was never reached in all cases. A normalization based on the maximum stress index was also employed combined with a slight random element evaluation of 0.75 of all elements per time increment.

The enrichment regions are divided using a crack initiation region. As relatively many of CLFs are used, this regions size (R_{init}) is defined such that it encompasses one ring of elements around the hole, thereby minimally hindering the total amount of damage that can initiate. Additionally, the mesh was aligned with the 45 and -45 degree plies in an attempt to prevent the joining of cracks.

Only a single set of results is provided, with uniform settings, to provide a realistic image of the applicability of the multiple crack model with Abaqus. This is the set of results that provided the best overall results for the whole range of test cases. For individual cases the use of different combinations of CLFs and enrichment regions can provide more realistic failure patterns, but this would result in higher level of case dependency and possibly additional convergence issues.

The results are provided in two subsections. One subsection for the results at 95% of the failure load and past the ultimate failure load for all the baseline cases. A second subsection provides again a comparison for the 2t case against experimental CT results.

4.5.6.1 Baseline results

Table 4.11 provides the relative errors for all the baseline cases. It can be noted that the results for the multiple crack model have a slightly larger error, but are still in good agreement considering experimental scatter.

Table 4.11: Model errors multiple crack model

	1t Case	2t Case	4t Case	8t Case
Single crack model	2%	2%	-4%	4%
Multiple crack model	-3%	2%	-11%	-9%

However, arguably more important are again the accompanying failure patterns, focussing this time specifically on matrix failure patterns. The failure patterns at 95% and past the ultimate failure load level are provided in Figures 4.36 to 4.43. All results suffer from some parallel cracks joining or cracks that grow away from the user defined fracture plane 4.5.5, even with the aligned mesh. Even tough the occurrence of this phenomenon is greatly reduced, its unphysical occurrence is still one of the major issues with the current implementation in Abaqus.

For the 1t case damage patterns are very similar to the single crack model, with the development of only a few very minor secondary cracks as can be observed in Figure 4.36. The most notable feature is for the 45 degree layer, in which a single crack follows a unphysical path. Only post final failure parallel crack really start to develop as can be observed in Figure 4.37.

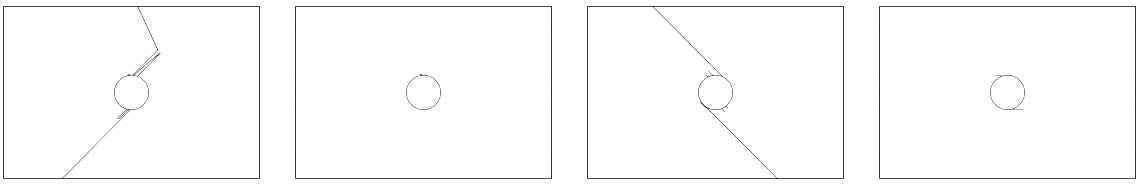

(a) 45 Degree ply **(b)** 90 Degree ply **(c)** -45 Degree ply **(d)** 0 Degree ply

Figure 4.36: Matrix failure at 95% of the failure load for the 1t case

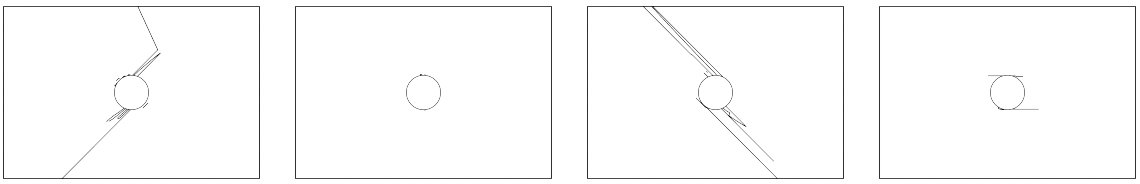

(a) 45 Degree ply **(b)** 90 Degree ply **(c)** -45 Degree ply **(d)** 0 Degree ply

Figure 4.37: Matrix failure at the ultimate failure load for the 1t case

Results for the 2t case show relatively little development of secondary cracks or parallel cracks. At a load level of 95%, as in Figure 4.38, only the -45 and 0 degree layer shows a clear increase in the total amount of cracks. This is in line with experimental results and is further discussed in the next subsection. Past ultimate failure this does not increase significantly. Further discussion is provided in the subsequent subsection for this case.

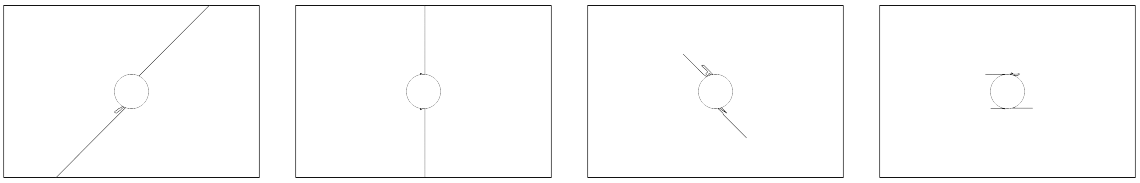

(a) 45 Degree ply **(b)** 90 Degree ply **(c)** -45 Degree ply **(d)** 0 Degree ply

Figure 4.38: Matrix failure at 95% of the failure load for the 2t case

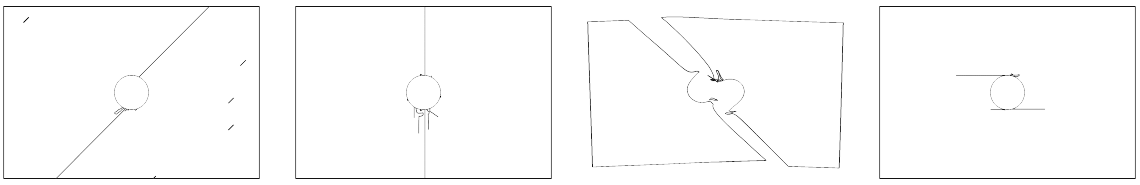

(a) 45 Degree ply **(b)** 90 Degree ply **(c)** -45 Degree ply **(d)** 0 Degree ply

Figure 4.39: Matrix failure at the ultimate failure load for the 2t case

For the 4t case the development of parallel cracks is again more dominant. Figure 4.40 shows

again the failure patterns at a 95% load level. Noticeable is again a crack in the -45 degree layer which is not aligned with the fibre direction. Past final failure the development of secondary cracks is more significant. Past final failure, ultimate failure is now also predicted relatively accurately with an error of -9%. This can be seen as promising, considering the single cracks model was not able to achieve such results with ultimate failure typically occurring significantly earlier for the 4t case. Still, not too much value should be attached to this error since it is just a single result for which also unphysical damage patterns are visible in the -45 degree layer.

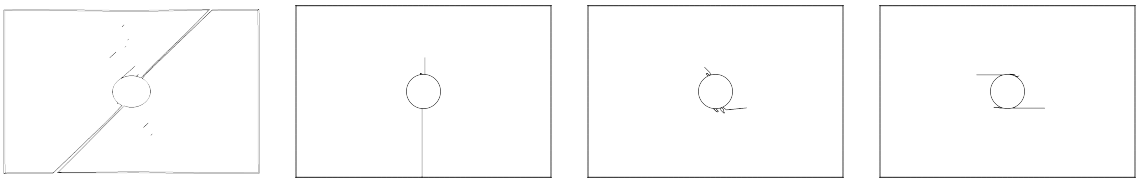

(a) 45 Degree ply **(b)** 90 Degree ply **(c)** -45 Degree ply **(d)** 0 Degree ply

Figure 4.40: Matrix failure at 95% of the failure load for the 4t case

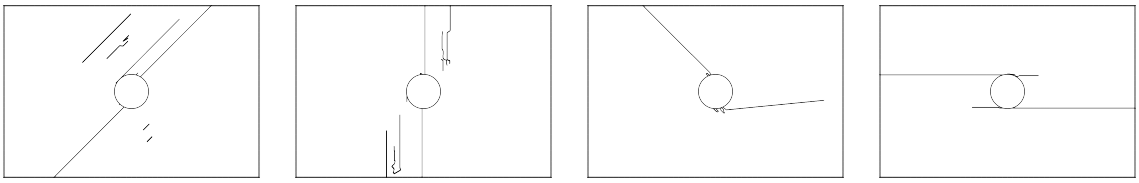

(a) 45 Degree ply **(b)** 90 Degree ply **(c)** -45 Degree ply **(d)** 0 Degree ply

Figure 4.41: Matrix failure at the ultimate failure load for the 4t case

The 8t case is finally presented in Figures 4.42 and 4.43. The 8t case clearly presents the development of multiple parallel cracks. Moreover the effect of the matrix-crack delamination coupling is clearly visible with the shift of cracks in the 90 degree ply. Whether this is a more accurate result can not be said without experimental evidence for this case. Again also strongly noticeable for this case is the development of four cracks in the 0 degree ply. This is in line with experimental evidence [3] and was not possible for the single crack model.

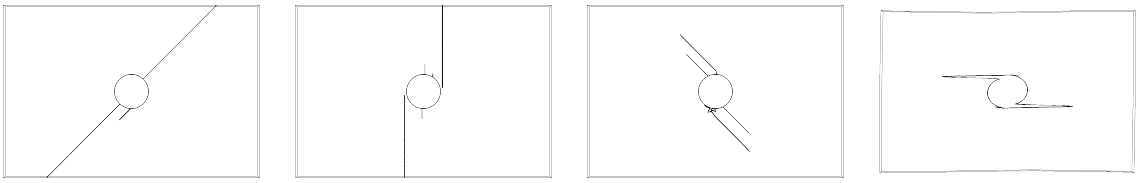

(a) 45 Degree ply **(b)** 90 Degree ply **(c)** -45 Degree ply **(d)** 0 Degree ply

Figure 4.42: Matrix failure at 95% of the failure load for the 8t case

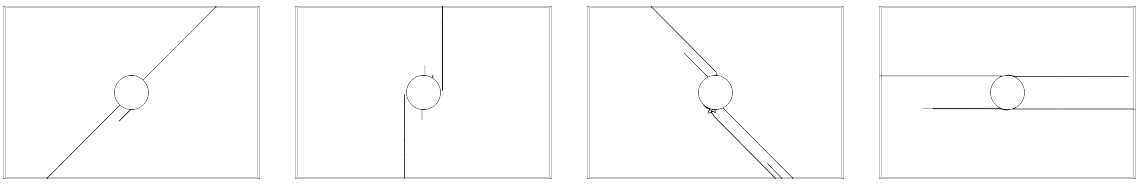

(a) 45 Degree ply **(b)** 90 Degree ply **(c)** -45 Degree ply **(d)** 0 Degree ply

Figure 4.43: Matrix failure at the ultimate failure load for the 8t case

4.5.6.2 Comparison with experimental CT scans

For the 2t case a comparison with experimental CT data [3] is again made. Figure 4.44 presents the results at a 60% load level and Figure 4.45 at a 80% load level.

A relatively good agreement with experimental results can be noted, specially when compared to the single crack model presented previously. At a 60% load level the only noticeable difference is observed in the 45% degree ply. This discrepancy was previously noted to be of relatively little significance as there was a high level of crack growth around this load level in the single crack model as discussed in Section 4.4.3. The same applies for the multiple crack model of this section.

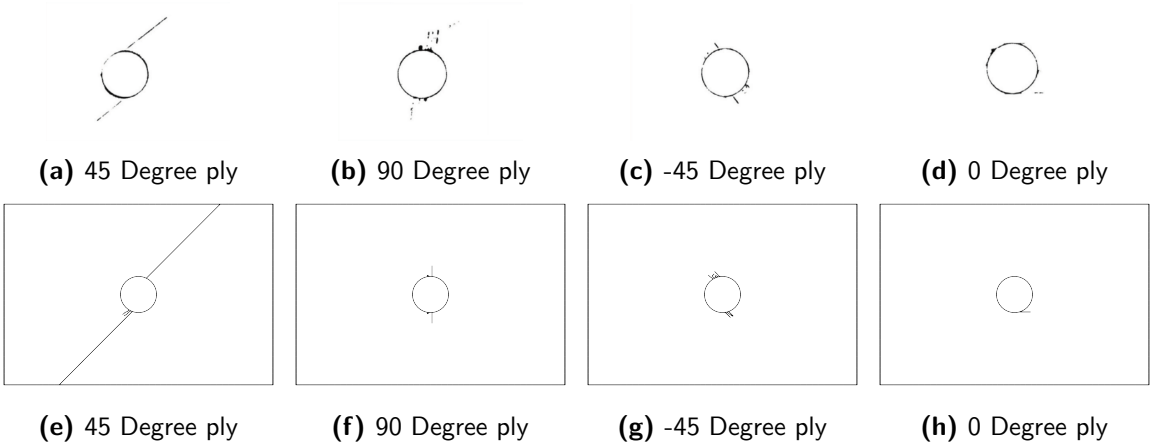

(a) 45 Degree ply **(b)** 90 Degree ply **(c)** -45 Degree ply **(d)** 0 Degree ply

(e) 45 Degree ply **(f)** 90 Degree ply **(g)** -45 Degree ply **(h)** 0 Degree ply

Figure 4.44: Matrix failure damage patterns at 60% of the failure load compared to experimental results [3]. Experimental top, model bottom.

At the 80% load level differences are more apparent, specifically in the 90 and -45 degree layers. The remaining differences also highlight the unsolved shortcomings within the current framework using Abaqus. In the 90 degree ply, the cracks in the experimental data are not continuous but rather form a band of multiple parallel cracks. The current numerical model, using Abaqus, is fundamentally unable to reproduce this behaviour for two reasons:

- The cracks do not all initiate around the hole;
- A band of discontinuous cracks is formed.

The forme issues relates to the definition of enrichment regions, for which the concept of a damage initiation region cannot be established. As such, the damage in these cases will be underestimated as new cracks can not initiate. This applies for all layers, but is most apparent for the 90 degree ply. Even if this issue could be solved by clever definitions of the enrichment regions within Abaqus the latter issues present itself. The development of multiple parallel cracks will not be possible as Abaqus will most likely join these cracks in the direction of the crack band creating unphysical failure patterns.

The -45 degree layer similarly presents an issue with multiple cracks joining. The joining of parallel cracks undermines the total amount of damage. It can be controlled by making more severe use of CLFs, but this as well undermines the total amount of damage. The only factor that could possibly better control this behaviour is the previously discussed switch to elements with triangular faces such as tet and wedge elements.

The matrix failure-delamination coupling does provide for this case better results for the 0 degree layer for which now longer cracks are present, driven by the reduction in strength due to delaminations at the -45/0 ply interface.

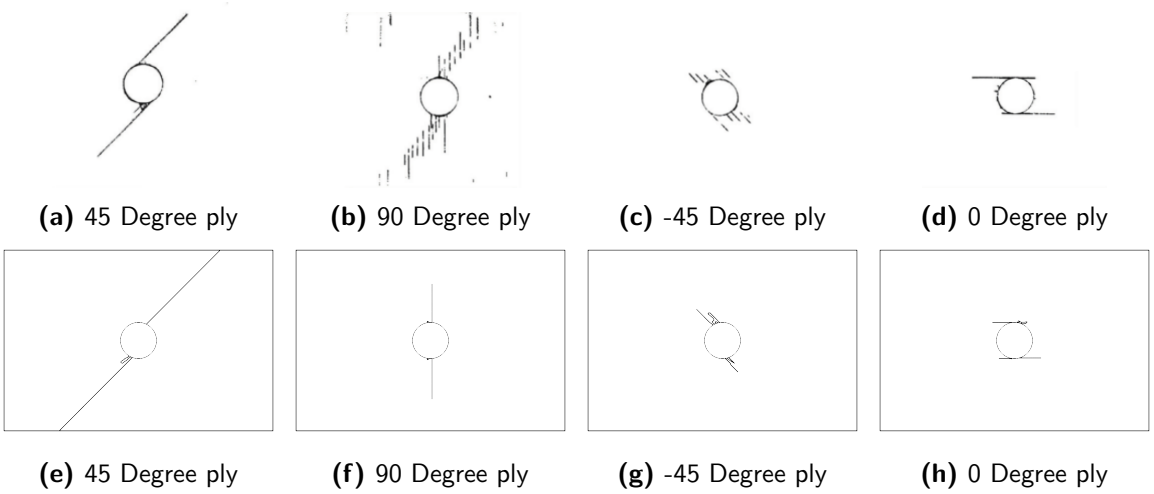

(a) 45 Degree ply **(b)** 90 Degree ply **(c)** -45 Degree ply **(d)** 0 Degree ply

(e) 45 Degree ply **(f)** 90 Degree ply **(g)** -45 Degree ply **(h)** 0 Degree ply

Figure 4.45: Matrix failure damage patterns at 80% of the failure load compared to experimental results [3]. Experimental top, model bottom.

4.6 Conclusions

While the results presented in this chapter appear promising, specifically when compared to previously obtained results for the CDM implementations [2], a large amount of issues are still apparent. This relates to issues on all fronts: Issues regarding the implemented damage models, also previously discussed in Chapter 3; Issues with the implementation of these damage models and the accompanying model uncertainty, specifically relating to the single crack and multiple crack model. Finally there are issues regarding computational efficiency.

Although already previously highlighted in Chapter 3 with the model description, a high level of uncertainty is present in the implemented damage models through a lack of physical

grounding and implementations at a meso-mechanical level. Even if acceptable results are obtained for some cases, these may not translate to other cases. The fibre dominated load case, without ply blocking, is relatively easy to predict, even with CDMs [2]. Such laminates may be more common in industry practice, but may not be applicable to test PDA models. The delamination dominated load cases feature a high level of interaction and (delamination driven) final failure is easily missed. The cohesive zone model for matrix cracks and delaminations provides an easy implementation but the true input parameters are too much unknown and based on assumptions. Strength corrections for cohesive zones, in-situ strengths both affect the traction-separation behaviour in a different way. Still it is assumed that fracture toughness values are similar for both delaminations matrix cracks, leading to very different traction-separation behaviour. It is impossible to justify this from the little physical meaning that the cohesive zone model possesses.

At the same time current implementation in Abaqus presents severe difficulties in properly assessing this. The single crack model, although now relatively stable to run, is very limiting in the damage it describes and is hard to extend to more generic laminates and loading conditions. This specifically relates to matrix cracking. The limitations of this model also make it hard to provide definitive conclusions on the obtained results. For the verification case of this chapter this was partly done by the investigation of a crack-spacing parameter in a previous implementation by Van der Meer [61]. Although both models are comparable, implementation is different on aspects such as the in-situ strength, material shear non-linearity and fracture toughness's making a comparison difficult.

The multiple crack model attempts to tackle the problems of the single crack model, but is only partially able to do so. Inherent limitations within Abaqus make it impossible to move forward and a true multiple crack model can not be considered. To do so, it is advised to move away from the framework using Abaqus to a framework in which more control is possible and limitations are removed. The example result set from the multiple crack model shows only a limited set of parallel cracks developing, which does seem slightly better in line with experimental results, but is still relatively unstable. The sudden cracking problem is however no longer present and, asymmetric more generic laminates are also no longer an issue.

If it is infeasible or undesirable to move away from Abaqus for any reason, an improved version of the single crack model is advised taking the most important aspects from the multiple crack model into account. The use of special enrichment regions, different from the one region per ply in the single crack model, is advised such that generic laminates can be considered. Specifically the model which considers a damage initiation region is suitable for this. A relatively large initiation region is advised considering at least three elements from the edge. Heavy use of CLFs is also advised such that closely spaced parallel cracks, causing the joining of cracks, do not initiate. For this the CLF which normalizes using the maximum failure index is advised, to prevent the sudden cracking problem, together with a strict limitation on the total amount of cracks that can initiate. The use of random CLFs, other than possibly a slight random element evaluation, is not advised as this can severely effect the convergence rate.

Still, it is important to note that this model will always be limited in the damage it can describe and it is very arguable whether a form of the single crack model is ever really sufficient, even with the results obtained in this chapter. Extreme care should therefore be taken when using present implementation for other laminates as it is impossible to quantify

how much the model is off.

Finally, computational efficiency is still a significant issue. The current model provides acceptable run times, on par with the less accurate CDMs. Although framework was implemented that should make scaling better, this can only be done to a limited extent. Different layups, such as the sub-laminate scaled specimens which were not considered are significantly more expensive to evaluate. The addition of cohesive zones for delaminations worsens this effect. Moreover this chapter considered relatively simple specimens with a clearly defined failure region. However, the main issue relates again to the limited amount of matrix damage. More widespread damage will further increase the runtimes. This, in conjunction with the issues related to the uncertainty in the damage models, poses problems in further research and use. Even if more advanced damage models are appropriate it is uncertain if such models could have any practical applicability if these are not at the same computational cost level or lower.

With these critical notes it is easy to forget that the model, although requiring a different framework, still presents great potential. The rate of matrix crack progression appears to match experimental evidence. Moreover the reported experimental triangular delamination patterns can be matched and failure loads are within the experimental scatter. This is all very promising, specifically when compared to CDM implementations [2], in which this was all not possible for some cases. Even for implementations within the current framework sensitivity analysis show these interactions to be very easily missed. It is the ability to capture these interaction that currently provides most of the confidence in the presented model.

5 Experimental campaign and model validation

In order to validate the blended model a validation campaign was performed for which both damage progression and final failure was monitored. This chapter presents the test set-up and the experimental results combined with the results of the implemented model. The conclusion of the previous chapter provided a recommended model which is in this chapter applied for OHT tests on a $[45/-45/0/90]_{2S}$ laminate. Testing combines a number of experimental monitoring techniques to track damage progression in an attempt to provide validation other than simply the failure loads. This includes Digital Image Correlation (DIC), Acoustic Emission and CT. Still this additional monitoring is insufficient and additional testing would be required to provide any real confidence in the model.

First Section 5.1 discusses the test set-up. Similarly, for the FEM model the set-up is discussed in Section 5.2. The test results are split in the final failure results (load-displacement) of Section 5.3.1 and the damage progression results of Section 5.3.2.

5.1 Test set-up

The experimental campaign was performed using a 60 kN MTS loading the specimens at a rate of $1[mm/s]$. A total of six specimens were loaded up to final failure. Two additional specimens were loaded up to approximately 60% and 80% of the final failure load at loads of 18 and 22 $[kN]$ respectively.

5.1.1 Test specimens

The test specimens consist of 8 laminates made of Hexply AS4/8552 UD prepregs. The specimens dimensions are $25[mm]$ wide with a nominal thickness of $2.7[mm]$ in a $[45/-45/0/90]_{2S}$ layup. A centrally located hole has a diameter of $6.35[mm]$. An overview of the relevant material properties is provided in Table 5.1.

Table 5.1: Material properties experimental campaign [7–10]

E_1	135.02	GPa	X_T	4900	MPa
ν_{12}, ν_{13}	0.3	–	X_C	2207	MPa
G_{12}, G_{13}	4.9	GPa	Z_T	–	MPa
E_2, E_3	9.5	GPa	Z_C	–	MPa
ν_{23}	0.45	–	Y_T	52.0	MPa
G_{23}	3.2	GPa	Y_C	199.8	MPa
β	$3 \cdot 10^{-10}$	MPa^{-3}	S_{12}	91.0	MPa
CTE_1	0	mm/deg			
CTE_2, CTE_3	0.00003	mm/deg	$G_{FF}^{(+)}$	$92.0 \cdot 10^3$	J
			$G_{FF}^{(-)}$	$80.0 \cdot 10^3$	J
G_{IC}	220	J			
G_{IIC}, G_{IIIC}	1000	J	$p_{\perp\perp}^{(-)}$	0.225	–
σ_1	80.7	Mpa	$p_{\perp\perp}^{(+)}$	0.225	–
σ_2, σ_3	114.5	MPa	$p_{\parallel\perp}^{(-)}$	0.25	–
$BK\ Value$	2.08	–	$p_{\parallel\perp}^{(+)}$	0.3	–

5.1.2 Acoustic Emission

To monitor the progression of non-visible damage use is made of acoustic emission. Acoustic emission functions by detecting shock waves at sensors placed on the specimens. Each of these shockwaves typically corresponds to a damage event such as matrix cracking, delaminations or fibre failure. The recorded energy corresponds to the intensity of each damage event. It does however not provide information on the type of damage and the location. With additional processing this may be retrieved in some cases as well but this was not done for this experimental campaign. Monitoring of the frequency of these damage events can be done live while testing, which sets the threshold for the interrupted tests. An example of the acoustic emission set-up is provided in Figure 5.1b.

5.1.3 Digital Image Correlation

At the back side of each specimen a spickle pattern was applied which can be tracked, allowing for the computation of local strain and displacement patterns. This allows for comparison of numerical strain patterns during loading up to the point of final failure. The set-up made use of a commercial VIC3D system using two 5MP cameras. The use of DIC, although limited to the outer plies of the specimen, allows for valuable information on the progression of damage as the evolution of strain patterns can be matched to the numerical model. Local failure, such as delamination or matrix cracking, will cause changes to the global behaviour of the specimen which can be observed in changing strain patterns. Limitations of the system are for this application primarily in the resolution of the cameras. An overview of the DIC set-up is provided in Figure 5.1a.

5.1.4 X-ray CT

For three of the tested specimens additional 3D X-ray CT is performed. Two specimens are scanned prior to failure, at load levels of 60 and 80% respectively. One specimen is scanned after final failure. The CT scans provide information on what the failure patterns look like, but only in limited extent on the rate of damage progression. Specimens are scanned at a resolution of 12 μm, without the use of additional dye penetrant. This resolution is too low for small damage or cracks that just initiated [77], but is sufficient for complete damage patterns after failure in an unloaded condition.

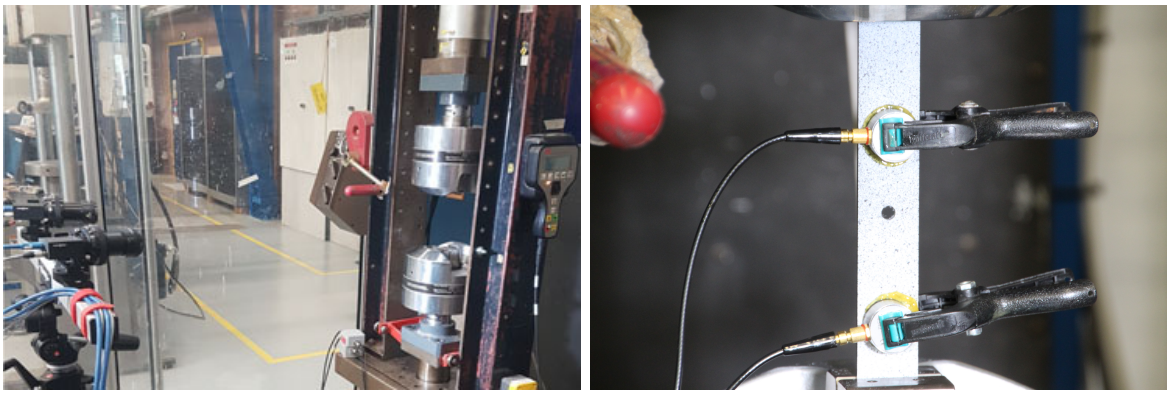

(a) DIC set-up **(b)** Acoustic emmision set-up

Figure 5.1: Overview test set-up experimental campaign

5.2 FEM implementation

The FEM implementation for the experimental campaign follows the same outline as for the Nixon-Pearson verification case of Chapter 4. The model is generated as outlined in Chapter 3 using both the single and multiple crack model of Chapter 4. The multiple crack model was applied with heavy use of CLFs, as followed from the conclusion of Chapter 4. This resulted in a model that was, in terms of results and specifically damage patterns, equivalent to the single crack model. The presented results of this chapter are based on the single crack model.

An overview of the test set-up is provided in Figure 5.2. Shear non-linearity is not taken into account other than for the computation of in-situ strengths. Cooldown residual stresses are accounted for by applying a thermal loading step of with a temperature offset of 160 degrees. A dynamic implicit analysis (with quasi static application) is used with automatic time incrementation, a maximum time step of 0.01 and a minimum time step of $1 \cdot 10^{-15}$.

5.3 Test Results

The test results are split into two section: Final failure and damage progressions. Both sections present the experimental results as well as the model predictions.

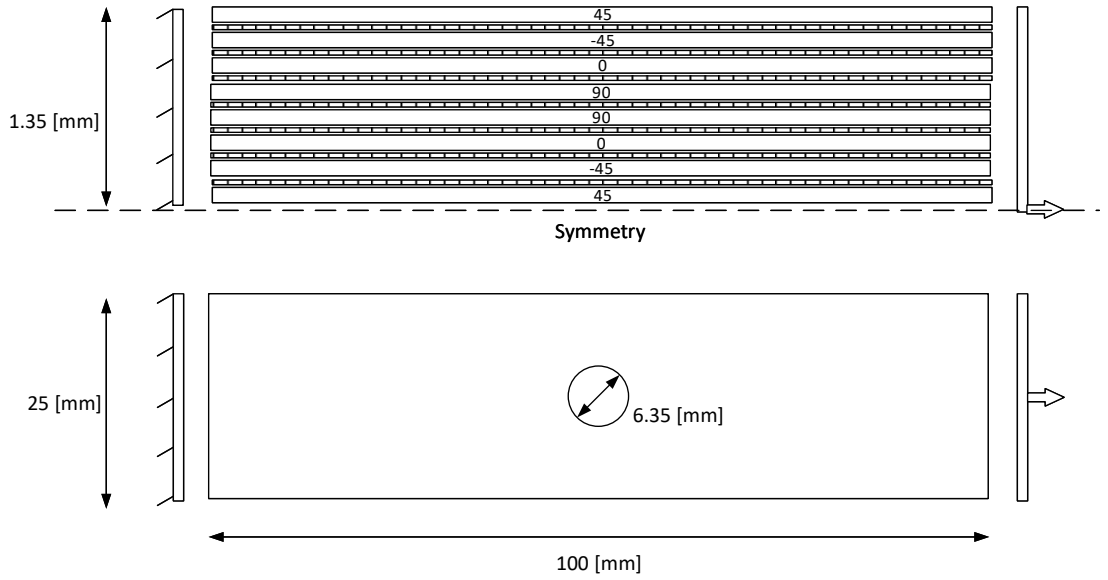

Figure 5.2: Basic setup experimental OHT tests

5.3.1 Final failure

The failure loads of the specimens that were loaded up to final failure are provided in Table 5.2. All specimens broke in a similar fashion by sudden (fibre) fracture at the holes with a low variance in failure loads. The exterior failure patterns for one of the specimens is provided in Figure 5.3.

Figure 5.4 provides the model prediction for final failure. As can be observed an extremely close match to experimental results is achieved, which was repeated for smaller mesh sizes as shown in Table 5.3. These results are obtained on a first try, without tweaking of the model using the same set-up as for the Nixon-Pearson case adjusted to the parameters of the experimental campaign.

Even though the load displacement results look promising, not too much value should be attached to these results. The model appears to be well suited for the prediction of fibre failure dominated load cases. However, for the applicability in general models, the progression of matrix and delamination damage is more interesting. Fibre failure dominated load cases are less influenced by this sequencing as was also found in the previous Chapter 4. The sequencing and progression is however very important for other load cases which are not considered in this experimental campaign.

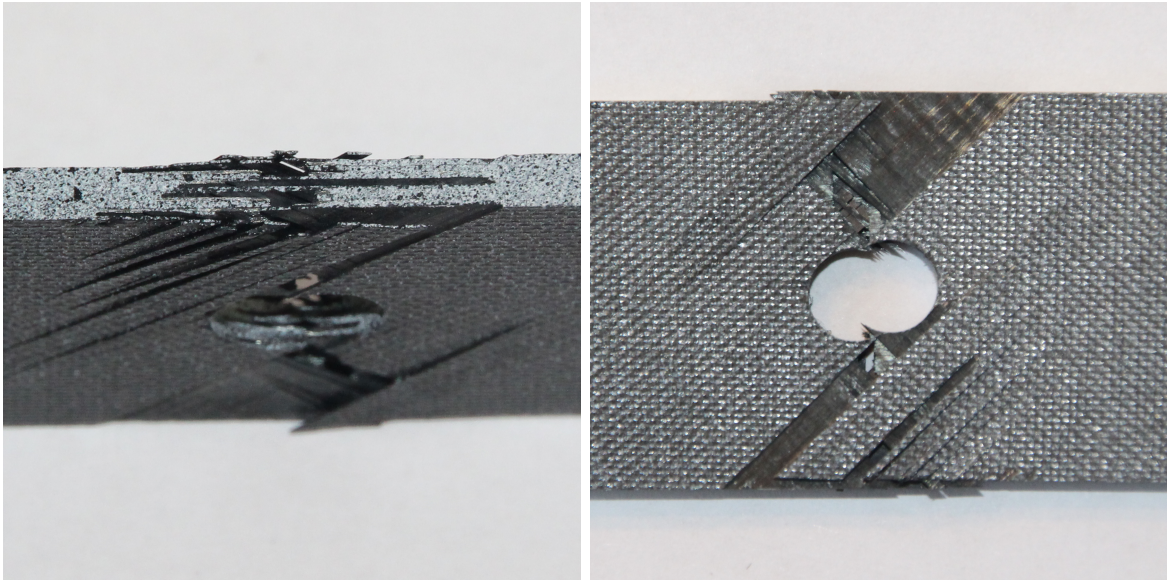

Figure 5.3: Typical exterior damage state after failure

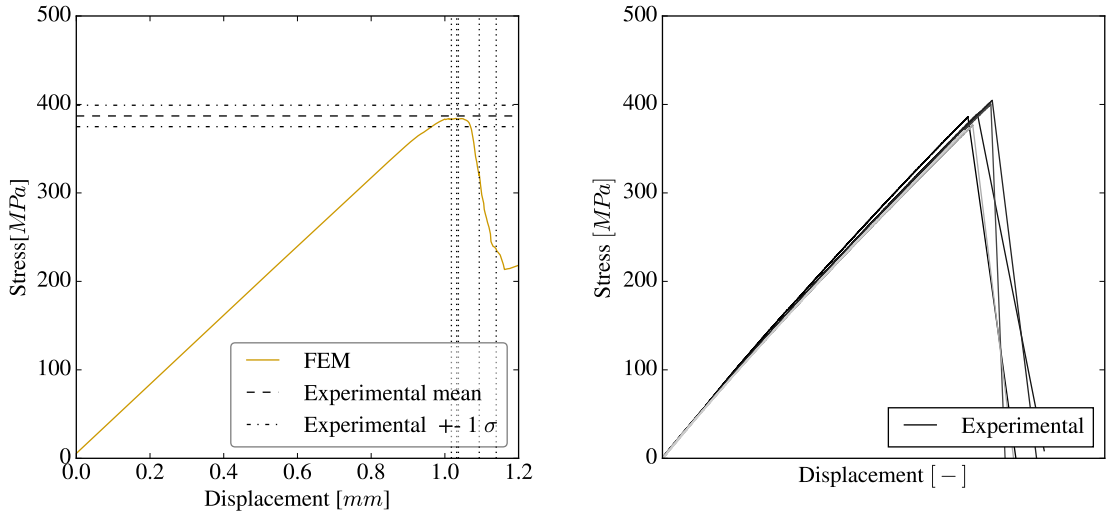

Figure 5.4: Load displacement behaviour

5.3.2 Damage Progression

Damage progression in the specimens was monitored in three different ways. Using acoustic emission, DIC and X-ray CT scans. Still, even with all this monitoring, the best that these methods can provide is proof that the model is not per-se wrong. This however does not mean that the model can be considered validated with just these experimental results. The need for additional experimental testing is highlighted.

Table 5.2: Specimen failure loads

Specimen	Failure Load [kN]	Failure Stress [MPa]
1	26.06	386.11
2	26.27	389.13
3	27.32	404.73
4	27.04	400.60
5	25.44	376.84
6	24.99	370.28
7	-	-
8	-	-
Mean	26.19	387.95
Standard Deviation	0.90 (3.13%)	13.28 (3.13%)

Table 5.3: Model failure loads for different mesh sizes

Mesh Size [mm]	0.5-1.5	0.33-0.67	0.25-0.75
Failure Load [kN]	25.82	25.07	25.90
Difference [%]	-1	-4	-1

5.3.2.1 Acoustic emission

Figure 5.5 provides the damage progression of the different failure modes as well as the experimental acoustic emission data. Figures 5.5a to 5.5c provide the model data on a layer to layer basis. For fibre failure, as a CDM is used, no appropriate physical quantity can be attributed to the damage. Damaged volume captures the meaning as to the damage the CDM applies, but clearly undermines physical meaning of the damage.

Figure 5.5d combines the means of Figures 5.5a to 5.5c with the experimental acoustic emission data. As the acoustic emission data has no units that can directly be physically associated with any particular type of damage all results are normalized using the damage state at the peak failure load. For the acoustic emission data it is important to mention that the data combines all failure modes, but not in equal parts.

If the acoustic emission data is considered, then this does not disprove the validity of the model but neither does it prove it. The acoustic emission data appears to closely match the fibre failure related damage. This is not unlikely as fibre failure has the highest fracture energy associated to it, making it likely that this dominates the acoustic damage data. Only just prior to final failure a mismatch exists, which is in line with Figure 5.4 where some flattening of the load displacement curve was observed just prior to final failure. This flattening behaviour prior to failure was not observed in the experimental campaign in which all specimens failed with a sharp load drop. Dynamic effects at failure likely trigger other sequential failures at these load levels, making the flattening behaviour a partial theoretical quasi-static effect. This dynamic behaviour and stochastic effects such as material inhomogeneity also drive the

scatter in the experimental campaign which can not be replicated with this FEM model.

Overall the acoustic emission data provides an indication that the fibre damage is well predicted considering this is the most energetic failure mode, and the match leading up to final failure is relatively close. For matrix and delamination failure this indication is only provided indirectly via the interactions with fibre failure. However, as previously noted these interactions are little for fibre failure dominated load cases. For example, lowering all delamination and matrix failure related strengths and fracture thoughness's by 25% did not change the final failure load, but did results in a significant increase in damage prior to final failure. An increase on the other hand for strengths and fracture thoughness's by 25% did increase the failure load but still provided a similar absolute error compared to the baseline model highlighting the insensitivity of fibre failure to other failure modes. Therefore no conclusion can be be made on the basis of acoustic emission data as to how well delamination and matrix failure is predicted.

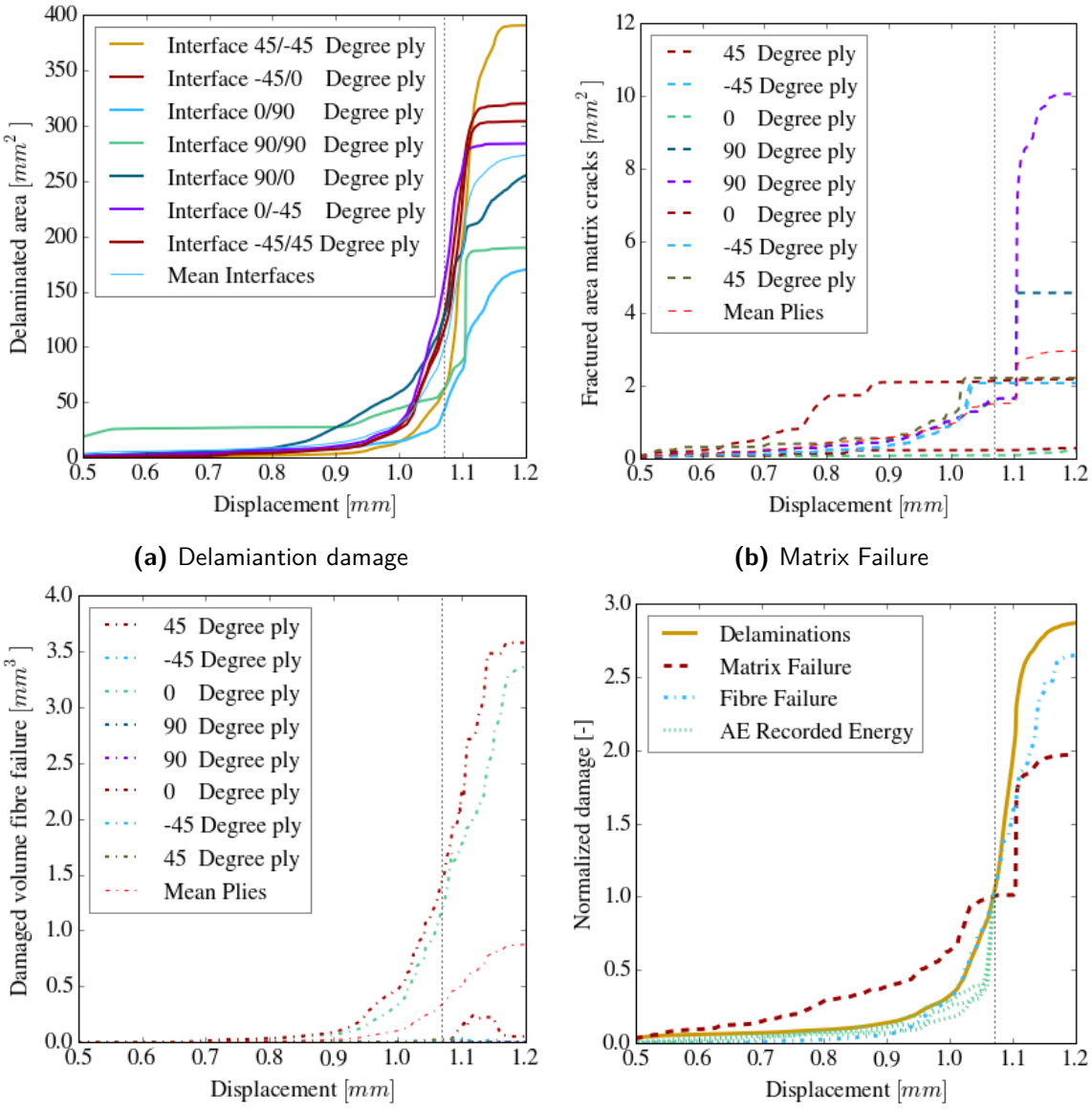

(a) Delamiantion damage

(b) Matrix Failure

(c) Fibre Failure

(d) Acoustic emission normalized energy

Figure 5.5: FEM damage progression and acoustic emisson data

5.3.2.2 DIC

The DIC data provides little useful information for this model other than again proving it not undeniably wrong. Up to final failure DIC results provide a good match with the model results in terms of both strain patterns and associated strain values. Exemplary for a load level of 80% and 95% comparison between the shear strains ϵ_{12} is provided. This example shows a good match between the model and experimental data, and more interestingly was not able to do so for CDM models previously implemented [2] which highlighted the need for fracture mechanics based damage models. Higher strains, outside the limits of the DIC, can

be seen around the hole at the 95% load level. This does not prove model in-correctness as this region is not captured by the limited resolution of the DIC set-up. Similarly the matrix crack, visible in the FEM model would not be visible in the DIC data due to the limited resolution. This again however only provides proof of the model's potential, but does not proof its correctness.

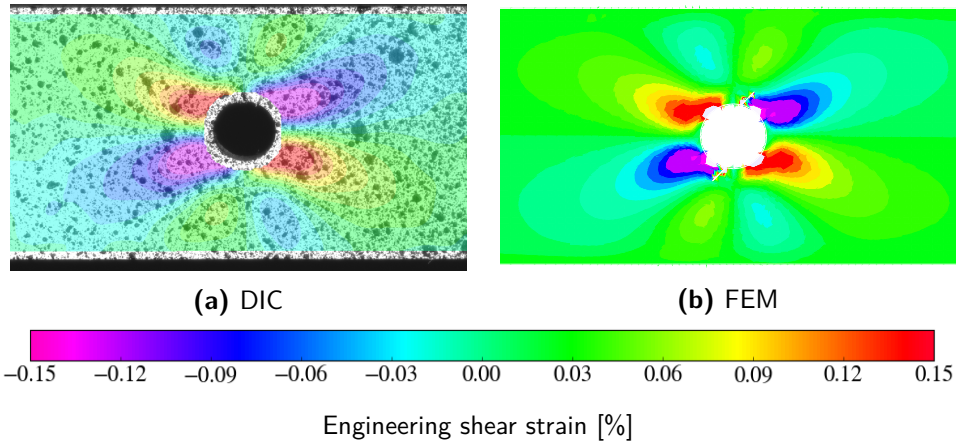

Figure 5.6: Comparison of measured and predicted strain field at 80 % of failure load

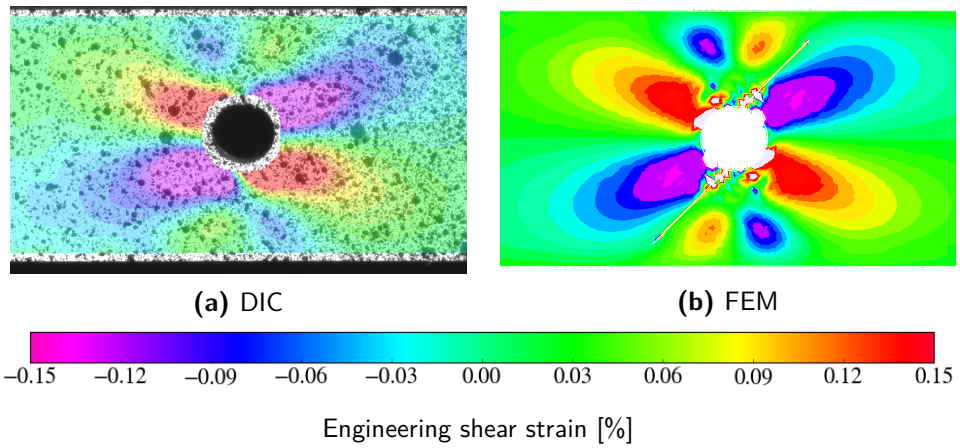

Figure 5.7: Comparison of measured and predicted strain field at 95 % of failure load

5.3.2.3 X-Ray CT

Finally, a comparison with CT scans is made. CT scans at 60% and 80% load levels provided no visible damage. This is partly in line with Figure 5.5 which predicts minimal damage at these load levels. Moreover small cracks cannot be detected at these load levels if the specimen is not scanned in loaded condition [77]. Damage which was monitored by the acoustic emission system showed a significant increase in the number of damage events just before the 60% load level, but these turned out to be of low energy. The interrupted tests were therefore stopped before any real damage could be observed. However, past final failure the CT scans show clear damage. Still, a comparison is hard to make for multiple reasons:

- The load levels at which damage is observed can never be matched
- The model can not capture the extreme dynamic effects past final failure
- The single crack model is limited in the total amount of damage
- Behaviour past the final failure load is increasingly stochastic

Considering these limitations a comparison with experimental CT scans is still made in Figure 5.8 and 5.9. For the FEM model the final recorded load level is taken to show the damage patterns. A few important observations can be made: The outline of the damage patterns roughly matches the experimental results. The experimental results show however significantly more damage, especially in the outer ply. This can be related to the concept of in-situ strengths and the corresponding lower strengths at the outer ply (Section 3.2.2). Both the crack models are inadequate for such damage. For the inner plies this is less the case and the single crack model seems to be appropriate to model the primary cracks. Moreover it can be observed that damage is very stochastic, with only a rough outline of the in-ply symmetry plane visible in each ply. Within the limitations of the single crack model the result are a good match.

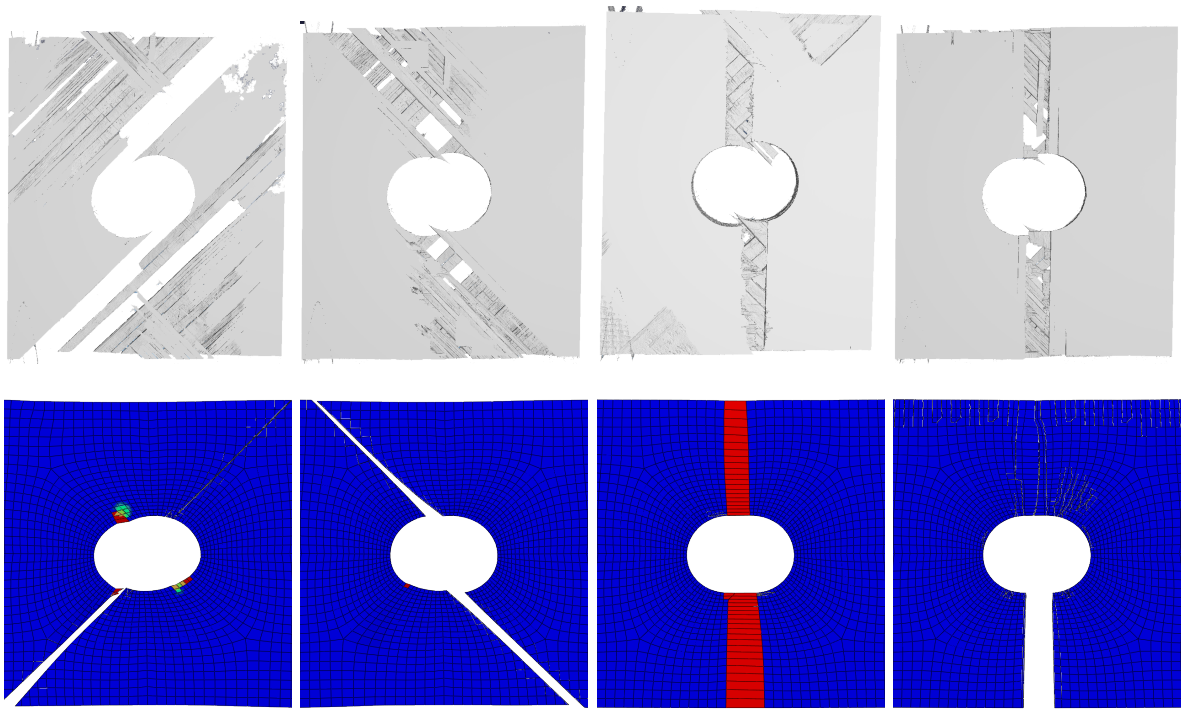

(a) 45 Degree ply **(b)** -45 Degree ply **(c)** 0 Degree ply **(d)** 90 Degree ply

Figure 5.8: Matrix failure (discrete) and fibre failure (red) damage patterns after final failure, plies 1 to 4

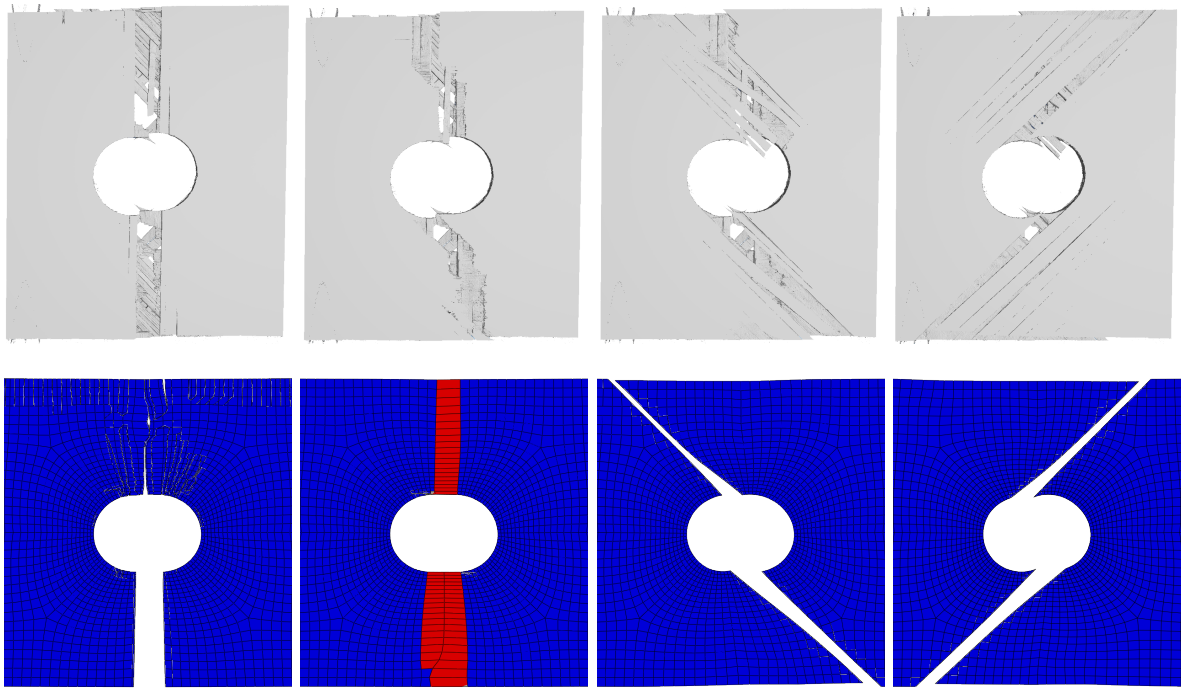

(a) 90 Degree ply **(b)** 0 Degree ply **(c)** -45 Degree ply **(d)** 45 Degree ply

Figure 5.9: Matrix failure (discrete) and fibre failure (red) damage patterns after final failure, plies 5 to 8

A comparison of delamination damage is also not really possible to make. Still, for two positions a side view comparison is made, but only very qualitative conclusions can be attached to it. The specimen is cut in the lengthwise direction, such that the loading would be applied out of plane in the figure. Two positions considered are at r=0.5R and r=R in Figure 5.10 and 5.11 respectively. The CT scans can only be considered for qualitative conclusions because both the scans and model are limited in the damage they show. Therefore only a comparison can be made showing the area that are strongly delaminated, hereby meaning plies with visible ply separation.

As can be observed the very rough outlines of delaminated areas seem to match, but that is all that can be concluded. Notably there is already a huge difference in the damage states between the upper and lower half of the specimen illustrating that failure in composites is also very much a stochastic process.

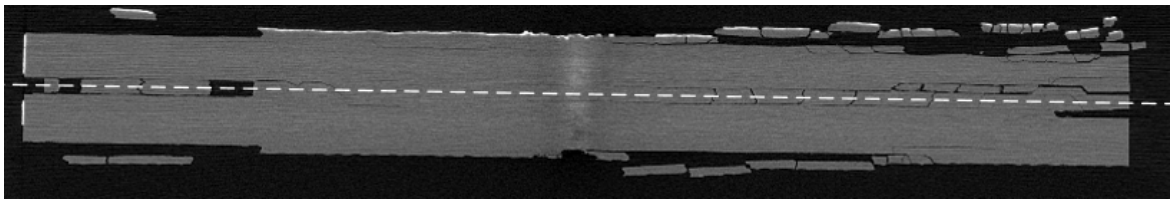

(a) Full laminate

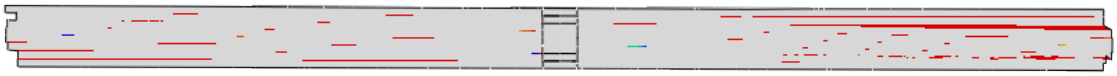

(b) Upper half of the laminate

Figure 5.10: Delamination patterns at r=R

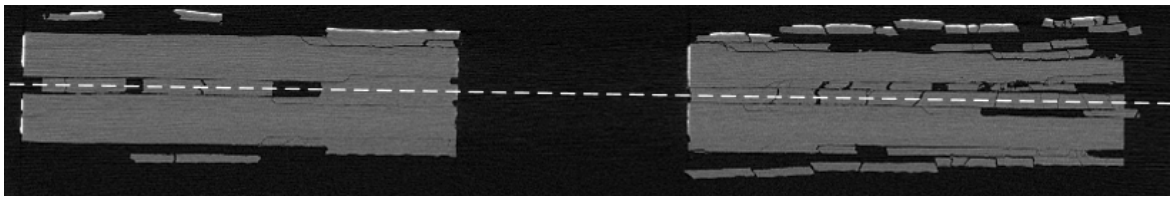

(a) Full laminate

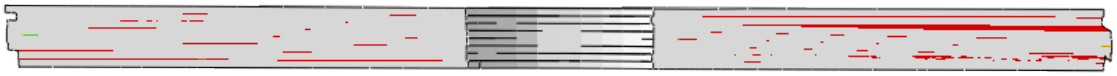

(b) Upper half of the laminate

Figure 5.11: Delamination patterns at r=0.5R

5.4 Conclusions

The experimental campaign echoes most of the issues discussed in the preceding chapters. These issues can be divided in three parts: suitability of the damage models, XFEM related issues and the need for additional experimental testing.

Even though the results are a close match in terms of the reported failure load, the same can not be said for the progression of damage. A softening behaviour slightly prior to final failure is observed which is not in line with experimental results for which final failure is sudden in all cases. As final failure is almost completely fibre failure dominated this relates most likely to the residual stiffness in the CDM which does not represent the physical reality.

The (in)adequacy of the single crack model is also again shown. Some unphysical cracks can be observed, and moreover the parallel cracking which is visible in the final failure patterns is not replicated. This holds also for the multiple crack model, for which results were not shown, but achieved similar results. Only with the use of severe use of CLFs does this model work adequately, but this prevents the development of parallel cracking and final results are similar to the single crack model. These results were therefore excluded. The requirement for the ability to model parallel cracks is however clear from the CT results.

Finally, this very small experimental campaign highlights again the need for additional experimental testing and validation, which may overall be the more pressing issue. This experimental campaign provided less confidence in the presented model than the verification discussed in the previous chapter. Experimental evidence, specifically failure loads, does not guarantee model applicability over a wide range of cases. This is especially true if failure is driven by interactions of failure modes. For this case this is clearly visible for the delamination and matrix damage, where a $\pm 25\%$ increase in fracture toughness did not change the final failure load in a significant way. Focus in experimental campaigns should therefore, apart from testing additional cases, be on damage patterns at different load levels. This is however both difficult and expensive. The former e.g. shown by the lack of observable damage via interrupted CT scans at 60% and 80% of the final failure load levels. The current experimental investigation was therefore also insufficient in proving model validity, other than not clearly disproving it.

Taking these critical notes into account it is easy to forget that the model still presents itself as very promising, specifically when compared to more traditional CDM models. Accuracy was indeed never clearly disproven. The most stringent issues are therefore a more stable framework, specifically relating to XFEM in Abaqus and experimental testing. Only then can the model be properly validated.

6 Conclusions and Recommendations

The work presented in this thesis sets small steps in increasing the predictability of composites allowing their true potential to be fully utilized one day. This research blended stress-strain and fracture mechanics based methods with the objective to improve the fidelity of current PDA methods under quasi-static loading. Fidelity herein primarily considers a trade-off between accuracy and computational effort. Stress-strain based methods, which are currently typically employed, were provided from a partly parallel research by Van Dongen and were in this thesis combined with fracture mechanics based methods in a PDA framework.

From a fracture mechanical perspective two meso mechanical failure modes are modelled: delamination and matrix failure. Selection of PDA methods was based primarily on aspects of practical application and suitability in a blended framework. Both of these failure modes are modelled using cohesive zones, which uses a gradual stiffness reduction via a traction-separation law to model the separation of fracture planes. More traditional methods such as VCCT in the framework of LEFM, which models cracks with sharp tips, were found to be unsuitable although they may make physically more sense, especially in the context of parameter selection. The true physical meaning is however arguable in both cases making currently the physical input parameters and assumptions with regards to cohesive zones the main downside of this selection. Delamination failure with cohesive zones is modelled by the insertion of cohesive elements in between all plies in an intrinsic approach. For matrix cracks the cohesive zones are combined with XFEM. XFEM allows for arbitrary fracture planes, using so called enriched elements with additional shape functions, which removes the strong mesh dependency if elements are not aligned with the physical fracture plane. For matrix failure an extrinsic approach is used in which cohesive zones are automatically inserted after fracture occurs.

The consequences of this choice continue in subsequent model implementation. XFEM in Abaqus presented significant modelling issues by software imposed limitations discussed further in the next paragraphs. The choice for cohesive zone modelling presented also a huge amount of parameter uncertainty, specifically in regard to the traction-separation behaviour. This behaviour is typically not known, requiring the assumption of simplistic softening laws. At locations where interactions between delaminations and matrix cracks are strong this may have a strong influence which was not investigated. A better investigation of these interactions with regards to softening laws would be key to understanding whether the model is able to correctly capture them. Certainty whether interactions are properly captured is currently

among the key issues to provide certainty for the validity of the model.

As part of the blended framework this thesis established, these fracture mechanics based methods for delaminations and matrix failure were combined with stress-strain based methods. The framework is driven by the compatibility with XFEM. An integration is required in the whole model from part generation as well as during the actual analysis. This strongly reduces the applicability and makes model application without the framework close to infeasible. Fibre failure was added in the blended framework by using a CDM with the LaRC05 criteria. The delamination failure was further specified by using a quadratic initiation criteria with a linear softening law. Based on the local element size a strength correction is applied for large interface elements. Matrix failure is initiated by the Puck initiation criteria with again a linear, but physically unsupported, softening law. Material strengths are adjusted to take increased strengths of embedded plies into account with an in-situ strength.

These corrections to strengths for cohesive zones add again to the uncertainty in the traction-separation behaviour discussed in the preceding paragraph. Although both corrections are supported, the ambiguity it yields in the traction-separation behaviour is not good for general model applicability.

Verification of the model was performed on data from a large set of external OHT specimens. This was the continuation of a preliminary joined model which was previously presented by Van Dongen. This model still had severe convergence issues coupled with no model certainty, but showed very promising results in terms of damage patterns, specifically when compared to more classical CDM methods implemented. The first of these continued models is a single crack model, which limits the total amount of cracks to one per ply, per side. The preliminary model's crashes in Abaqus were driven by a sudden increase cracks resulting from limitations in Abaqus, which was unphysical and prevented analysis from continuing, which was required to prove final failure had occurred. With the single crack model a clear definition of a 5% load drop for final failure could be established allowing the model to be more properly verified. This presented good results in terms of final failure loads and damage patterns for the four main verification cases under consideration. Differences in error for reported failure loads were within a few percent. Delamination showed a triangular damage pattern, which was also reported for these tests, and were driven by a high amount of delamination-matrix crack interaction. Sensitivity for this interaction was found to be high making this a very good achievement for the model. This was seen as an essential requirement for the model to be valid. Matrix failure was however not fully in line with experimental results, primarily in the damage it could describe in the single crack model. This main issue related to the use of XFEM in Abaqus and limited crucial further model investigation. As the model undermined damage in an unquantifiable way it can not provide a fully justified conclusion on how well the model really performs, which is also key to knowing whether interactions between damage modes are captured for more generic cases.

In order to tackle the issues of the single crack model a multiple crack model was established. Previous issues of the preliminary model, which were partly solved in the single crack model, are all resulting from the Abaqus implementation of XFEM. The multiple crack model attempted to allow for more cracks to be modelled and at the same time provide scalability to more generic laminates and loading conditions which was both impossible in the single crack model. It was only partly able to do the latter of these. Small spaced parallel cracks are not possible in the framework with Abaqus. The use of a Crack Limiting Function (CLF)

in conjunction with specially tailored enrichment regions did however create model which allowed for more damage than the single crack model, as long as the matrix cracks are not closely spaced. Moreover it presented a more fundamental solution to a sudden cracking problem that the single crack model featured. Real fundamental solutions can however only be provided if a move is made to a framework with less limitations thereby moving away from commercial software.

A final model validation on a in-house experimental campaign echoes all these issues. A good match, within a few percent points difference, is obtained with experimental results in terms of final failure load. Additional DIC, CT and acoustic emission data also does not contradict this image. Failure modes are however not strongly coupled. It is therefore impossible to say whether the model suffices, although it still looks promising. A new framework would be required to adequately model the effects of multiple cracks combined with moreover additional experimental testing focussing particularly on damage patterns and interactions. Only in a more stable framework the main uncertainties presented in this conclusion can be properly investigated.

Main recommendations for future work therefore focus on two parts: Within the current framework it can be further tested against more experimental cases. Compressive loading would be particularly suited for this. This was outside the scope of this thesis, but was considered in the framework and all the required aspects have been integrated. This included a compressive fibre failure criteria (Larc05), compressive matrix failure under an angle (Puck) with a contact interaction between the fracture planes. The latter of these would allow for a strong matrix failure-delamination coupling by the slipping of fracture planes and may prove very interesting, considering compressive load case are significantly more difficult to predict than tensile load cases.

The other main recommendation is the establishment of a more stable framework, outside commercial software, and use this to further investigate the current model. There is still a great amount of model uncertainty which needs to be addressed. This includes further testing with additional experimental campaigns but also within what is currently available. Stochastic effects are clear in all experiential results and have been left completely untouched although it is an important aspect in regards to composites. Also the sensitivity to model parameters is highlighted in just some of the most important parameters, but is far from complete.

The results in this thesis presented themselves as very promising and it is clear that a fracture mechanics based framework is the way forward compared to more classical CDM implementations. However, the presented work captures only a very small subset of what damage in composites encompasses, and was for this small subset unable to provide full confidence in the model. Although promising, it is clear that there is still a very long road to go.

References

[1] M. Kuna, *Finite Elements in Fracture Mechanics*. Dordrecht: Springer, 1st ed., 2013.

[2] B. R. van Dongen, *Progressive damage modelling of FRPs using a blended stress-strain and fracture mechanics approach in FEM*. Msc thesis, Delft University of Technology, 2017.

[3] O. J. Nixon-Pearson, S. R. Hallett, P. W. Harper, and L. F. Kawashita, "Damage development in open-hole composite specimens in fatigue. Part 2: Numerical modelling," *Composite Structures*, vol. 106, pp. 890–898, 2013.

[4] P. P. Camanho, P. Maimí, and C. G. Dávila, "Prediction of size effects in notched laminates using continuum damage mechanics," *Composites Science and Technology*, vol. 67, no. 13, pp. 2715–2727, 2007.

[5] B. G. Green, M. R. Wisnom, and S. R. Hallett, "An experimental investigation into the tensile strength scaling of notched composites," *Composites Part A: Applied Science and Manufacturing*, vol. 38, no. 3, pp. 867–878, 2007.

[6] S. Giannis and C. Jeenjitkaew, "Fatigue Performance of Tapered Laminates with Internal Ply Drop-Offs: Experiments and Numerical Predictions.," in *26th Annual Technical Conference of the American Society for Composites* (M. Hyer, S. Hoa, O. Ochoa, and M. Hojjati, eds.), pp. 643–659, 2011.

[7] N. G. Perogamvros and G. N. Lampeas, "Experimental and numerical investigation of AS4/8552 interlaminar shear strength under impact loading conditions," *Journal of Composite Materials*, vol. 50, no. 19, pp. 2669–2685, 2016.

[8] N. Ersoy, T. Garstka, K. Potter, M. R. Wisnom, D. Porter, M. Clegg, and G. Stringer, "Development of the properties of a carbon fibre reinforced thermosetting composite through cure," *Composites Part A: Applied Science and Manufacturing*, vol. 41, no. 3, pp. 401–409, 2010.

[9] P. Badalló, *Analysis and Optimization of Composite Stringers*. PhD thesis, Universitat de Girona, 2015.

[10] H. M. Deuschle, *3D Failure Analysis of UD Fibre Reinforced Composites: Puck's theory within FEA*. Phd thesis, Universität Stuttgart, 2010.

[11] J. A. Pascoe, R. C. Alderliesten, and R. Benedictus, "Methods for the prediction of

fatigue delamination growth in composites and adhesive bonds - A critical review," *Engineering Fracture Mechanics*, vol. 112-113, pp. 72–96, 2013.

[12] M. J. Hinton, A. S. Kaddour, and P. D. Soden, *Failure Criteria in Fibre Reinforced Polymer Composites: TheWorld-Wide Failure Exercise*. 2004.

[13] G. Vigueras, F. Sket, C. Samaniego, L. Wu, L. Noels, D. Tjahjanto, E. Casoni, G. Houzeaux, A. Makradi, J. M. Molina-Aldareguia, M. Vázquez, and A. Jérusalem, "An XFEM/CZM implementation for massively parallel simulations of composites fracture," *Composite Structures*, vol. 125, pp. 542–557, 2015.

[14] F. P. van der Meer, C. Oliver, and L. J. Sluys, "Computational analysis of progressive failure in a notched laminate including shear nonlinearity and fiber failure," *Composites Science and Technology*, vol. 70, no. 4, pp. 692–700, 2010.

[15] V. K. Goyal, N. R. Jaunky, E. R. Johnson, and D. R. Ambur, "Intralaminar and interlaminar progressive failure analyses of composite panels with circular cutouts," *Composite Structures*, vol. 64, no. 1, pp. 91–105, 2004.

[16] K. Friendrich, *Application of Fracture Mechanics to Composite Materials*. Elsevier, first ed., 1989.

[17] G. Irwin, "Analysis of Stresses and Strains Near the End of a Crack Traversing a Plate," *Journal of Applied Mechanics*, vol. 24, no. September, pp. 361–364, 1957.

[18] G. Sih, P. Paris, and G. Irwin, "On cracks in rectilinearly anisotropic bodies," *International Journal of Fracture Mechanics*, vol. 1, no. 3, pp. 189–203, 1965.

[19] M. L. Benzeggagh and M. Kenane, "Measurement of mixed-mode delamination fracture toughness of unidirectional glass/epoxy composites with mixed-mode bending apparatus," *Composites Science and Technology*, vol. 56, no. 4, pp. 439–449, 1996.

[20] M. D. Wood, X. Sun, L. Tong, Q. Luo, a. Katzos, and a. Rispler, "A New ENF Test Specimen for the Mode II Delamination Toughness Testing of Stitched Woven CFRP Laminates," *Journal of Composite Materials*, vol. 41, no. 14, pp. 1743–1772, 2007.

[21] F. Shen, K. Lee, and T. Tay, "Modeling delamination growth in composites," *Composites Science and Technology*, vol. 61, pp. 1239–1251, 2001.

[22] J. R. Reeder, "3D Mixed-Mode Delamination Fracture CriteriaâĂŞAn Experimentalist's Perspective," *American Society for Composites 21st Annual Technical Conference*, pp. 1–18, 2006.

[23] ASTM D7905/D7905M - 14, "Standard Test Method for Determination of the Mode II Interlaminar Fracture Toughness of Unidirectional Fiber-Reinforced Polymer Matrix Composites," *American Society for Testing and Materials (ASTM)*, pp. 1–18, 2014.

[24] ASTM D5528 - 13, "Standard Test Method for Mode I Interlaminar Fracture Toughness of Unidirectional Fiber-Reinforced Polymer Matrix Composites," *American Society for Testing and Materials (ASTM)*, pp. 1–13, 2014.

[25] J. Reeder, "A Bilinear Failure Criterion for Mixed-Mode Delamination," *Eleventh Volume: Composite Materials-Testing and Design*, vol. 94, pp. 303–322, 1993.

[26] T. H. Walker, W. B. Avery, L. B. Ilcewicz, J. Poe, C. C., and C. E. Harris, "Tension fracture of laminates for transport fuselage. Part 1: Material screening," in *Ninth DOD(NASA)FAA Conference on Fibrous Composites in Structural Design*, pp. 747–787, 1992.

[27] R. Krueger, "Virtual crack closure technique: History, approach, and applications," *Applied Mechanics Reviews*, vol. 57, no. 2, p. 109, 2004.

[28] P. Elisa, "Virtual Crack Closure Technique and Finite Element Method for Predicting the Delamination Growth Initiation in Composite Structures," *Advances in Composite Materials - Analysis of Natural and Man- Made Materials*, pp. 463–480, 2011.

[29] R. Haber and H. Koh, "Explicit expressions for energy release rates using virtual crack extensions," *International Journal for Numerical Methods in Engineering*, vol. 21, no. 2, pp. 301–315, 1985.

[30] S. C. Lin and J. F. Abel, "Variational approach for a new direct-integration form of the virtual crack extension method," *International Journal of Fracture*, vol. 38, no. 3, pp. 217–235, 1988.

[31] T. K. Hellen and W. S. Blackburn, "The calculation of stress intensity factors for combined tensile and shear loading," *International Journal of Fracture*, vol. 11, no. 4, pp. 605–617, 1975.

[32] H. Ishikawa, "A finite element analysis of stress intensity factors for combined tensile and shear loading by only a virtual crack extension," *International Journal of Fracture*, vol. 16, no. 5, pp. 243–246, 1980.

[33] G. P. Nikishkov and S. N. Atluri, "Calculation of fracture mechanics parameters for an arbitrary three-dimensional crack, by the 'equivalent domain integral' method," *International Journal for Numerical Methods in Engineering*, vol. 24, no. 9, pp. 1801–1821, 1987.

[34] B. R. Davis, P. a. Wawrzynek, and A. R. Ingraffea, "Simulation of Arbitrary Delamination Growth in Composite Structures Using the Virtual Crack Extension Method," in *27th Technical Conference of the American Society for Composites*, (Ithaca), 2012.

[35] S. J. Lord and E. S. Greenhalgh, "Modelling of Delamination and Debonding in Laminated Composites using a Moving Mesh Approach," in *11th European Conference on Composite Materials*, (Rhodes), pp. 1–10, 2004.

[36] L. Mishnaevsky, M. Dong, S. Hönle, and S. Schmauder, *Computational mesomechanics of particle-reinforced composites*, vol. 16. 1999.

[37] A. B. De Morais, "Cohesive zone beam modelling of mixed-mode I-II delamination," *Composites Part A: Applied Science and Manufacturing*, vol. 64, pp. 124–131, 2014.

[38] J. F. Molinari, G. Gazonas, R. Raghupathy, A.Rusinek, and F. Zhou, "The cohesive element approach to dynamic fragmentation: The question of energy convergence," *International Journal for Numerical Methods in Engineering*, vol. 69, pp. 484–503, 2006.

[39] L. Wu, D. Tjahjanto, G. Becker, A. Makradi, A. Jérusalem, and L. Noels, "A micro-meso-model of intra-laminar fracture in fiber-reinforced composites based on a discontinuous Galerkin/cohesive zone method," *Engineering Fracture Mechanics*, vol. 104, pp. 162–183, 2013.

[40] M. Samimi, J. A. W. van Dommelen, and M. G. D. Geers, "A three-dimensional self-adaptive cohesive zone model for interfacial delamination," *Computer Methods in Applied Mechanics and Engineering*, vol. 200, no. 49-52, pp. 3540–3553, 2011.

[41] P. P. Camanho, C. G. Davila, and S. S. Pinho, "Fracture analysis of composite co-cured structural joints using decohesion elements," *Fatigue and Fracture of Engineering Materials and Structures*, vol. 27, no. 9, pp. 745–757, 2004.

[42] S. L. Lemanski, J. Wang, M. P. F. Sutcliffe, K. D. Potter, and M. R. Wisnom, "Modelling failure of composite specimens with defects under compression loading," *Composites Part A: Applied Science and Manufacturing*, vol. 48, no. 1, pp. 26–36, 2013.

[43] A. Needleman, "Some issues in cohesive surface modeling," *Procedia IUTAM*, vol. 10, pp. 221–246, 2013.

[44] P. P. Camanho, C. G. Davila, and M. F. De Moura, "Numerical Simulation of Mixed-mode Progressive Delamination in Composite Materials," *Journal Of Composite Materials*, vol. 37, no. 16, 2003.

[45] D. Xie and A. M. Waas, "Discrete cohesive zone model for mixed-mode fracture using finite element analysis," *Engineering Fracture Mechanics*, vol. 73, no. 13, pp. 1783–1796, 2006.

[46] T. Belytschko and T. Black, "Elastic crack growth in finite elements with minimal remeshing," *International Journal for Numerical Methods in Engineering*, vol. 45, no. 5, pp. 601–620, 1999.

[47] S. Mohammadi, *XFEM fracture analysis of composites*. Wiley, 2012.

[48] L. Zhao, J. Zhi, J. Zhang, Z. Liu, and N. Hu, "XFEM simulation of delamination in composite laminates," *Composites Part A: Applied Science and Manufacturing*, vol. 80, pp. 61–71, 2016.

[49] Simulia, "Abaqus 6.14 Users Manual," 2014.

[50] M. Meo and E. Thieulot, "Delamination modelling in a double cantilever beam," *Composite Structures*, vol. 71, no. 3-4, pp. 429–434, 2005.

[51] P. W. Harper and S. R. Hallett, "Cohesive zone length in numerical simulations of composite delamination," *Engineering Fracture Mechanics*, vol. 75, no. 16, pp. 4774–4792, 2008.

[52] L. Lampani, "Finite element analysis of delamination of a composite component with the cohesive zone model technique," *Engineering Computations*, vol. 28, no. 1-2, pp. 30–46, 2011.

[53] S. T. Pinho, *Modelling failure of laminated composites using physically-based failure models*. Phd thesis, Imperical College London, 2005.

[54] F. P. Van Der Meer and L. J. Sluys, "Continuum Models for the Analysis of Progressive Failure in Composite Laminates," *Journal of Composite Materials*, vol. 43, no. 20, pp. 2131–2156, 2009.

[55] H. Puck and Schürmann, "Failure Analysis of Frp Laminates By Means of Physically Based Phenomenological Models *," *Composites Science and Technology*, vol. 3538, no. 96, pp. 1633–1662, 1998.

[56] A. M. Girão Coelho, "Finite element guidelines for simulation of fibre-tension dominated failures in composite materials validated by case studies," *Archives of Computational Methods in Engineering*, vol. 23, pp. 363–388, 2016.

[57] M. M. Shokrieh, L. B. Lessard, and C. Poon, "Three-Dimensional Progressive Failure Analysis of Pin/Bolt Loaded Composite Laminates," in *83rd Meeting of the AGARD SMP on "Bolted/Bonded Joints in Polymeric Composites"*, (Florence, Italy), 1996.

[58] L. Tong, "An Assessment of Failure Criteria to Predict the Strength of Adhesively Bonded Composite Double Lap Joints," *Journal of Reinforced Plastics and Composites*, vol. 16, no. 8, pp. 698–713, 1997.

[59] J. Lee, "Three dimensional finite element analysis of damage accumulation in composite laminate," *Computers & Structures*, vol. I, no. 3, pp. 335–350, 1982.

[60] A. Turon, C. G. Dávila, P. P. Camanho, and J. Costa, "An engineering solution for mesh size effects in the simulation of delamination using cohesive zone models," *Engineering Fracture Mechanics*, vol. 74, no. 10, pp. 1665–1682, 2007.

[61] F. P. Van der Meer, *Computational Modeling of Failure in Composite Laminates*. Phd thesis, Delft University of Technology, 2010.

[62] A. Kaddour and M. Hinton, "Maturity of 3D failure criteria for fibre-reinforced composites: Comparison between theories and experiments: Part B of WWFE-II," *Journal of Composite Materials*, vol. 47, no. 6-7, pp. 925–966, 2013.

[63] O. Mohr, "Welche Umstände bedingen die Elastizitätsgrenze und den Bruch eines Materials," *Zeitschrift des Vereins Deutscher Ingenieure*, vol. 46, no. 1524-1530, pp. 1572–1577, 1900.

[64] M. W. Czabaj and J. G. Ratcliffe, "Comparison of intralaminar and interlaminar mode-I fracture toughness of unidirectional IM7/8552 graphite/epoxy composite," *NASA Technical Report*, pp. 1–18, 2012.

[65] P. P. Camanho, C. G. Davila, S. T. Pinho, L. Iannucci, and P. Robinson, "Prediction of in situ strengths and matrix cracking in composites under transverse tension and in-plane shear," *Composites Part A: Applied Science and Manufacturing*, vol. 37, no. 2, pp. 165–176, 2006.

[66] F. Crossman, W. Warren, A. Wang, and G. Law, "Initiation and Growth of Transverse Cracks and Edge Delamination in Composite Laminates Part 2. Experimental Correlation," *Journal of Composite Materials*, vol. 14, no. 1, pp. 88–108, 1980.

[67] P. P. Camanho, W. Sanders, C. Davila, and J. Mayugo, "Progressive failure analysis of

advanced composites," *University of Porto FA8655-06-1-3072 Report*, vol. 44, no. 0704, 2009.

[68] R. G. Cuntze and T. Ag, "Failure Conditions for Isotropic Materials , Unidirectional Composites , Woven Fabrics - their Visualization and Links -," pp. 1–18, 2006.

[69] S. T. Pinho, R. Darvizeh, P. Robinson, C. Schuecker, and P. P. Camanho, "Material and structural response of polymer-matrix fibre-reinforced composites," *Journal of Composite Materials*, vol. 46, no. 20, pp. 2313–2341, 2012.

[70] A. Matzenmiller, J. Lubliner, and R. L. Taylor, "A constitutive model for anisotropic damage in fiber-composites," *Mechanics of Materials*, vol. 20, no. 2, pp. 125–152, 1995.

[71] I. Lapczyk and J. A. Hurtado, "Progressive damage modeling in fiber-reinforced materials," *Composites Part A: Applied Science and Manufacturing*, vol. 38, no. 11, pp. 2333–2341, 2007.

[72] O. J. Nixon-Pearson and S. R. Hallett, "An investigation into the damage development and residual strengths of open-hole specimens in fatigue," *Composites Part A: Applied Science and Manufacturing*, vol. 69, pp. 266–278, 2015.

[73] R. Gutkin, M. L. Laffan, S. T. Pinho, P. Robinson, and P. T. Curtis, "Modelling the R-curve effect and its specimen-dependence," *International Journal of Solids and Structures*, vol. 48, no. 11-12, pp. 1767–1777, 2011.

[74] O. J. Nixon-Pearson, S. R. Hallett, P. W. Harper, and L. F. Kawashita, "Damage development in open-hole composite specimens in fatigue. Part 2: Numerical modelling," *Composite Structures*, vol. 106, pp. 890–898, 2013.

[75] Y. Masuko and M. Kawai, "Application of a phenomenological viscoplasticity model to the stress relaxation behavior of unidirectional and angle-ply CFRP laminates at high temperature," *Composites Part A: Applied Science and Manufacturing*, vol. 35, no. 7-8, pp. 817–826, 2004.

[76] G. Jeronimidis and a.T. Parkyn, "Residual Stresses in Carbon Fibre-Thermoplastic Matrix Laminates," *Journal of Composite Materials*, vol. 22, no. 5, pp. 401–415, 1988.

[77] F. Sket, A. Enfedaque, C. Alton, C. González, J. M. Molina-Aldareguia, and J. Llorca, "Automatic quantification of matrix cracking and fiber rotation by X-ray computed tomography in shear-deformed carbon fiber-reinforced laminates," *Composites Science and Technology*, vol. 90, pp. 129–138, 2014.